A STUDY ON THE METAL ION SENSING ABILITY AND AGGREGATION BEHAVIOUR OF SOME SQUARAINE DYES

THESIS SUBMITTED
TO THE UNIVERSITY OF KERALA
IN PARTIAL FULFILMENT OF THE REQUIREMENTS
FOR THE DEGREE OF
DOCTOR OF PHILOSOPHY
IN CHEMISTRY
UNDER THE FACULTY OF SCIENCE

BY

K. J. THOMAS

PHOTOCHEMISTRY RESEARCH UNIT
REGIONAL RESEARCH LABORATORY (CSIR)
TRIVANDRUM-695 019, KERALA, INDIA

SEPTEMBER, 1996

A STUDY ON THE METAL ION SENSING ABILITY AND AGGREGATION BEHAVIOUR OF SOME SQUARAINE DYES

THESIS SUBMITTED
TO THE UNIVERSITY OF KERALA
IN PARTIAL FULFILMENT OF THE REQUIREMENTS
FOR THE DEGREE OF
DOCTOR OF PHILOSOPHY
IN CHEMISTRY
UNDER THE FACULTY OF SCIENCE

BY

K. J. THOMAS

PHOTOCHEMISTRY RESEARCH UNIT
REGIONAL RESEARCH LABORATORY (CSIR)
TRIVANDRUM-695 019, KERALA, INDIA

SEPTEMBER, 1996

STATEMENT

I hereby declare that the matter embodied in this thesis is the result of the investigations carried out by me at the Photochemistry Research Unit of the Regional Research Laboratory, Trivandrum, under the guidance of Dr. Suresh Das and the same has not been submitted elsewhere for a degree.

In keeping with the general practice of reporting scientific observations, due acknowledgment has been made wherever the work described is based on the findings of other investigators.

K. J. Thomas

CR
667·2:546·3-128

PHOTOCHEMISTRY RESEARCH UNIT
REGIONAL RESEARCH LABORATORY (CSIR)
TRIVANDRUM-695 019, INDIA

Dr. SURESH DAS
SCIENTIST

Telephone : 91-471-490392 Fax : 91-471-490186
E. mail: das@csrrltrd.ren.nic.in

CERTIFICATE

Certified that the work embodied in this thesis entitled: "**A Study on the Metal Ion Sensing Ability and Aggregation Behaviour of Some Squaraine Dyes**" has been carried out by Mr. K. J. Thomas under my supervision and the same has not been submitted elsewhere for a degree.

Suresh Das
(Thesis Supervisor)

ACKNOWLEDGMENTS

It is with great pleasure that I place on record my sincere thanks to Dr. Suresh Das, my research supervisor, for suggesting the research problem and encouraging me for a successful completion of the work.

I would like to express my sincere thanks to Professor M. V. George for his constant encouragement and help throughout the tenure of my work. Also, I wish to thank Dr. A. D. Damodaran, Director, RRL, Trivandrum for providing the facilities for carrying out my work and for his constant support.

I express my sincere thanks to Dr. K. George Thomas for his help and encouragement during various stages of my work. Thanks are also due to other members of the Photochemistry Research Unit for their help and support. I wish to acknowledge the help rendered by Dr. P. V. Kamat of the Notre Dame Radiation Laboratory, USA for the laser flash photolysis experiments reported in this thesis.

Also, I would like to thank Dr. Vijay Nair, Dr. Mangalam Nair and other members of the Organic Chemistry Division and Professor C. P. Joshua, of the University of Kerala for their help and cooperation.

Financial assistance from CSIR is gratefully acknowledged.

Finally, I am deeply indebted to all the members of my family for their invaluable support and encouragement.

Trivandrum
September, 1996

K. J. Thomas

CONTENTS

PREFACE

Squaraine dyes possess sharp and intense absorption bands in the visible and near infrared region which become broad and red shifted in the solid state. These properties combined with their ability to photoconduct make them important for a number of applications such as in solar energy conversion and xerography. The intense bands of these dyes arise from an intramolecular charge transfer transition and these bands are highly sensitive to substitutional changes as well as to changes in the surrounding medium. The main objectives of the present investigations were, (i) the design and study of squaraine based chromo- and fluoroionophores and (ii) study of the aggregation behaviour of squaraines in homogeneous and heterogeneous media.

In Chapter 1 of the thesis, a brief review on the photophysical, photochemical and aggregation properties of squaraines in homogeneous and heterogeneous media is presented.

Chapter 2 deals with the synthesis and photophysical characterization of a few crown ether derivatives of squaraines, **12-14**. The excited singlet, triplet and radical ion formation in these squaraines were studied by picosecond and nanosecond laser flash photolysis. Although complexation of the crown ether squaraines with different alkali metal ions did not bring about significant changes in the shape of their absorption and emission spectra, a significant decrease in the quantum yield of fluorescence of these dyes was observed. These effects have been attributed to partial inhibition of the intramolecular charge transfer process brought about by metal ion

complexation. The association constants of these dyes with metal ions vary with the size of the crown ether moiety. The changes in the redox properties of these dyes brought about by metal ion complexation were studied using cyclic voltammetry.

The third Chapter of the thesis describes the photophysical and photochemical properties, as well as metal ion complexation properties of a cationic squaraine dye, **10**. Complexation of this dye with metal ions brings about significant changes in the absorption properties of the dye giving rise to a new band. The position of this band is dependent upon the metal ions used, making it possible to distinguish various metal ions. Interestingly, it was observed that alkali and alkaline earth metal cations have no effect on the absorption properties of this dye, enabling thereby the detection of millimolar to nanomolar quantities of metal ions such as Cu^{2+}, Hg^{2+} and lanthanides even in the presence of millimolar quantities of alkali and alkaline earth metal ions.

The last chapter of the thesis (Chapter 4) describes the detailed photophysical studies of two bis(benzothiazolylidene)squaraine dyes, **7** and **8** containing carboxylic functional groups. The presence of the carboxylic functional groups make these dyes water soluble in basic medium (pH ~8). These dyes form sandwich type H-aggregates in water and the photophysical properties of these aggregates have been investigated. Addition of low concentrations of polyvinylpyrrolidone (PVP) ($<3 \times 10^{-4}$ M) brought about an enhancement in the aggregation of **7**, whereas that of **8** remained unaffected. At high concentrations of PVP ($>3 \times 10^{-4}$ M), the formation of highly fluorescent species was observed for **7** and **8** and these species have

been attributed to the polymer microencapsulated monomeric forms of these dyes. The nature of the interaction between PVP and these dyes has been discussed. Picosecond laser flash photolysis studies of the aggregates showed that they break-up in the excited state to yield both excited and ground state monomeric molecules. Rapid recombination of these solvent caged monomers lead to the reformation of the ground state aggregates.

The compound numbers listed in this preface refer to those given in the different Chapters of this thesis.

CHAPTER 1

PHOTOCHEMISTRY AND PHOTOPHYSICS OF SQUARAINE DYES: A BRIEF REVIEW AND OBJECTIVES OF THE PRESENT INVESTIGATION

1.1. Introduction

During the past couple of decades squaraine dyes have been extensively investigated for their diverse applications such as in xerography,[1] organic solar cells,[2,3] optical recording media,[4] and non-linear optical devices[5-7] by many research groups. Squaraine dyes are 1,3-disubstituted squaric acid derivatives, possessing sharp and intense absorption in the visible region which become broad and red shifted in the solid state due to the strong intermolecular donor-acceptor interactions.[8,9] A brief review on the synthesis, photophysics and photochemistry of squaraine dyes with special emphasize on the microenvironment effect and aggregation properties as well as the objectives of the present investigation are presented in this Chapter.

1.2. Synthesis

Squaric acid undergoes condensation reactions with a variety of nucleophiles to form 1,3-disubstituted products possessing intense absorption in the visible and near-infrared region.[10-14] Schmidt[15] has proposed the widely accepted name 'squaraine' for this class of dyes which was first reported by Treibs and Jacobs.[10] The major part of the earlier work on the synthesis of squaraines was carried out by the former group[10,16] and by Sprenger and Ziegenbein.[17-19] Later, Law and co-workers have

contributed extensively on the synthesis of unsymmetric squaraines.[20-23] More recently, Nakasumi and co-workers[24] have reported a new class of cationic squaraines.

1.3. Absorption and Emission Spectra

Squaraine dyes can be generally described as molecules consisting of two donor moieties (D) connected to a central C_4O_2 electron withdrawing group (A) (Chart 1). The optical properties of squaraines, are very similar

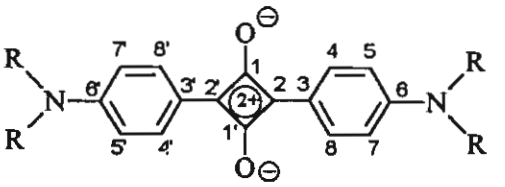

1, R = CH_3

2, R = C_4H_9

Chart 1

to those of polymethine cyanine dyes, suggesting a cross-conjugated structure as shown in Chart 2. In such a structure the bond lengths between the conjugated carbons are expected to be equal, with values in between those of a single and double bond. X-ray crystallographic studies suggest that the average C-C bond length is about 1.414 Å indicating considerable amount of double bond character, suggesting extensive delocalization throughout the molecule.[25-28] Whereas the C_4-C_5 bond length of 1.366 Å is suggestive of a quinoid like structure, the C-C bond length of the cyclobutane ring deviates closest to that of a single bond.[25] Thus, while the net molecular carbon-carbon bond order suggests a cross-conjugated cyanine like structure, squaraine also possesses a cyclobutadienylium dication

character. The true structure must therefore be a complex mixture of the two resonance forms, shown in Chart 2.

MNDO and CNDO calculations have showed that the S_0-S_1 electronic excitation involves a charge transfer process which is primarily confined to the central cyclobutane ring, from each oxygen atom to the four membered ring with minor contributions from the donor groups. The intramolecular CT character of this transition, combined with an extended conjugated π-electron donor network gives rise to the sharp and intense bands in the visible region observed for squaraines.[29]

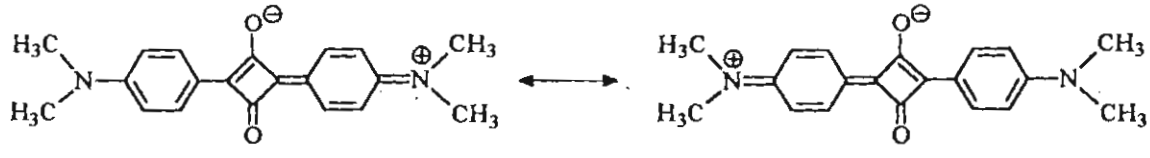

Chart 2

The effect of substituents and solvents on the ground and excited state properties of bis[4-(dimethylamino)phenyl]squaraine, **1** (Chart 1) and its derivatives have been studied in detail by Law.[30] Increase in the chain length of the N-alkyl group as well as substitution at the C_4 and C_5 positions brought about bathochromic shifts in the absorption spectra of these squaraines. These effects could partly be attributed to the minor involvement of the donor groups in the S_0-S_1 excitation. The enhancement in the D-A-D CT character brought about by the substituents can lead to a stabilization of the polarized charges. Law[30] has suggested that the bathochromic shifts can mainly be attributed to improved formation of solute-solvent complexes with increase in the stabilization of these charges.

The absorption and emission properties of [4-methoxyphenyl-4'-(dimethylamino)phenyl]squaraine, **3** (Chart 3) and its derivatives, a class of unsymmetrical D'-A-D compounds showed interesting differences from those of the symmetrical squaraines.[31,32] Their absorption spectra are blue-shifted relative to those of the symmetrical squaraines, due to the presence

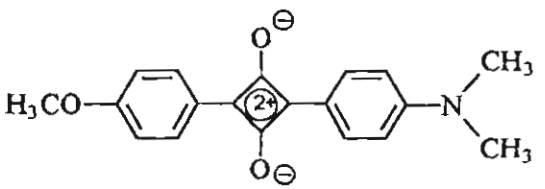

3

Chart 3

of the less electron donating anisole ring. Introduction of asymmetry through the anisole ring enhances vibronic coupling during electronic transition, producing vibrational fine structure in both absorption and fluorescence spectra. The multiple fluorescence observed for these compounds has been shown to be the sum of vibronic bands of the unsymmetrical squaraine and its solvent complex. The fluorescence quantum yields of the unsymmetrical squaraines are a factor of 30 lower than those of symmetrical squaraines and these differences have been attributed to radiationless decay, due to enhanced rotation of the C-C bond between the anisole ring and the central four-membered ring.

For the symmetrical bis[4-(dimethylamino)phenyl]squaraine, **1** (Chart 1) and its derivatives, complexation with alcoholic solvents was shown to bring about bathochromic shifts in their absorption spectra.[33] For the bis(benzothiozolylidene)squaraines such as **4** (Chart 4), however,

complexation with alcoholic solvents brought about marked hypsochromic shifts in their absorption maxima.[34] The hypsochromic shifts have been attributed to formation of hydrogen bonds between the alcohols and the oxygen atoms of the central cyclobutane ring, which can hinder the intramolecular charge-transfer process. A strong correlation was observed

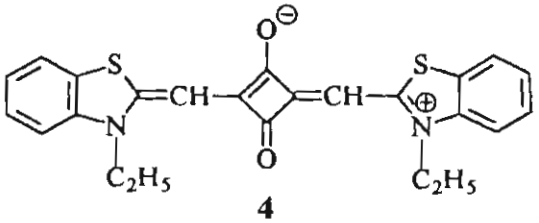

4

Chart 4

between the extent of the hypsochromic shift and the hydrogen bonding strength of the alcohol. Such hypsochromic shifts have also been observed for similar squaraine dyes.[35] The differences in the behaviour of the [4-(dialkylamino)phenyl]squaraines and bis(benzothiozolylidene)squaraines suggest that the quinoid like structure may be more pronounced in the latter.

1.4. Excited State Properties

The properties of the excited states and the reduced and oxidized forms of bis[4-(dimethylamino)phenyl]squaraine, **1** and bis[4-(dimethylamino-2-hydroxy)phenyl]squaraine, **5** (Chart 5) have been investigated by picosecond and nanosecond laser flash photolysis.[36]

The transient absorption spectra recorded at different time intervals, following 532-nm laser pulse (18 ps) excitation of **5** show an absorption maximum around 480 nm.[36] The lifetime of the excited singlet state and the fluorescence quantum yield of **5** are about twice that of **1**. This has been

attributed to hydrogen bonding between the OH group in the phenyl ring and the CO-group in the central cyclobutane ring, which can restrict the rotational relaxation of the excited state of **5** as proposed earlier by Law.[30]

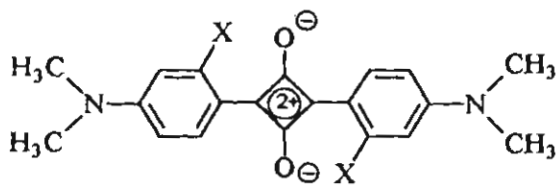

1, X = H
5, X = OH

Chart 5

The intersystem crossing efficiencies of **1** and **5** were very small (1%). The triplet-triplet spectra of these dyes were obtained using the triplet-triplet energy transfer method using 9,10-dibromoanthracene (DBA) as the sensitizer. The transient absorption spectrum recorded immediately after laser pulse excitation (λ_{max} 425 nm) corresponds to the sensitizer triplet while those recorded at time intervals greater than 10 μs correspond to the triplet state of **1**. The triplet lifetimes of **1** and **5** were identical, indicating that the triplet excited states, unlike the singlet excited states, are insensitive to the presence of OH groups on the phenyl ring.

1.5. Photophysical Properties of Squaraines in Heterogeneous Media

The intramolecular charge-transfer nature of the electronic transitions of squaraines makes their photophysical properties highly sensitive to the properties of the surrounding medium. In addition, the ability of these dyes to form solute-solvent complexes and their sensitivity to pH, polarity and hydrogen bonding ability of solvents can make these dyes useful as probes for assessing the microstructures of organized assemblies and of polymers.

1.5.1. Effect of β-Cyclodextrin

Addition of β-cyclodextrin (β-CD) to aqueous solutions of **6b** (Scheme 1) brought about a gradual red shift in the absorption and emission bands with an enhancement in fluorescence yield.[37] At the highest concentration of β-CD studied the fluorescence yield of **6b** ($\Phi_f = 0.18$) was nearly

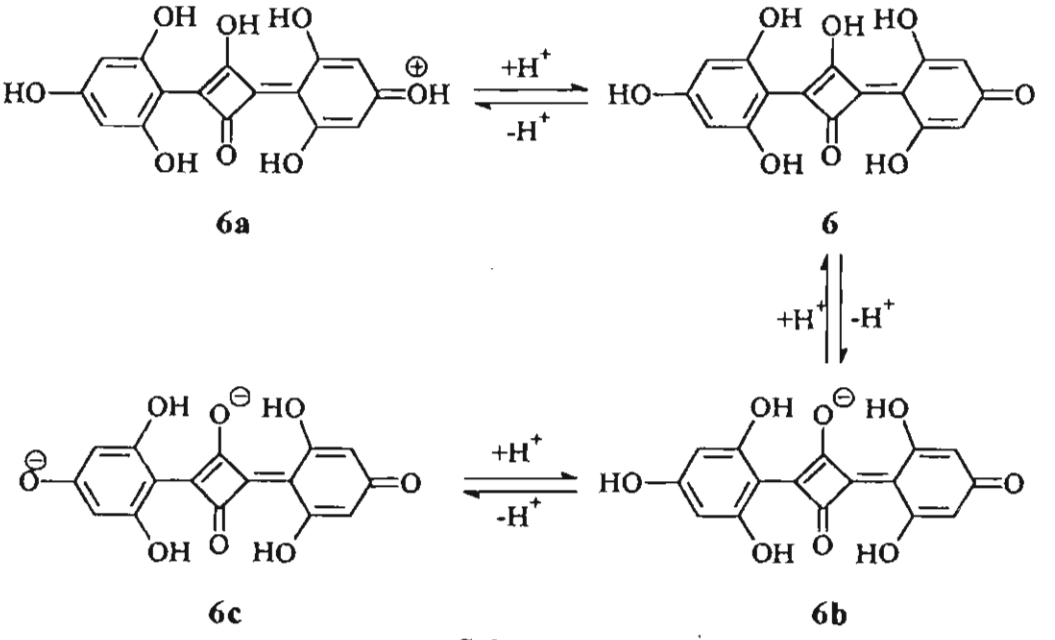

Scheme 1

90 fold of that observed in water. Benesi-Hildebrand analysis of the dependence of fluorescence yield of **6b** on β-CD concentration indicated a 2:1 complex formation between β-CD and **6b**.

Encapsulation by β-CD molecules can enhance the microviscosity around the dye anion which can restrict the free rotation of the two phenyl groups. Additionally, the hydrogen bonding of **6b** with the solvent molecules will also be restricted. Due to a combination of these effects the

non-radiative decay routes become far less efficient leading to the observed enhancement in fluorescence yield. From picosecond laser flash photolysis studies the rate constant for non-radiative internal conversion was estimated as 1.18×10^{10} s^{-1} and 6.6×10^{8} s^{-1} in the absence and presence of β-CD, respectively.

1.5.2. Effect of Polymers

In basic methanolic solutions of **6**, addition of poly(4-vinylpyridine), (P4VP) brought about a marked red shift in the absorption band of the dye anion[38] which was accompanied by a significant enhancement in the fluorescence quantum yield. At low concentrations of P4VP employed in these studies, the change in macroviscosity would not sufficient to affect the fluorescence yields significantly. It was proposed that entrapment of the dye anion by the polymer macrocages leads to the observed effects, with the driving force for the entrapment being hydrophobic interactions between P4VP and the dye anion.

1.6. Aggregation Properties of Squaraines

Photoconducting and other solid state properties of materials are dependent both upon the intrinsic molecular properties of the material as well as the intermolecular interactions that occur in the solid state. The sharp and intense bands of squaraines for example, become broad and red shifted in the solid state. Studies on aggregates can help in developing a molecular level understanding of their solid state properties. In view of this, the aggregation behaviour of squaraines in solutions[39-41], vesicles[42,43] thin films[44-47] in the solid state[48] and on semiconductor surfaces[49-52] has been extensively studied.

1.6.1. Aggregation in Solutions

The equilibrium constants and thermodynamic parameters for aggregate formation of bis(2,4-dihydroxyphenyl)squaraine (7) and bis(2,4,6-trihydroxyphenyl)squaraine (6) (Chart 6) have been studied by absorption spectroscopy.[41] In dry acetonitrile, at low concentrations, the dyes exhibited a broad absorption band centered around 480 nm. At higher concentrations a sharp new band centered around 565 nm was observed. Based on the dependence of the absorption spectral changes on dye concentration the aggregated forms were determined to be dimeric species and intermolecular hydrogen bonding has been proposed to be responsible for the dimerization process. This was confirmed by addition of hydrogen bond donating or accepting solvents to these solutions which led to a decrease in the intensity of the dimer band and a concomitant increase in the intensity of the monomer band.

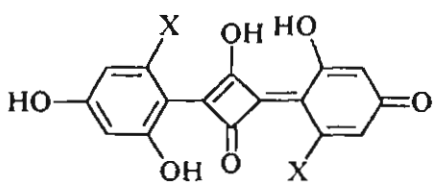

6, X = OH

7, X = H

Chart 6

According to exciton theory[53,54] the excited state energy level of the monomeric dye splits into two upon aggregation, one level being lower and the other higher in energy than the monomer excited state. The transition to the higher state is forbidden for head-to tail (J-type) dimers, whereas the lower excited state is forbidden for sandwich type (H-type) dimers. The

sharp bands observed in the red region of the monomer bands indicate that J-type aggregates predominate in the case of these dyes.

Addition of iodine to acetonitrile solutions of **6** led to an increase in aggregate formation and this has been attributed to the formation of charge-transfer complexes between iodine and **6**. Squaraine dyes such as bis[4-(dimethylamino)phenyl]squaraine, **1** have been observed to form charge transfer complexes with iodine.[55]

The emission and excitation spectra of **7** in acetonitrile suggest that the dimer aggregates tend to dissociate in the excited state.[41] At lower concentration the dye is predominantly in the monomer state and exhibits emission in the 580 nm region. The excitation spectrum closely matches the absorption spectrum of the monomer. The large Stoke's shift in emission is suggestive of deprotonation of the monomeric form in the excited state. The emission and excitation bands measured in solution containing higher concentrations of the dye indicate that the emission from the aggregate closely matches that of the monomer emission. This is suggestive of dissociation of the aggregate in the excited state, possibly involving proton exchange as well. Confirmation of dissociation of the dimer in the excited state was obtained from picosecond laser flash photolysis studies.

The excited singlet states of **6** and **7** in the neutral form exhibited characteristic transient absorption in the 430-450 nm with lifetimes of 130 and 30 ps, respectively. Corresponding bleach and recovery of the ground state absorption were also observed.[41] At higher concentrations of the dye, bleaching of the dimer band was observed and this was accompanied by formation of a transient absorption band in the 430-450 nm region indicating formation of the excited singlet state of the monomer. These results

suggest that the squaraine aggregate dissociate in the excited state. The decay time of the excited singlet state matched the recovery time of the *dimer band. The rapid recovery of the dimer band suggests that dissociation* of the dimer in the excited state leads to a solvent caged excited state/ground state dye pair.

UV-vis spectroscopic studies showed that the squaraine dye, **8** (Chart 7) can exist in the form of two aggregates which form preferentially in different DMSO-water compositions.[39] In pure DMSO and DMSO-water mixtures containing more than 70% DMSO, **8** exists in the monomeric form

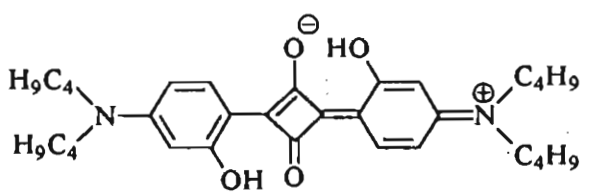

8

Chart 7

which has a sharp absorption band with a maximum around 600 nm. In 70% v/v DMSO-water mixtures, **8** exists in a stable aggregated form which has a blue shifted absorption band (λ_{max} = 530 nm, $\varepsilon \approx 80{,}000\ M^{-1}\ cm^{-1}$). In DMSO-water mixtures containing 20-50% of DMSO a second type of aggregate form with a broad absorption band in the region 550-700 nm was observed. This species underwent a time dependent change to the aggregated species observed in the DMSO-rich solvent mixture. The rate of this change increased with increase in the DMSO content. Similar observations on the formation of thermodynamically and kinetically preferred aggregates were made for other bis[4-(dialkylamino)phenyl] squaraine derivatives.[40]

1.6.2. Aggregation in Langmuir-Blodgett Films

The aggregate properties of surfactant squaraines **9-11** (Chart 8) which were designed to orient the "bricklike" squaraine chromophore in three different directions when organized in monolayers and Langmuir-Blodgett films (LB films) have been reported.[45]

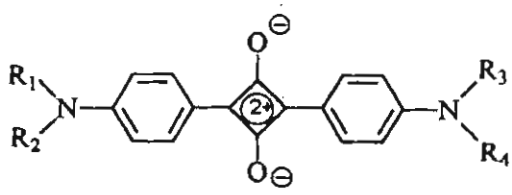

9, $R_1 = R_2 = CH_3$; $R_3 = R_4 = n\text{-}C_{18}H_{37}$

10, $R_1 = R_3 = CH_3$; $R_2 = R_4 = n\text{-}C_{18}H_{37}$

11, $R_1 = R_2 = R_3 = R_4 = n\text{-}C_{18}H_{37}$

Chart 8

Surface pressure-area isotherm studies showed that the squaraine chromophores of **9**, **10** and **11** orient as designed, namely being laid down vertically along the long axis, vertically along the short axis and flat on water. Thus, the surface pressure area isotherm of **9** on water surface exhibits only one transition with a limiting area of 52 $Å^2$/molecule. From single crystal X-ray structure of bis(4-methoxyphenyl)squaraine,[28] X-ray powder diffraction patterns of bis[4-(dialkylamino)phenyl]squaraines[56] and molecular modeling studies, the dimensions of the squaraine chromophore have been estimated as 17 Å x 7 Å x 3.5 Å. Based on these values, the limiting area upon compression for **9** residing vertically on its long axis on water, would be 25 $Å^2$/molecule. However, depending upon the nature of the stearyl chain attachment a spread of about 20-25 Å can be expected in these values.[57] Based on this and the nature of the intermolecular interaction of the aggregates which involve C-O dipole-dipole interactions, it was proposed that **9** aligns vertically on its long molecular axis. The limiting

area of the isotherm was 60 $Å^2$/molecule for **10**, which agrees well with the assumption that the molecule resides vertically along the short axis. Compound **11** showed two transitions of limiting areas of 126 and 85 $Å^2$/molecule. Since the calculated molecular area of squaraine chromophore of **11** is 119 $Å^2$/molecule, excluding the molecular chains, these results suggest that this dye lays flat on the water surface upon compression. Since the limiting area of the second transition is smaller than the molecular area of a squaraine chromophore, the pressure-isotherm curve suggests that the chromophores may become tilted and stack on each other at surface pressures higher than 10 mN/m.

The aggregation of **9** and **10** was studied by absorption spectroscopy. By comparison with the absorption spectra of model squaraine aggregates, it was concluded that **9** forms sandwich type dimers which is essentially controlled by C-O dipole-dipole interactions. For **10**, the aggregate band is red-shifted to that of the monomer and this has been attributed to an aggregated form involving intermolecular charge-transfer interactions between the electron-donor and electron-acceptor groups of squaraines. The difference in aggregational behaviour was attributed to orientational effects induced by the LB film technique.

More recently it was observed that the blue shifted aggregate of **9** could be converted to two different aggregates at higher temperatures from 65 to 100 °C.[45] The absorption spectrum of a monolayer of **9** on a glass substrate showed an absorption peak at 530 nm which was attributed to the blue shifted aggregate. On heating the film at 65 °C under ambient conditions, the absorption peak at 530 nm decreases in intensity and an increase in absorption around 660 nm was observed, indicating conversion

of one aggregated form to another. Interestingly, the heat-generated by the red-shifted aggregate in the LB film of **9** was similar to that obtained in freshly prepared LB film of **10**. When the blue-shifted and the red-shifted aggregates of **9** were heated at 105 °C for 10-20 min, absorption due to these species was replaced by that of a new species with a maximum at 695 nm. This new species has been assigned to a J-aggregate of **9** based on similar characteristics of other squaraine dyes[41,58-60] and cyanine dyes.[61,62] When both the red-shifted and the J-aggregated films were treated with water vapour at 65 °C a gradual reversal in the aggregation process leading to regeneration of the blue shifted aggregate was observed. The formation of J-aggregates were not observed for **10** and **11**. Steam treatment of the red shifted aggregates of these dyes did however, lead to the formation of blue shifted aggregates. It was also observed that these dyes form blue shifted aggregates in DMSO. On addition of the dye to DMSO-water mixtures of increasing water concentration, a decrease in the intensity of the 530 nm band and an increase in intensity of absorption at 650-680 nm were observed. Similar effects in DMSO-water mixtures were observed earlier for other bis[4-(dialkylamino)phenyl]squaraines by Buncel et al.[39] and Mckerrow et al.[40]

Based on these studies, Liang et al.[45] have proposed the molecular arrangement for the blue-shifted, J-aggregates of **9** in LB films. In the LB films of **9**, each squaraine molecule occupies 26 $Å^2$ in the vertical orientation whereas its limiting molecular area in LB films was estimated as 51 $Å^2$.[45] The excess free area, enables tilting movement of the squaraine chromophores within the LB film on heating. Due to the relatively good match of the estimated areas occupied by the squaraines **10** and **11** to the limiting

molecular areas in LB films, these films are less susceptible to rearrangement on heating.

The observed aggregational behaviour has been rationalized in terms of an optimization between hydrophobic interactions (between hydrocarbon chains) and charge-transfer interactions (between the squaraine chromophores). In the air-water interface, due to the predominance of hydrophobic interactions the card pack arrangement (blue-shifted aggregate) is formed. On being transferred to a glass substrate this arrangement is maintained. Heating at 105 °C, however, leads to the more stable J-aggregate which are stabilized by the intermolecular charge transfer interactions. On exposure to steam, the hydrophobic interactions again become the dominating force leading to reformation of the card-pack arrangement. These studies have recently been extended to several amphiphilic squarainces containing carboxylic units.[47]

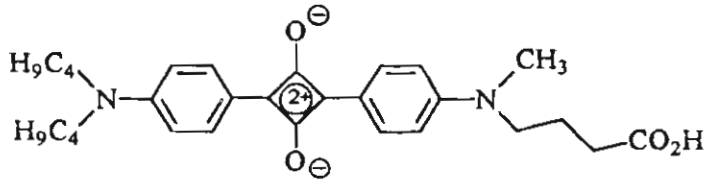

12

Chart 9

The aggregation of a surfactant squaraine, 4-[N-methyl-N-(carboxypropylamino)phenyl-4'-(N,N-dibutylamino)phenyl]squaraine, **12** (Chart 9) has been studied in a variety of media, including organic solvents, aqueous cyclodextrin solutions, vesicles, monolayers, LB films and pure dry films.[44]

In dilute aqueous solution, **12** has a strong absorption at 650 nm with a shoulder at 590 nm. At higher concentrations, the 594 nm band increases

in relative intensity and this band has been attributed to the H-dimer form of **12**. The monomeric form fluoresces with a maximum at 678 nm, whereas the dimeric form is non-fluorescent. The structural assignment of the dimeric form was supported by studying the spectroscopic properties of **12** in cyclodextrin (CD) solutions. Compound **12** formed 1:1 inclusion complexes with α-and β-CD, which absorb at λ_{max} 650 nm and emit at λ_F ~672 nm with fluorescence quantum yields of 2-3 times higher than in pure water. In γ-CD solution due to its larger cavity size, a 2:1 complex between **12** and γ-CD was observed. The absorption and emission characteristics of the 2:1 complex was similar to those of the dimeric form. A further blue shift in absorption, λ_{max} 500-540 nm, was observed when **12** was incorporated in vesicles, monolayers, supported on LB films and in pure solid dye film. Intermolecular interactions between squaraine chromophores involving the C-O dipole-dipole interactions similar to those observed in microcrystals[28,48] have been proposed as the main driving force for the aggregations of these dyes.

1.6.3. Aggregation in Vesicles

The synthesis and aggregation behaviour of several amphiphilic squaraines in aqueous and mixed aqueous-organic solutions as well as in bilayer vesicles have been reported.[42,43] In aqueous solutions containing the amphiphilic squaraines and phospholipids, clear solutions could be obtained upon sonication. Light scattering and membrane filtration studies indicate that the mixed vesicles were much larger than the corresponding pure phospholipid vesicles. At higher concentrations of squaraine to phospholipid the blue-shifted (520 nm) aggregate with spectra similar to those observed in

LB films or in DMSO-water mixtures were observed, whereas at lower dye/phospholipid ratios, an increase in the intensity of the monomer band was observed. These squaraines were also capable of forming stable large vesicles upon probe sonication. Under these conditions only the blue shifted aggregate band was observed.

The tendency for aggregation was found to increase with the increase in the length of the alkyl chain substituent on nitrogen. Squaraines with quarternary ammonium head groups exhibited less tendency for aggregation, probably due to electrostatic repulsion of the head groups. The aggregation number was determined by Benesi-Hildebrand type analysis to be ~4 for several of these squaraines. Based on the induced circular dichroism observed for the aggregate and Monte Carlo simulation results, Chen et al.[42,43] propose that the unit aggregate is a tetramer with chiral pin-wheel structure.

1.7. Interaction with Semiconductors

Squaraines are capable of sensitizing large band-gap semiconductors such as TiO_2, SnO_2 and ZnO. The dynamics of the charge injection from the excited state of squaraines to the conduction band of semiconductors have been investigated by picosecond spectroscopy.[36,50,63] The sharp absorption band of bis[4-(dimethylamino-2-hydroxy)phenyl]squaraine, **5** with λ_{max} at 636 nm became broad and red-shifted (λ_{max} 670 nm) in the presence of colloidal TiO_2. The red-shift of 35 nm, in the absorption band has been attributed to a strong charge transfer interaction of the dye with the TiO_2 surface. Concurrently a quenching of fluorescence is also observed which could be attributed to charge injection from the excited singlet of the dye to the conduction band of TiO_2. The formation of the dye radical cation was

further confirmed by picosecond laser flash photolysis experiments. The J-type dimer of bis(2,4,6-trihydroxyphenyl)squaraine, **6** was found to form charge transfer complex with TiO_2.[52] Squaraines were found to have much better solar energy conversion efficiencies than a variety of other merocyanine dyes.[2,3]

1.8. Biological Applications

There is considerable interest in the study of fluorescent dyes absorbing in the near infrared region for a number of biological applications. Such dyes have applications in fluorescence lifetime sensing techniques for intracellular chemical imaging of analytes such as pH, O_2, K^+, or Ca^{2+}.[64] However, very few NIR dyes possessing high quantum yields of fluorescence are known. Several squaraine dyes are known which absorb in the NIR region and also possess strong emission properties which are highly sensitive to the nature of the surrounding medium. In view of this, the use

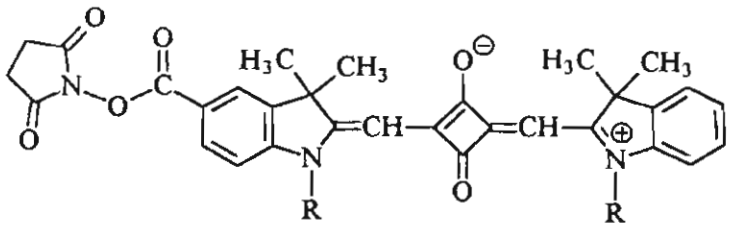

13, R = C_2H_5

14, R = $(CH_4)_2SO_3^{\ominus}$

Chart 10

of squaraines as fluorophores or fluoroionophores for biological applications is gaining increased attention. Lakowicz and co-workers have synthesized and studied the biological applications of several new squaraine dyes.[65-69] It was found that indolenine-containing squaraines were the most photostable and that their lifetimes are significantly increased in the

presence of bovine serum albumin (BSA). Two amine reactive N-hydroxy-succinimide esters of squaraines **13** and **14** (Chart 10) were synthesized. Squaraine dye **14** is water soluble due to the presence of a sulfobutyl group and **13** was made water soluble by reacting it with taurine.

The fluorescence quantum yields and lifetimes of the Sq-taurine derivative increased by 28-fold and 31-fold, respectively on binding to BSA. The short lifetimes and low quantum yields of fluorescence in water of these squaraines, increase significantly when bound to proteins. Also, their absorption maxima around 635 nm in water and 640 nm when bound to proteins allow excitation with diode lasers making these dyes highly suited for applications as reactive fluorescent labels in immunochemical assays and biophysical studies of proteins.

1.9. Non-linear Optical Properties

Non-linear optical (NLO) materials play an important role in modern technology, such as in imaging and information processing, telecommunication, integrated optics and optical computing.[70,71] The origin of the second-order optical nonlinearities in organic conjugated molecules is fairly well explained by distortion of π-electrons induced by electron donating (donor) and electron accepting (acceptor) groups. In most such molecules however, formation of centrosymmetric crystal structures is observed due to electrostatic interaction between adjacent molecules. One of the major problems to be addressed in these studies is the requirement of non-centrosymmetric alignment of molecules in crystals and thin films.

The large values reported for squaraines indicate that noncentrosymmetric crystals or film of these dyes should be capable of efficient second

harmonic generation (SHG). A new class of chiral D'-A-D squaraines, obtained by 1,2-substitution of squaric acid showed second harmonic generation intensities of upto 64 times that of urea in the powder form.[5,6] X-ray crystal analysis indicated that two hydrogen bonds between adjacent molecules and the chirality of the molecule contribute to one dimensional molecular alignment in spite of the strong dipole-dipole interactions and that the conjugated system of D'-A-D molecule extend from amino groups to cyclobutenedione ring to enhance the second harmonic nonlinearity of these crystals.

In a recent study Ashwell et al. have observed that centrosymmetric squaraine dyes incorporated into LB monolayers showed high second harmonic generation efficiencies.[7] It has been proposed that formation of non-centrosymmetric aggregates is responsible for these effects. Nonlinear optical studies have also shown that symmetric squaraines have quite large molecular second hyperpolarizabilities.[72-76]

1.10. Objectives of the Present Investigation

Though the photophysical and photochemical properties of squaraines have been investigated extensively, many aspects of squaraine photophysics have yet to be addressed. The design of squaraine fluoro- and chromoionophores is important with reference to their use in intracellular trace metal analysis. Additionally, aggregation of squaraine dyes can play an important role in many device applications such as in second harmonic generation and solar energy conversion. In order to explore these aspects, we have undertaken the synthesis and detailed photophysical studies of a few squaraine dyes. The main objectives of the present investigation are (i)

the design and study of squaraine based chromo- and fluoroionophores and (ii) study of the aggregation behaviour of squaraines in homogeneous and heterogeneous media.

1.11. References

1. Tam, A. C. *Appl. Phys. Lett.* **1980**, *37*, 978.
2. Morel, D. L.; Stogryn, E. L.; Ghosh, A. K.; Feng, T.; Purwin, P. E.; Shaw, R. F.; Fishman, C.; Bird, G. R.; Piechowski, A. P. *J. Phys. Chem.* **1984,** *88*,923.
3. Piechowski, A. P.; Bird, G. R.; Morel, D. L.; Stogryn, E. L. *J. Phys.Chem.* **1984**, *88*, 934.
4. Emmelius, M.; Pawlowski, G.; Vollmann, H. W. *Angew. Chem. Int. Ed. Engl.* **1989**, *28*, 1445.
5. Pu, L. S. In *Materials for Nonlinear Optics, Chemical Perspectives,* Marder, S. R.; Sohn, J. E.; Sluck, G. D. Eds.; ACS Symposium Series 455, American Chemical Society ,Washington DC, **1991**, p 331.
6. Pu, L. S. *J. Chem. Soc. Chem. Commun.* **1991**, 429.
7. Ashwell, G. J.; Jefferies, G.; Hamilton, D. G.; Lynch, D. E.; Roberts, M. P. S.; Bahra, G. S.; Brown, C. R. *Nature (London),* **1995**, *375*, 385.
8. Loutfy, R.O.; Hsiao, C. K.; Kazmaier, P. M. *Photogr. Sci. Eng.* **1983**, *27*,5.
9. Law, K.-Y.; Facci, J. S.; Bailey, F. C.; Yanus, J. F. *J.Imaging Sci.* **1990**, *34*, 31.
10. Treibs, A.; Jacob, K. *Angew. Chem. Int. Ed. Engl.* **1965**, *4*, 694.
11. Sprenger, H.-E.; Ziegenbein, W. *Angew. Chem. Int. Ed. Engl.* **1968**, *7*, 530.
12. Schmidt, A. H. *Synthesis*, **1980**, 961.
13. Seitz, G.; Imming, P. *Chem. Rev.* **1992**, *92*, 1227.

14. Law, K. Y. *Chem. Rev.* **1993**, *93*, 449.

15. Schmidt, A. H. In *Oxocarbons*, West, R. Ed.; Academic Press: New York, **1980**, Chapter 10.

16. Treibs, A; Jacob, K. *Justus Liebigs Ann. Chem.* **1966**, *699*, 153.

17. Ziegenbein, W.; Sprenger, H.-E. *Angew. Chem. Int. Ed. Engl.* **1966**, *5*, 893.

18. Sprenger, H.-E.; Ziegenbein, W.; *Angew. Chem. Int. Ed. Engl.* **1966**, *5*, 894.

19. Sprenger, H.-E.; Ziegenbein, W.; *Angew. Chem. Int. Ed. Engl.* **1967**, *6*, 553.

20. Law, K.-Y.; Bailey, F. C. *J. Chem. Soc. Chem. Commun.* **1990**, 863.

21. Law, K.-Y.; Bailey, F. C. *J. Chem. Soc. Chem. Commun.* **1991**, 1156.

22. Law, K.-Y.; Bailey, F. C. *J. Org. Chem.* **1992**, *57*, 3278.

23. Law, K.-Y.; Bailey, F. C. *Can. J. Chem.* **1993**, *71*,. 494.

24. Nakazumi, H.; Natsukawa, K.; Nakai, K.; Isagawa, K. *Angew Chem. Int. Ed. Engl.* **1994**, *33*, 1001.

25. Dirk, C. W. Herndon, W. C.; Cervantes-Lee, P.; Selnau, H.; Martinez, S.; Kalamegham, P.; Tan. A.; Campos, G.; Velez, M.; Zyss, J.; Ledoux, I.; Cheng, L-T. *J. Am. Chem. Soc.* **1995**, *117*, 2214.

26. Farnum, D. G.; Neuman, M. A.; Suggs, W. T.(Jr.) *J. Cryst. Mol.Struct.* **1974**, *4*, 199.

27. Kobayashi, Y.; Goto, M.; Kurahashi, M. *Bull. Chem. Soc. Jpn.* **1986**, *59*, 311.

28. Bernstein, J.; Goldstein, E. *Mol. Cryst. Liq. Cryst.* **1988**, *164*, 213.

29. Bigelow, R. W.; Freund, H.-J. *Chem. Phys.* **1986**, *107*, 159.

30. Law, K.-Y. *J. Phys. Chem.* **1987**, *91*, 5184.

31. Law, K.-Y. *J. Phys. Chem.* **1995**, *99*, 9818.

32. Law, K.-Y. *Chem. Phys. Lett.* **1992**, *200*, 121.

33. Law, K.-Y. *J. Photochem. Photobiol. A: Chem.* **1994**, *84*, 123.

34. Das, S.; Thomas, K. G.; Ramanathan, R.; George, M. V.; Kamat, P. V. *J. Phys. Chem.* **1993**, 97, 13625.

35. Chen, C-T.; Marder, S. R.; Cheng, L.-T.; *J. Chem. Soc. Chem. Commun.* **1994**, 259.

36. Kamat, P. V.; Das, S.; Thomas, K. G.; George, M. V. *J. Phys. Chem.* **1992,** *96,* 195.

37. Das, S.; Thomas, K. G.; George, M. V.; Kamat, P. V. *J. Chem. Soc. Faraday Trans.* **1992**, *88,* 3419.

38. Das, S.; Kamat, P. V.; De la Barre, B.; Thomas, K. G.; Ajayaghosh, A.; George, M. V. *J. Phys. Chem.* **1992**, *96*, 10327.

39. Buncel, E.; Mckerrow, A. J.; Kazmaier, P. M. *J. Chem. Soc. Chem. Commun.* **1992**, 1242.

40. Mckerrow, A. J.; Buncel, E.; Kazmaier, P. M. *Can. J. Chem.* **1995**, *73*, 1605.

41. Das, S.; Thanulingam, T. L.; Thomas, K. G.; Kamat, P. V.; George, M. V. *J. Phys. Chem.* **1993,** *97*, 13620.

42. Chen, H.; Farahat, M. S.; Law, K.-Y.; Whitten, D. G. *J. Am. Chem. Soc.* **1996**, *118*, 2584.

43. Chen, H.; Law, K.-Y.; Perlstein, J.; Whitten, D. G. *J. Am. Chem. Soc.* **1995**, *117*, 7257.

44. Chen, H.; Herkstroeter, W. G.; Perlstein, J.; Law, K.-Y.; Whitten, D. G. *J. Phys. Chem.* **1994**, *98*, 5138.

45. Liang, K.; Law, K.-Y.; Whitten, D. G. *J. Phys. Chem.* **1994**, *98*, 13379.

46. Law, K.-Y.; Chen, C. C. *J. Phys. Chem.* **1989**, *93*, 2533.

47. Chen, H.; Law, K.-Y.; Whitten, D. G., *J. Phys. Chem.* **1996**, *100*, 5949.

48. Law, K.-Y. *J. Phys. Chem.* **1988**, *92*, 4226.

49. Kim, Y.-S.; Liang, K.; Law, K.-Y.; Whitten, D. G.; *J. Phys. Chem.* **1994**, *98*, 984.

50. Das, S.; Thomas, K. G.; Kamat, P. V.; George, M. V. *Proc. Indian Acad. Sci. (Chem.Sci.),* **1993**, *105*, 513.

51. Kamat, P. V. ; Hotchandani, S.; de Lind, M.; Thomas, K. G.; Das, S.; George, M. V. *J. Chem. Soc. Faraday Trans.* **1993**, *89*, 2397.

52. Hotchandani, S.; Das, S.; Thomas, K. G.; George, M. V.; Kamat, P. V. *Res. Chem. Intermed.* **1994**, *20*, 927.

53. McRae, F. G.; Kasha, M. In *Physical Processes in Radiation Biology*, Augenstein, L.; Rosenberg, B.; Mason, S. F.; Eds.; Academic: New York, **1963**, p 23.

54. Kasha, M.; Rawls, H. R.; El Bayoumi, A. *Pure Appl. Chem.* **1965**, *11*, 371.

55. Das, S.; Thanulingam, T. L.; Thomas, K. G. (unpublished results).

56. Law, K. Y.; Bailey, F. C. *J. Imaging Sci.* **1987**, *31*, 172.

57. Nutting, G. C.; Harkin, W. D. *J. Am. Chem. Soc.* **1939**, *61*, 1182.

58. Kim, S.; Furuki, M.; Pu, L. S.; Nakahara, H.; Fukuda, K. *J. Chem. Soc. Chem. Commun.* **1987**, 1201.

59. Tanako, M.; Sekiguchi, T.; Matsumoto, M.; Nakamura, T.; Manda, E.; Kawabata, Y. *Thin Solid films* **1988**, *160*, 299.

60. Iwamoto, M.; Majima, Y.; Hirayama, F.; Furuki, M.; Pu, L. S. *Chem. Phys. Lett.* **1992**, *195*, 45.

61. Makio, S.; Kanamaru, N.; Tanaka, J. *Bull. Chem. Soc. Jpn.* **1980**, *53*, 3120.

62. Hada, H.; Hanawa, R.; Haraguchi, A.; Yonezawa, Y. *J. Phys. Chem.* **1985**, *89*, 560.

63. Kamat, P. V. ; Das, S.; Thomas, K. G.; George, M. V. *Chem. Phys. Lett.* **1991**, *178*, 75.

64. Lackowicz, J. R. *Laser Focus World*, **1992**, *28*, 60.

65. Terpetsching, E.; Lakowicz, J. R. *Dyes Pigm.* **1993**,*21*, 227.

66. Terpetschnig, E.; Szmacinski, H.; Lakowicz, J. R. *Anal. Chim. Acta*, **1993**, *282*, 633.

67. Terpetschnig, E.; Szmacinski, H.; Ozinskas, A.; Lakowicz, J. R.; *Anal. Biochem.* **1994**, *217*, 197.

68. Terpetschnig, E.; Szmacinski, H.; Lakowicz, J. R. *Proc. SPIE-Int. Soc. Opt. Eng.* **1994**, *2137*, 608.

69. Terpetschnig, E.; Szmacinski, H.; Lakowicz, J. R. *J. Flouoresc.* **1993**, *3*, 153.

70. Ulrich, D. R. In *Organic Materials for Non-Linear Optics*, Hann, R. A.; Bloor, D. Eds.; The Royal Society of Chemistry Proceedings, Special Publication No. 69, The Royal Society of Chemistry, London, 1989, p 241.

71. Prasad, P. N.; Williams, D. J. *Introduction to Nonlinear Optical Effects in Molecules and Polymers*, John Wiley and Sons, New York, 1991.

72. Scott, G. W.; Tran, K.; Funk, D. J.; Moore, D. S. *J. Mol. Struct.* **1995,** *348*, 425.

73. Dirck, C. W.; Kuzyk, M. G. *Chem. Mater.* **1990**, *2*, 4.

74. Kuzuk, M. G. Paek, U. C.; Dirk, C. W. *Appl. Phys. Lett.* **1991**, 59, 902.

75. Dirck, C. W.; Kuzyk, M. G. In *Materials for Nonlinear Optics: Chemical Perspectives*, Marder, S. R.; Sohen, J. E.; Stucky, G. D. Eds.; ACS Symp. Ser. No. 455, ACS Washington D. C., **1991**, p 687.

76. Dirk C. W.; Cheng, L.-T.; Kuzyk, M. G. *Int. J. Quantum Chem.* **1992**, *43*, 27.

CHAPTER 2

SYNTHESIS AND PHOTOPHYSICAL STUDIES OF CROWN ETHER SQUARAINES

2.1. Abstract

The synthesis and photophysical properties of three new red-sensitive highly fluorescent bis[4-(monoaza-crown-ether)phenyl]squaraine fluoroionophores **12-14** are reported. The dyes are soluble in both polar and nonpolar solvents with fluorescence quantum yields varying from 0.01 to 0.89. Complexation of the fluoroionophores with alkali metal ions brings about drastic reductions in their fluorescence quantum yields as well as significant changes in redox properties. These effects could be attributed to a cation induced reduction in the electron donating ability of the aza-crown-ether moiety of these dyes. Dyes **13** and **14** form aggregates in aqueous solutions which could be disrupted by the formation of a *1:1* complex between these dyes and β-cyclodextrin. This complexation is accompanied by a significant enhancement in the fluorescence yields of these dyes. Direct laser excitation of these dyes lead to the formation of excited triplets as well as dye radical cations and anions via a biphotonic photoionization process.

2.2. Introduction

Interest in the design of fluoro- and chromoionophores has increased significantly during recent years because of their potential as chemical sensors for metal and molecular cations as well as for neutral molecules.[1-4]

Chromoionophores generally comprise of two functionally different chemical groups; an ionophore, capable of recognizing specific ions, and a chromophore, capable of transducing the chemical information produced by the interaction of the ionophore and ion into an optical signal.

After the discovery of crown-ethers as a new generation of complexing agents, they have found many applications in analytical chemistry.[5] Chromoionophoric macrocycles are interesting primarily because of their utility in the identification and quantitative detection of metal cations.[6] For the design of chromo- and fluoroionophores for detection of metal ions the following aspects are of particular interest;[7] (i) fluorophores which respond with high sensitivity to local electronic disturbances by cations, (ii) connections between ionophore and fluorophore which allow the strongest electronic interactions with complexed cations and, (iii) the mechanism of interaction between the metal ions and the fluorophore or chromophore. The replacement of an amino substituent of the chromophore by aza-crown-ethers provides an effective method for designing new fluoro- and chromoionophores.[8] In such molecules the amino nitrogen of the crown-ether moiety plays the role of an electron-donor with respect to both complexed cation and the chromophore.[8] A majority of the donor-acceptor chromoionophores (**1-11**) reported in the literature meet this requirement.

When a group acting as an electron donor within the chromoionophore interacts with a cation, the latter reduces the electron donating character of this group, owing to the reduction of conjugation and a blue shift in the absorption and emission spectra of the molecule is observed.[8] On the contrary, a cation interacting with the acceptor moiety enhances the electron pulling capacity of the group and the absorption and emission

spectra undergo bathochromic shifts.[8] There are many reports on these kind of fluoro- and chromoionophores. It is well known that the fluorescence of anthracene and its derivatives are quenched by amines because of the electron transfer from the latter to the flourophore. Based on this observation many systems were developed in which anthracene was linked to aza-crown-ether ionophores (Chart 1). In these fluoroionophores the anthracene fluorescence, which is efficiently quenched by electron transfer from the lone pair of the nitrogen atom, recovers on complexation with metal cations, which suppresses the electron transfer.[8]

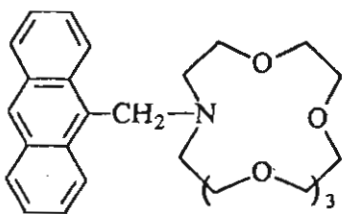

1

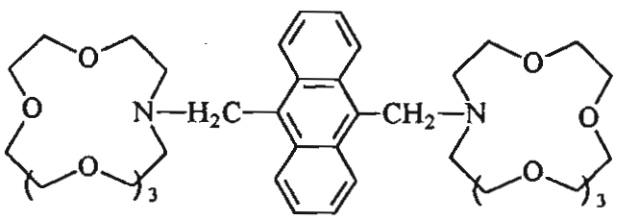

2

Chart 1

Valeur and co-workers have demonstrated that alkaline earth metal ions could be selectively detected using benzoxazinone dyes linked to crown-ether moieties such as **3** (BOZ-crown) (Chart 2).[9-11] The emission band of **3** undergoes remarkable shifts upon complexation with cations; the emission maximum shifts from 642 nm for the free ligand to 578 nm in the presence of 2×10^{-4} M calcium perchlorate. Besides, a significant enhancement of the fluorescence quantum yield was also observed. The quantum yield of fluorescence increases from 0.33 for the free ligand to

0.64 for the calcium complex. It was observed that alkali metal ions have only slight effect on the spectral features of **3**.

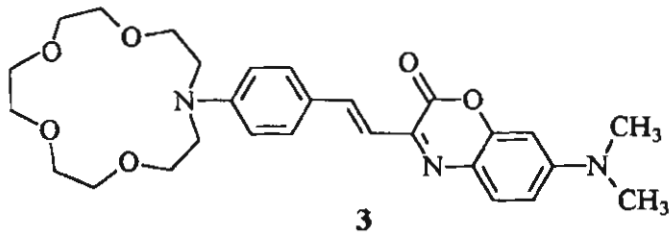

3 BOZ-crown

Chart 2

The fluoroionophore, **4** (Chart 3) obtained by the replacement of the dimethylamino group of the 4-dicyanomethylene-2-methyl-6-[p-(dimethyl-amino)styryl]-4H-pyran (DCM) by monoaza-15-crown-5-ether, was found to be highly sensitive to the presence of alkaline earth metals.[12] Intramolecular charge transfer is responsible for the fluorescence emission of DCM derivatives which in fact arises from a relaxed intramolecular charge transfer state, whereas the locally excited state is nonemissive. This charge transfer from the amino group to the dicyanomethylene group can be diminished if the electron-donating character of the donor moiety is reduced.

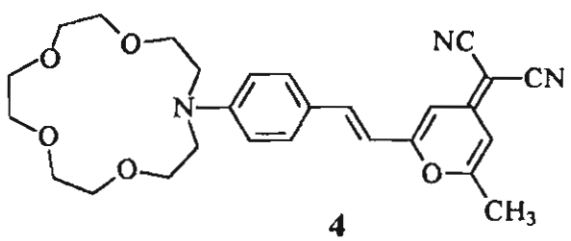

4 DCM-crown

Chart 3

On complexation with metal cations, the donor character of the nitrogen atom reduces depending upon the size and charge of the cation

used. The strongest effect was observed for Ca^{2+} which offers the best compromise regarding charge and size, with respect to the crown-ether moiety. Eventhough, Mg^{2+} possess a higher charge density, due to its small size the complex formed is not very stable and relatively high salt concentrations are required to bring about significant changes in the observed absorption and emission properties of the chromoionophore. Based on picosecond laser flash photolysis studies of DCM crown, they have suggested a temporary photoejection of the cation in less than 5 and 20 ps, takes place on excitation of the respective complexes of lithium and calcium.[13] They have attributed this phenomenon to photoinduced charge transfer from the nitrogen atom of the crown-ether to the dicyanomethylene group, so that the nitrogen atom of the crown-ether becomes positively polarized, and the resulting repulsion with the complexed cation causes photoejection. Based on these studies stability constants of the complexes in their excited states were estimated to be two orders of magnitude lower than those in the ground states.

Bourson et al. [14] have synthesized a series of coumarin dyes, covalently linked to crown-ether moieties such as **5-7** (Chart 4). These crown-ether coumarin derivatives undergo interesting photophysical changes upon cation binding. The changes in the absorption spectra are attributed to the direct interaction between the bound cation and the carbonyl group of the coumarin moiety. The electron withdrawing character of this group is reinforced by the cation, which leads to a bathochromic shift of the absorption spectrum with an increase in the extinction coefficient. The fluorescence spectra were also red shifted upon cation binding, but to a lesser extent than the absorption spectra. For the free ligand, the fluorescence is quenched statically due to the interaction between the carbonyl group and the

aza-crown-ether moiety. Upon complexation with metal ions these interactions disappear and an increase in the quantum yields is generally observed. However, complexation of Ca^{2+} and Mg^{2+} with **5**, for example leads to fluorescence quenching, indicating the presence of additional competitive routes for nonradiative decay which seem to be related to the charge density of the cation. The quantum yield of 7 is much lower than the quantum yield of other coumarin derivatives. Self quenching is indeed possible because the flexibility of the crown-ether allows the two coumarin moieties to come into close contact. It is interesting to note that upon complexation

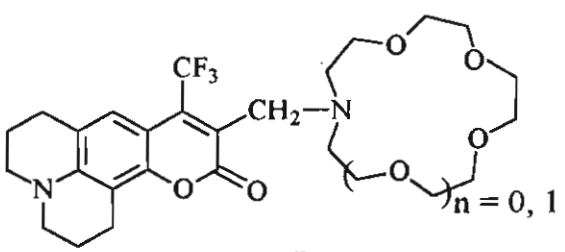

5, n = 1

6, n = 0

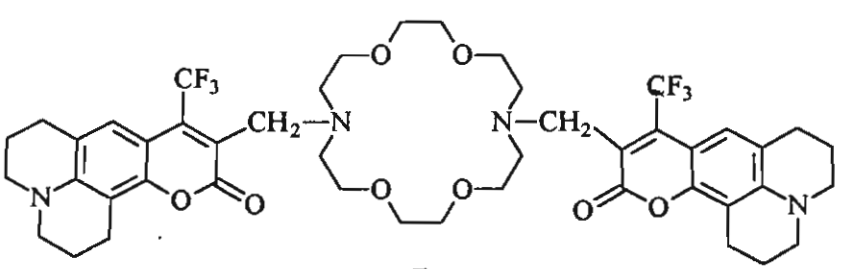

7

Chart 4

there is an increase in the quantum yield only with Ba^{2+} and K^+ ions and not with other cations. Ba^{2+} and K^+ are the cations that fit best into the crown-ether cavity. Therefore, it is anticipated that in the complexes of

these cations the carbonyl groups of the two coumarins are preferentially on opposite sides with respect to the cation and thereby self quenching is partially suppressed. However, for complexes of smaller cations, the preferred conformation may be such that the two carbonyls are in close proximity as in the free ligand, which may account for the static quenching.

The alkali and alkaline earth metal complexation properties of a series of 4-(N-monoaza-15-crown-5-ether)stilbene derivatives, **8-10** (Chart 5) were investigated by Letard et al. [15] These compounds exhibit generally drastic blue shift in their absorption spectra, upon cation binding. The alkaline earth metal cations were found to induce larger effects than the alkali

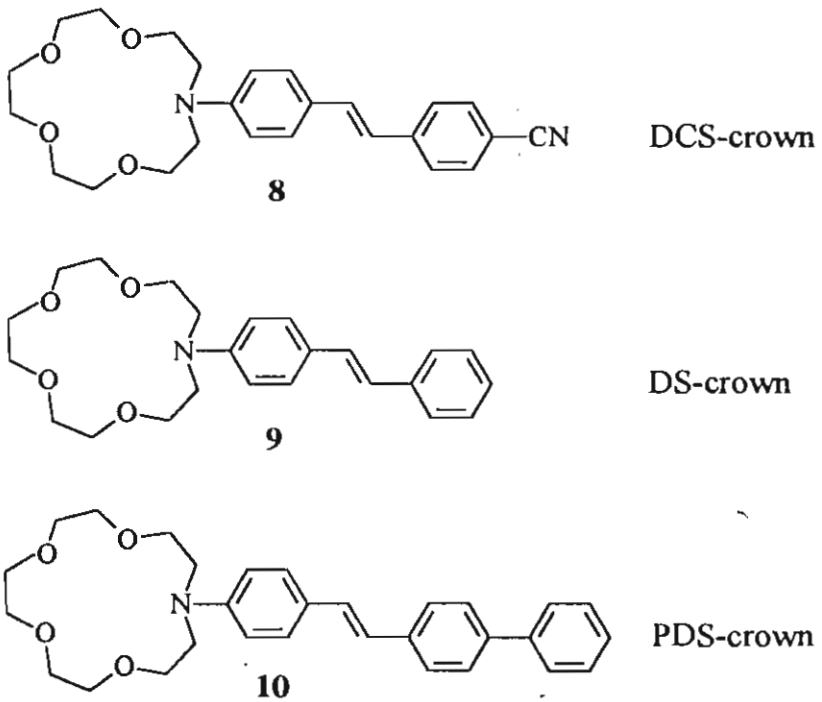

Chart 5

metal cations, as expected from the double charge of the former. They have observed a dual fluorescence for the PDS-crown complexed with Ca^{2+} in

n-BuCN. They ascribed this phenomenon to an equilibrium, in the excited state, between the cation complexed ligand and a species consisting of the cation-ligand separated by a solvent molecule brought about by the photoejection of the cation. They have suggested that the planar excited state of these donor-acceptor stilbenes can undergo single bond twist to a TICT (twisted intramolecular charge transfer) state which may be responsible for the emission.

The alkali metal ion complexation properties of 4-[4-(N-aza-15-crown-5-ether)styryl]-1-methylpyridinium iodide, **11** (Chart 6) was investigated.[16] Complexation of alkali metal ions (Li^+ and Na^+) induces suppression of its intramolecular charge transfer transitions, which lead to a blue shift in the absorption and emission spectra. The twisting of the excited state was hindered on complexation with cations, leading to an enhancement in the fluorescence quantum yield. It was observed that the chromoionophore, **11** shows more selectivity to Li^+ than Na^+, owing to the greater charge density of the former.

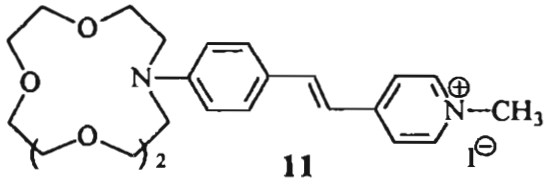

11

Chart 6

There are several reports on redox active ion responsive ligand systems, which are highly useful for biological applications.[17] Crown-ether linked ferrocenes, bipyridyls and ruthenium (II) bipyridyls are the noted examples of these classes of ligands. Cyclic voltammetric studies of a series

of ferrocene crown-ethers have shown positive shifts in the oxidation potentials, on complexation with lithium and sodium ions.[18] These anodic perturbations were attributed to the bound metal cation withdrawing charge from the ferrocene redox centre making it less easy to oxidize. Interestingly, it was observed that the magnitudes of anodic shifts increased with increasing charge/radius ratio of the guest cation.[17] The electrochemical properties of ferrocene crown-ether systems containing a saturated linkage between the crown-ether and redox-active centre were found to be totally insensitive to the presence of metal ions.[17] Significant amperometric selectivity for potassium ions were also obtained using certain ferrocene crown-ether derivatives.[17] Beer and co-workers have synthesized few crown-ether linked ruthenium (II) bipyridyl systems.[19-21] Although the electrochemical response of these systems with Na^+, K^+ and Mg^{2+} were not satisfactory, spectrochemical recognition capability were found to be good. It was observed that the MLCT emission maxima for the ruthenium (II) complexes were shifted significantly to lower wavelengths with increase in intensity in the presence of Li^+, Na^+ or Mg^{2+}.

Eventhough there are several reports on the design of chromo- and fluoroionophores for the selective recognition of biologically important cations such as Li^+, Na^+, K^+ and Ca^{2+},[6-16,22-28] the application of these systems are limited since the absorption and emission properties of most of the systems studied are in the UV and visible region of the spectrum. For biological applications it is desirable to synthesize water soluble flouro- or chromoionophores which absorb at longer wavelengths, preferably in the near infrared region[2] inorder to reduce overlap with tissue autofluorescence *and to avoid absorptions of the nucleic acids and amino acids.*[29] *Since the*

fluorescence signaling permits the monitoring of both excitation and emission wavelengths and are more sensitive to changes in the surrounding medium,[30] molecules which possess high quantum yield of fluorescence are more suited for the recognition of ions and molecules.

This Chapter of the thesis describes the synthesis as well as the photophysical studies of three new crown-ether squaraines, **12-14** (Chart 7). This includes the study of absorption and excited state properties in different solvents, aggregation behaviour as well as study of the alkali metal ion recognition ability using fluorescence quenching and electro-chemical techniques.

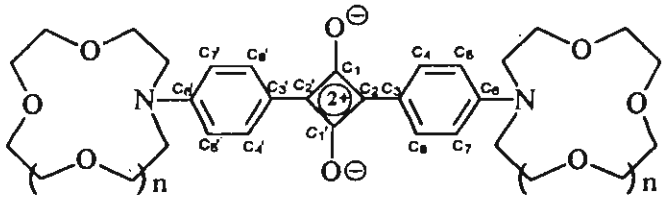

12, n = 1
13, n = 2
14, n = 3

Chart 7

2.3. Experimental Section

2.3.1. Materials and Methods

All melting points are uncorrected and were determined either on a Büchi melting point apparatus or on a Aldrich meltemp apparatus. All new compounds were fully characterized on the basis of analytical results and spectral data. IR spectra were recorded on a Perkin Elmer Model 882 IR

spectrometer and the UV-visible spectra on a Shimadzu 2100 spectrometer. ^{1}H and ^{13}C NMR spectra were recorded on a JEOL EX 90 spectrometer. ^{13}C NMR (22.5 MHz) resonances were assigned using QUAT and DEPT programs to determine the number of hydrogen attachments. Mass spectra were recorded on a Finnigan MAT Model 8340 or JEOL JMS AX 505 HA mass spectrometer. Quantum yields of fluorescence were measured by the relative method using optically dilute solutions with bis[4-(dimethylamino)-2-hydroxyphenyl]squaraine (Φ_f = 0.84) in dichloromethane[31] as reference. Corrections have been made in fluorescence quantum yield measurements for the changes in the absorbance at the excitation wavelength. Spectroscopic solvents were used throughout. For metal binding studies, anhydrous metal perchlorates and dried solvents were used.

2.3.2. Laser Flash Photolysis[32]

Picosecond laser flash photolysis experiments were performed with 532-nm laser pulses from a mode-locked, Q-switched Quantel YG-501 DP Nd: YAG laser system (output 2-3 mJ/pulse, pulse width ~18 ps). The white continuum picosecond probe pulse was generated by passing the fundamental output through a D_2O/ H_2O solution. The excitation and the probe pulse were incident on the sample cell at right angles. The output was fed to a spectrograph (HR-320, ISDA Instruments, Inc.) with fiber optic cables and was analyzed with a dual diode array detector (Princeton Instruments, Inc.) interfaced with an IBM-AT computer. Time zero in these experiments corresponds to the end of the excitation pulse. All the lifetimes, rate constants and equilibrium constants reported in this study are within an experimental error of ± 5%.

Direct excitation of the squaraine dye solution was carried out using the second harmonic of a Quanta-Ray CDR-1 Nd:YAG pulsed laser (532-nm, 6 ns pulse width, 10-50 mJ/pulse). The third harmonic of the same laser (355-nm, 10 mJ/pulse) was used for triplet-triplet (T-T) sensitization and electron transfer reactions of squaraine triplets with triphenylamine. For the T-T energy transfer studies the Molectron UV-400 nitrogen laser system (337.1-nm, 8 ns pulse, 1 mJ/pulse) was also used.

2.3.3. Synthesis of 12-14

N-Phenylmonoaza-12-crown-4-ether[33], N-phenyl-monoaza-15-crown-5-ether[34] and N-phenyl-monoaza-18-crown-6-ether[34] were synthesized, adopting methods similar to reported procedures. Crown-ether bearing squaraine dyes were synthesized by refluxing the corresponding N-phenyl-monoaza-crown-ether (0.3 mmol) and squaric acid (0.15 mmol) in a solvent mixture containing 3 mL of benzene and 5 mL of 1-butanol, accompanied by azeotropic distillation of water. Recrystallization from a mixture (3:1) of chloroform and *n*-hexane gave a 44% yield of bis[4-(monoaza-12-crown-4-ether)phenyl]squaraine, **12**, mp 225 °C (decomp.) and a 27% yield of bis[4-monoaza-15-crown-5-ether)phenyl]squaraine, **13**, mp 215 °C (decomp.), while recrystallization from a mixture (1:3) of chloroform and benzene gave a 36% yield of bis[4-(monoaza-18-crown-6-ether)phenyl]squaraine, **14**, mp 176 °C.

Analytical results and spectral data of fluoroionophores **12-14** are summarized below.

12: (44%) mp 225 °C (decomp); IR ν_{max} (KBr) 1586 cm^{-1}; UV λ_{max} ($CHCl_3$) 634 nm (ε 3,00,000 M^{-1} cm^{-1}); ^1H NMR ($CDCl_3$, TMS) δ 3.6-4.0 (32 H, m,

CH_2), 6.85 (4 H, d, aromatic), 8.4 (4 H, d, aromatic); ^{13}C NMR ($CDCl_3$) δ 189.00 (C), 183.32 (C), 154.57 (C), 133.08 (CH), 120.29 (C), 113.31 (CH), 71.41 (CH_2), 69.87 (CH_2), 69.21 (CH_2), 52.94 (CH_2); HRMS, exact mol wt calcd for $C_{32}H_{41}O_8N_2$ (MH^+), 581.2863; found, 581.2862 (FAB high resolution mass spectroscopy).

13: (27%) mp 215 °C (decomp); IR ν_{max} (KBr) 1595 cm^{-1}; UV λ_{max} ($CHCl_3$) 632 nm (ε 2,70,000 M^{-1} cm^{-1}); ^1H NMR ($CDCl_3$, TMS) δ 3.6-4.0 (40 H, m, CH_2), 6.8 (4 H, d, aromatic), 8.4 (4 H, d, aromatic); ^{13}C NMR ($CDCl_3$) δ 188.64 (C), 182.97 (C), 153.56 (C), 133.00 (CH), 119.90 (C), 112.59 (CH), 71.00 (CH_2), 70.23 (CH_2), 69.81 (CH_2), 68.08 (CH_2) 53.13 (CH_2); HRMS, exact mol wt calcd for $C_{36}H_{49}O_{10}N_2$ (MH^+) 669.3387; found 669.3372 (FAB high resolution mass spectroscopy).

14: (36%) mp 176 °C; IR ν_{max} (KBr) 1615 cm^{-1}; UV λ_{max} ($CHCl_3$) 634 nm (ε 2,80,000 M^{-1} cm^{-1}); ^1H NMR ($CDCl_3$) δ 3.6-3.9 (48 H, m, CH_2), 6.8 (4 H, d, aromatic), 8.35 (4 H, d, aromatic); ^{13}C NMR ($CDCl_3$) δ 188.58 (C) 183.27 (C), 153.89 (C), 133.18 (CH), 128.05 (C), 112.59 (CH), 70.88 (CH_2), 70.79 (CH_2), 70.65 (CH_2), 68.44 (CH_2), 51.70 (CH_2); HRMS exact mol wt calcd for $C_{40}H_{57}O_{12}N_2$ (MH^+), 757.3912; found 757.3916 (FAB high resolution mass spectroscopy).

2.4. Results and Discussion

2. 4. 1. NMR studies of 12-14

The ^1H NMR spectrum of **13** in $CDCl_3$ is shown in Figure 2.1. The CH_2 protons of the crown-ether moieties appear together as a multiplet at

3.6-4.0 ppm. The aromatic protons appear as two sets of doublets at 6.8 and 8.4 ppm. Similar ^{1}H NMR spectra were obtained for **12** and **14** also.

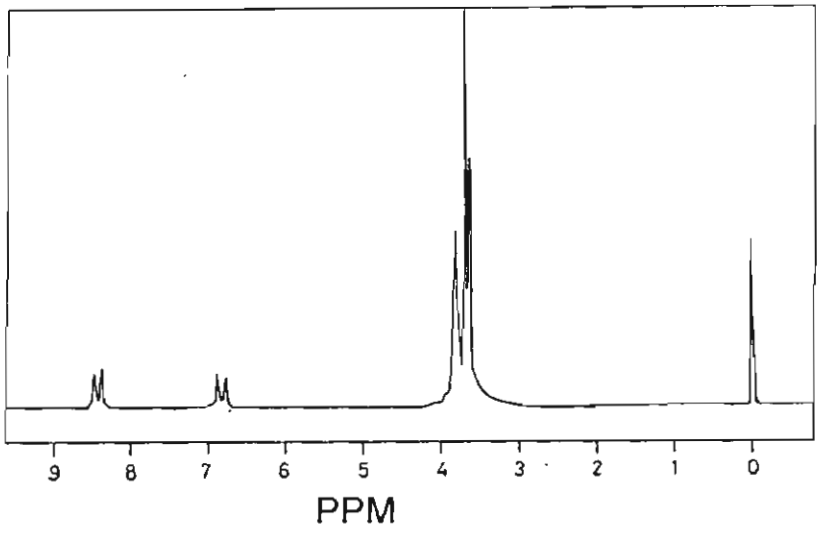

Figure 2.1. ^{1}H NMR spectrum of **13** in $CDCl_3$

The high solubility of these newly synthesized squaraine dyes in $CDCl_3$ facilitated the recording of their ^{13}C NMR specra (solubility of **13** in $CDCl_3$ is greater than 1.5 M). The ^{13}C NMR spectrum of **13** in $CDCl_3$ (Figure 2.2), for example, showed two tertiary carbon signals, four quarternary carbon signals and five secondary carbon signals. The two tertiary carbon peaks observed at 133.00 ppm and 112.59 ppm have been assigned to the two sets of identical carbon atoms at C_4, C_8, C_4', C_8' and C_5, C_7, C_5', C_7' positions (Chart 7). The quarternary carbon signals at 153.56 ppm and 119.90 ppm were attributed to the two sets of identical carbon atoms situated at the C_3, C_3' and C_6, C_6', positions and the quarternary carbon signals

at 188.64 ppm and 182.97 ppm could be attributed to the two sets of identical carbon atoms at the C_1, C_1' and C_2, C_2' positions of the central cyclobutane ring. In the case of **13** and **14**, the secondary carbons of the crown-ether moiety appear as five peaks, whereas for **12** they appear as four peaks. All the other spectral features of **12** and **14** are similar to those of **13**.

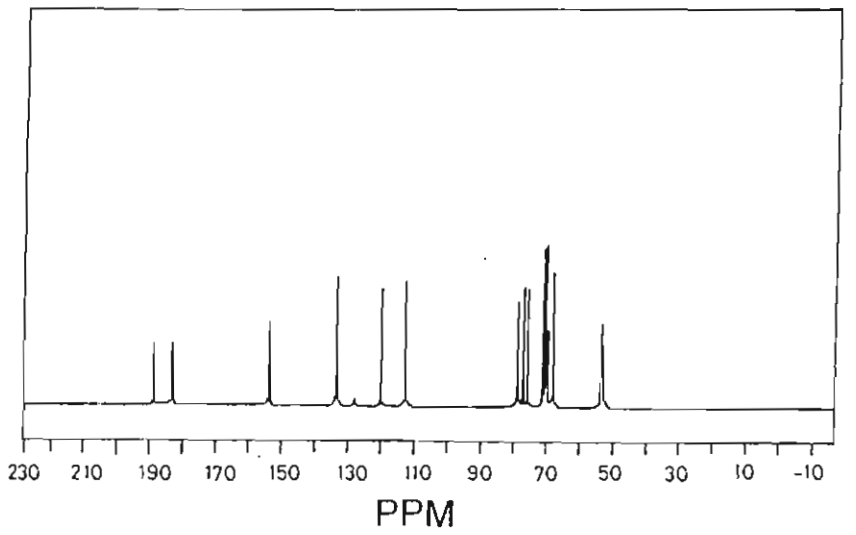

Figure 2.2. ^{13}C NMR spectrum of **13** in $CDCl_3$

The spectral features of **12-14** indicate that the two halves of the molecules are identical, indicating the highly symmetric donor-acceptor-donor nature of these molecules.

2.4.2. Absorption and Excited State Properties

The photophysical properties of **12-14** have been studied in solvents of varying polarities and the results are summarized in Table 2.1. MNDO and CNDO calculations have shown that the singlet-singlet excitation of bis[4-(dimethylamino)phenyl]squaraine and its derivatives arise from the

Table 1: Absorption and emission characteristics of bis[4-(monoaza-crown-ether)phenyl]squaraines 12-14 in different solvents

Solvents	12			13			14		
	λ_{max} Abs	λ_{max} Em	Φ_f	λ_{max} Abs	λ_{max} Em	Φ_f	λ_{max} Abs	λ_{max} Em	Φ_f
Benzene	635	652	0.84	633	652	0.89	635	654	0.78
Chloroform	634	655	0.74	632	652	0.83	634	656	0.76
Dichloromethane	636	660	0.48	634	657	0.50	636	660	0.43
Acetonitrile	637	662	0.11	634	659	0.14	636	661	0.13
Trifluoroethanol	634	661	0.06	631	657	0.07	629	655	0.07
t-butanol	-	-	-	-	-	-	635	658	0.55
iso-propanol	638	662	0.23	636	660	0.34	638	663	0.28
Ethanol	640	664	0.14	638	662	0.18	640	666	0.17
Methanol	-	-	-	638	661	-	-	-	-
Methoxyethanol	646	672	0.15	643	670	0.20	646	672	0.19
Water	-	-	-	640	667	0.015	644	667	0.015
Water + 2.7 mM β-CD	-	-	-	645	664	0.20	647	663	0.14

charge transfer transitions involving the central cyclobutane ring and the oxygen atoms with a minor contribution from the amino moieties.[35] The slight red-shift in the absorption spectra of crown-ether derivatives of squaraines in comparison to that of bis[4-(dimethylamino)phenyl]squaraine could be attributed to the electron rich crown-ether moieties on the two nitrogen atoms. Similar effects were earlier reported for squaraines with long alkyl chain substitution on the N atoms.[36]

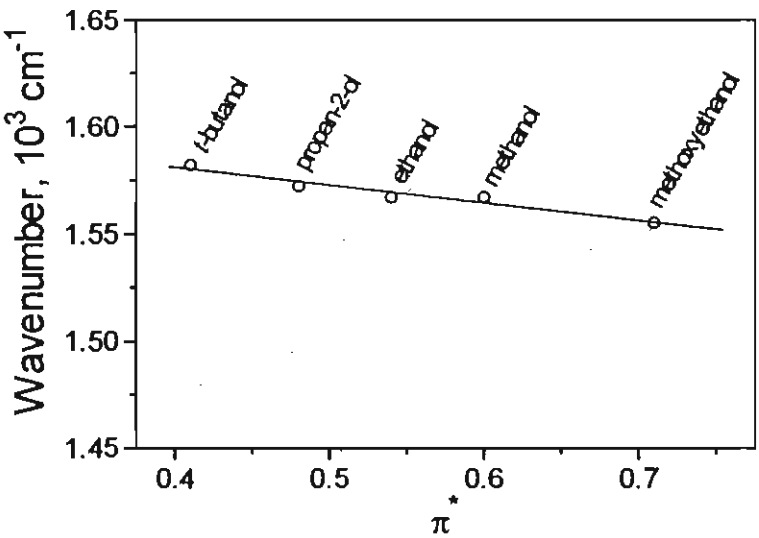

Figure 2.3. Plot of absorption maxima of **13** in wavenumbers versus the solvent Taft parameter, π^* in protic solvents.

In protic solvents the absorption and emission spectra are more or less independent of the nature of the solvent. However, in protic solvents they depend largely on the hydrogen bonding ability of the solvent. For example in a strongly hydrogen bonding solvent such as trifluoroethanol the absorption maximum was at 629 nm for **14** whereas it was considerably red shifted to 646 nm in a weakly hydrogen bonding solvent such as

methoxyethanol. In the case of protic solvents, the plot of absorption maxima in wavenumbers versus solvent Taft parameter, π^* (Figure 2.3) showed a linear dependence for all these dyes. The observed hypsochromic shift in absorption maxima can be attributed to the formation of specific hydrogen-bonded solute solvent complexes. Similar solvent hydrogen bonding effects were earlier observed for bis(benzothiazolylidene)squaraines.[37]

Solvent polarity has a drastic effect on the fluorescence quantum yields (Φ_f) and singlet excited state life times (τ_s) of these dyes (Tables 2.1 and 2.2). In a relatively nonpolar solvent such as benzene ($\pi^* = 0.59$), the quantum yield of fluorescence of **13** was very high ($\Phi_f = 0.89$) whereas in a polar solvent such as acetonitrile ($\pi^* = 0.75$), it was very low ($\Phi_f = 0.14$). The singlet excited state spectra and fluorescence lifetimes were determined using picosecond laser flash photolysis with 532-nm laser

Table 2.2. Singlet excited state characteristics of 12-14

Solvent	λ_{max} (S_1-S_n), nm[a]			Lifetime (τ_s), ns[b]		
	12	**13**	**14**	**12**	**13**	**14**
Benzene	495	495	495	2.36	2.13	2.50
Chloroform	480	480	480	1.25	1.20	1.45
Water	-	465	468	-	0.07	0.11
Water + β-CD[c]	-	480	480	-	0.90	0.94

[a] Difference absorption maximum of the excited singlet state.
[b] Measured from the decay of the transient absorption at the λ_{max}.
[c] 2.7 mM.

pulse as the source of excitation. Figure 2.4 shows the time resolved transient absorption spectra of the singlet excited state of **14** in benzene. Singlet excited state shows absorption maximum around 495 nm, whose decay closely matches with the recovery of the ground state at 635 nm.

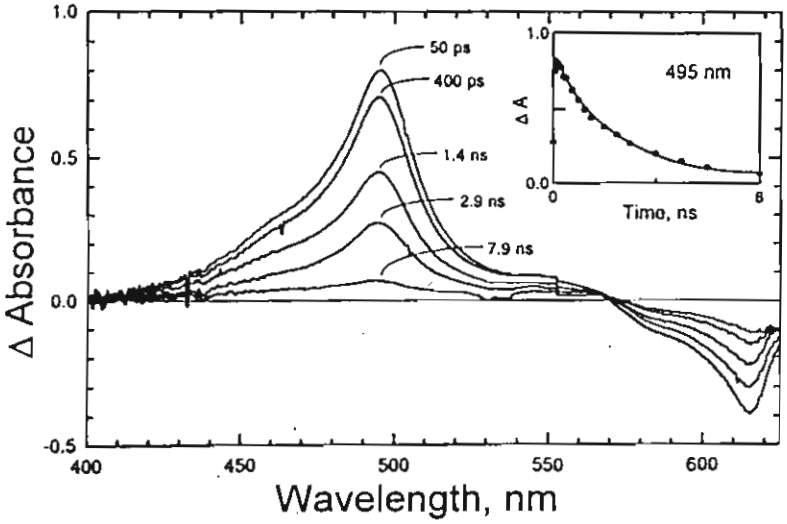

Figure 2.4. Time-resolved transient absorption spectra recorded following 532-nm laser pulse (pulse width 18 ps) excitation of **14** in benzene. Inset shows the decay profile of the singlet excited state as monitored from its absorbance at 495 nm.

The transient profiles were fitted to first order kinetics and the life-times thus obtained are given in Table 2.2. The fluorescence lifetimes of these dyes varied from 70 ps in water to 2.5 ns in benzene indicating its direct dependence on the nature of the solvent. Picosecond studies have revealed the absence of long lived transients which could arise due to the triplet states. These results are in agreement with the earlier reports that the intersystem crossing efficiency of squaraine dyes are very low.[31,38,39]

The decrease in singlet excited-state lifetimes and fluorescence quantum yields with increasing solvent polarity could be attributed to specific complex formation between the dye and solvent molecules as reported earlier.[36,37] The values of radiative and nonradiative decay rate constants listed in Table 2.2 indicates the influence of such solute-solvent complexation on the deactivation pathways of the excited singlet state.

When solutions of these dyes were made in water from stock acetonitrile solutions, a rapid decrease in the absorbance was observed until they reached a stable value and this was accompanied by a broadening of the absorption band. Since the solubilities of these dyes in water are low,

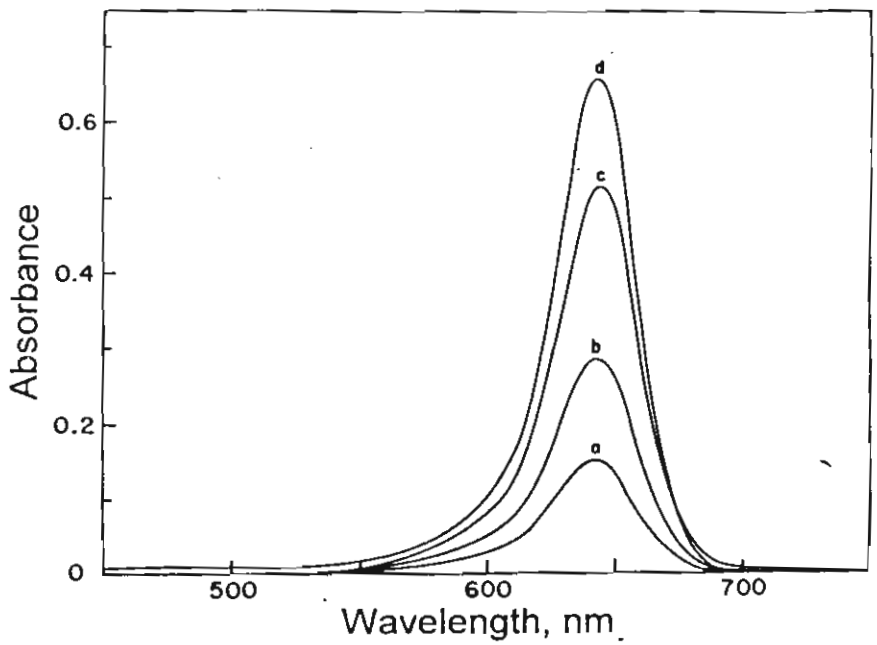

Figure 2.5. Effect of addition of acetonitrile on the absorption spectra of an aqueous solution of **14** (1.7 μM). Acetonitrile v/v (a) 0%, (b) 5%, (c) 20% and (d) 40%.

these changes in absorption spectra with time could be attributed to formation of aggregated species. Addition of acetonitrile leads to the recovery of the original absorption band (Figure 2.5). Since the dyes are expected to be better solvated in acetonitrile this effect may be attributed to a break-up of the aggregate form of the dye to its monomer form.

Since the photoconducting properties of squaraine dyes arise from intermolecular interactions, the understanding of those forces involved in the aggregation process is important. There have been few studies on the formation of squaraine dye aggregates in solution as well as in the solid state.[40-49] It was reported that both bis(2,4-dihydroxyphenyl)squaraine and bis(2,4,6-trihydroxyphenyl)squaraine form head-to-tail (J-type) aggregates in dry acetonitrile solutions.[41] However, in the present case the exact nature of the dye aggregate could not be ascertained. The intermolecular charge-transfer interactions between the donor (amino) and acceptor (cyclobutane ring) as proposed earlier for the formation of aggregates of bis(alkylamino-phenyl)squaraines in DMSO/water solutions[40] and Langmuir-Blodgett films[42] could lead to the formation of the aggregates of the crown-ether squaraines in the present case.

2.4.3. Interaction with β-cyclodextrin

In polar solvents the nonradiative decay is the predominant pathway of deactivation of the singlet excited state of the squaraine dyes **12-14**. In water the fluorescence quantum yield of the crown-ether derivatives of squaraines (**13** and **14**) were found to be very low (Φ_f = 0.015 for **14**). However, the emission properties can be significantly improved by encapsulating the dye in a hydrophobic environment. Addition of low concentrations of β-cyclodextrin (β-CD) (< 3 mM) to aqueous solutions of **13** and **14**

brings about a drastic enhancement in the intensity of their absorption bands, indicating that complexation of the dye with β-CD also leads to a breaking up of the aggregates. This was accompanied by a significant enhancement in the fluorescence quantum yield (Figure 2.6). The enhancement in fluorescence yields cannot be attributed to a simple breaking up of the aggregate, since addition of acetonitrile, which also leads to a break up of the aggregate does not lead to any significant change in the emission properties. The fluorescence quantum yield, Φ_f was 0.02 in water and 0.03 in 40% acetonitrile-water mixture and this very minor effect may be attributed to the changes in the solvent polarity brought about by the addition of acetonitrile. The enhancement of fluorescence yield on addition of β-CD can therefore be attributed to specific complex formation between the dye

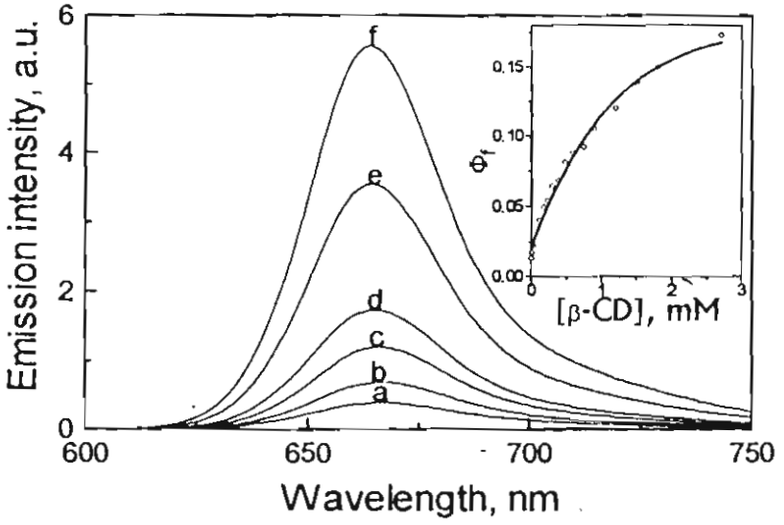

Figure 2.6. Influence of β-cyclodextrin [β-CD] on the emission spectrum of **13** (5.1 μM) in aqueous solutions. [β-CD] (a) 0, (b) 0.06, (c) 0.18, (d) 0.39, (e) 1.2 and (f) 2.7 mM. Inset shows the plot of quantum yield of fluorescence of **13** versus [β-CD] in aqueous solutions.

and β-CD. Similar interaction with β-CD has also been observed for other squaraine dyes.[46,50] The formation of dye-β-CD complexes which would lead to the break-up of the aggregate could be described by Equation 1,

$$M_2 \underset{+M}{\overset{-M}{\rightleftharpoons}} 2M \underset{-\beta\text{-CD}}{\overset{+\beta\text{-CD}}{\rightleftharpoons}} 2[M\cdots\cdots\beta\text{-CD}] \qquad (1)$$

where, M_2 = aggregate and M = monomer.

The fluorescence enhancement of **13** and **14** could be analyzed by the Benesi-Hildebrand equation for a 1:1 complex formation between monomer and β-cyclodextrin (Equation 2),

$$\frac{1}{\Phi_f^0 - \Phi_f} = \frac{1}{\Phi_f^0 - \Phi_f'} + \frac{1}{K_s(\Phi_f^0 - \Phi_f')\,[\beta\text{-CD}]} \qquad (2)$$

where, K_s is the equilibrium constant, Φ_f is the fluorescence quantum yield of the monomer, Φ_f' is the quantum yield of fluorescence of the dye-β-CD

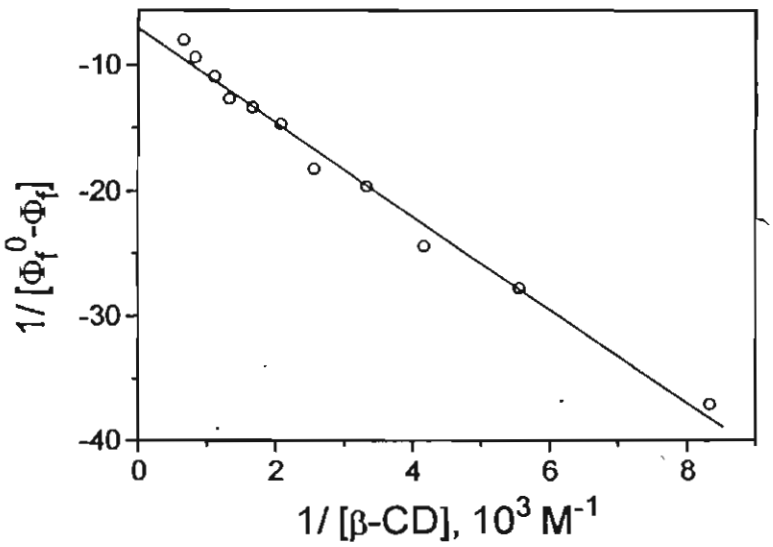

Figure 2.7. Plot of $1/(\Phi_f^0-\Phi_f)$ versus reciprocal of β-CD concentration for the fluorescence enhancement of **13** upon addition of β-CD.

complex and Φ_f, the observed quantum yield of fluorescence. The dependence of $1/(\Phi_f^0 - \Phi_f)$ on the reciprocal concentration of β-CD, was found to be linear, indicating a 1:1 complex formation between the dye and β-CD (Figure 2.7). The values for the equilibrium constant K_s and fluorescence quantum yield of the dye-β-CD complex, Φ_f' determined from the slope and intercept of these plots were 1100 M^{-1} and 0.24 for **13** and 1750 M^{-1} and 0.16 for **14**, respectively.

Picosecond laser flash photolysis studies on the dye-β-CD complexes (of **13** and **14**) showed that the absorption spectra of the excited singlet states were very similar to those for the uncomplexed dyes (Figure 2.8). However, the excited singlet state lifetime was much longer for the complex

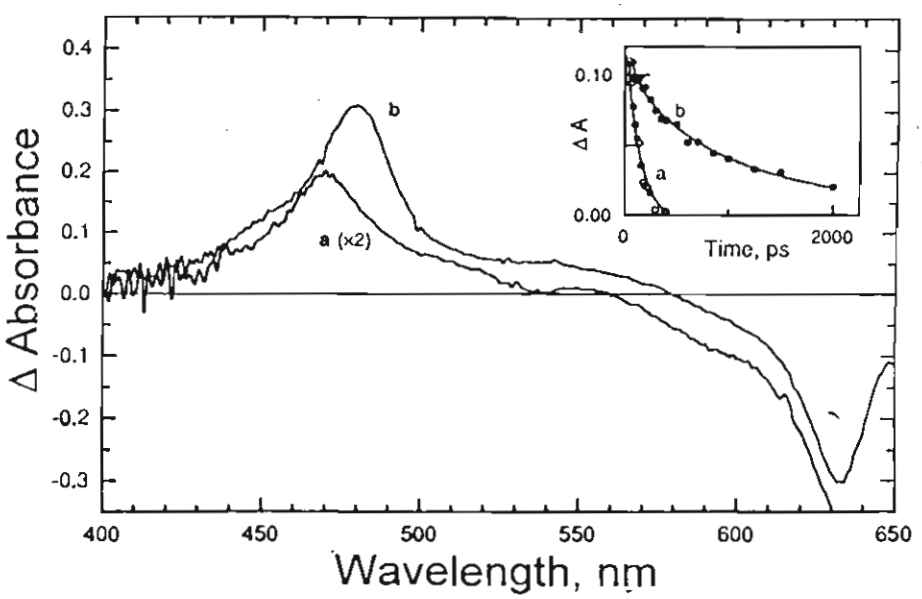

Figure 2.8. Transient absorption spectra of excited singlet of **14** in aqueous solution containing (a) 0 mM β-CD and (b) 3 mM β-CD (excitation 532-nm, Δ_t = 0 ps). Inset shows the decay of the transient absorption at 465 nm.

than for the free dye. Similar observations were made for **13** also. These results are summarized in Table 2.2. The nearly ten-fold enhancement in singlet excited state lifetime observed in the solutions containing β-CD, parallels the increase in fluorescence yield observed for these dyes, indicating suppression of the non-radiative internal conversion modes of the excited singlet state. For the dye **13**, the non-radative decay rate constant (k_{nr}) value decreased from 1.4 x 10^{10} to 8.9 x 10^{8} s^{-1}, and for **14** it decreased from 8.95 x 10^{9} to 9.16 x 10^{8} s^{-1} in β–CD solutions. The two major modes of non-radiative decay for dimethylaminophenylsquaraines and its derivatives have been proposed to be via rotation of the adjacent phenyl groups and hydrogen bonding with the solvent molecules.[50] Both these processes will be restricted to a certain extent on microencapsulation of the dye molecules by β-CD. These studies indicate that although the crown-ether squaraine dyes are relatively non fluorescent in aqueous media, hydrophobic interactions would lead to substantial enhancement of their fluorescence quantum yield.

2.4.4. Alkali Metal Ion Recognition using 12 and 13

The alkali metal ion binding abilities of crown-ether squaraine dyes were investigated using absorption and emission spectroscopy. These studies were carried out in 70% (v/v) toluene-30% (v/v) acetonitrile mixture. Under these conditions the fluorescent quantum yield of the dyes are high. It was observed that complexation of alkali metal cations induces significant changes in the photophysical properties of fluoroionophores **12** and **13** whereas, the photophysical properties of **14** was almost unaffected by the presence of Na^{+} or Li^{+}.

Fluoroionophore **12** has an absorption maximum at 639 nm and an emission maximum at 661 nm (Φ_f = 0.51) in 30% (v/v) acetonitrile-toluene mixture. The photophysical properties of **12** are highly sensitive to the presence of alkali metal ions such as Na^+ and Li^+. Although the alteration in the shape of the absorption and emission spectra are small, the quantum yield of fluorescence was drastically quenched by these metal ions. The quenching of fluorescence of **12** on addition of lithium perchlorate as well as sodium perchlorate is shown in Figure 2.9. Even at low concentrations of lithium perchlorate (1 mM), a substantial quenching of fluorescence (8%) was observed. An isobestic point and a gradual red shift in

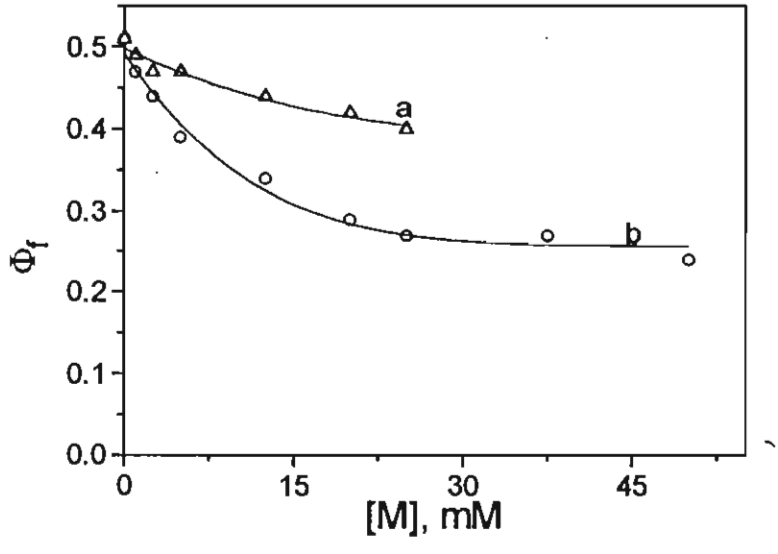

Figure 2.9. Plot of quantum yield of fluorescence (Φ_f) of **12** (3.0 μM) versus metal ion concentration in 30% (v/v) acetonitrile-toluene mixture. (a) $NaClO_4$; (b) $LiClO_4$.

absorption maximum were observed upon further addition of lithium perchlorate. Concurrently, there was a shift in emission maximum and a

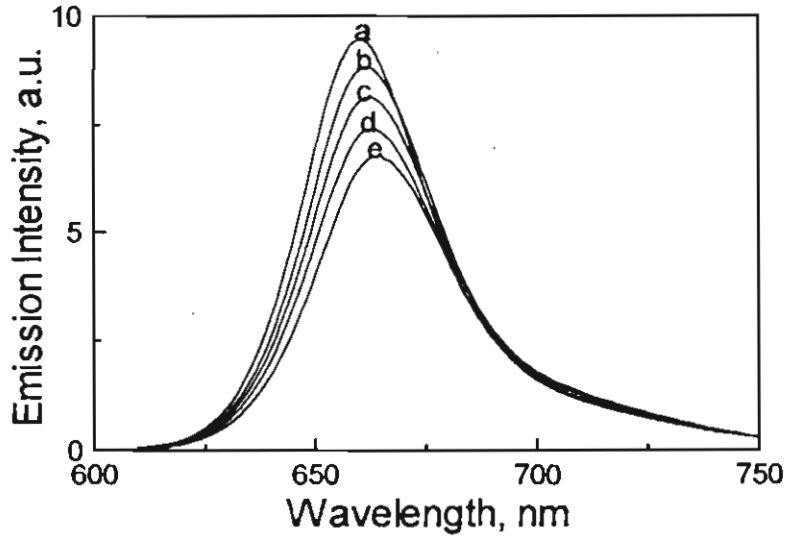

Figure 2.10. Influence of $LiClO_4$ concentrations on the emission spectrum of **12** (3.0 μM) in 30% (v/v) acetonitrile-toluene mixture. [$LiClO_4$] (a) 0, (b) 1.88, (c) 3.75, (d) 6.25 and (e) 12.5 mM

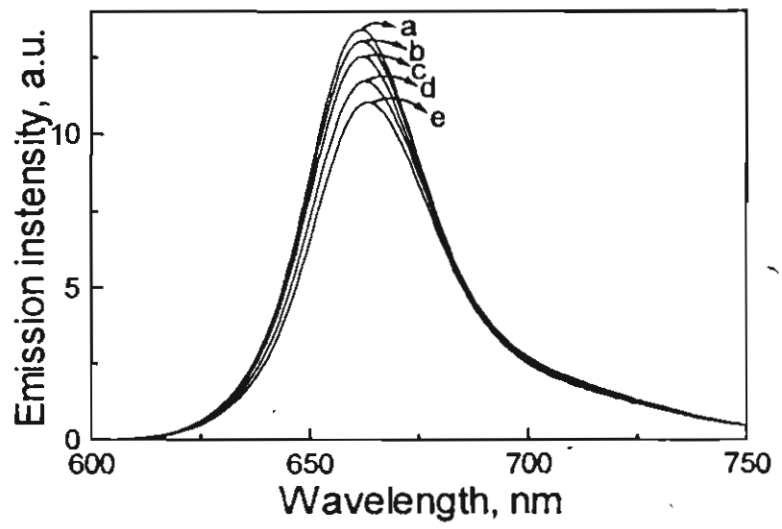

Figure 2.11. Influence of $NaClO_4$ concentrations on the emission spectrum of **12** (3.0 μM) in 30% (v/v) acetonitrile-toluene mixture. [$NaClO_4$] (a) 0, (b) 2.5, (c) 5.0, (d) 12.5 and (e) 25 mM.

significant quenching of fluorescence (38%) upon addition of 20 mM of lithium perchlorate (Figure 2.10, Table 2.3). In the case of sodium perchlorate, the absorption and emission maxima remain unchanged, while 4% quenching of fluorescence was observed on addition of 1 mM of sodium perchlorate and 18% quenching of fluorescence was observed on addition of 20 mM of sodium perchlorate (Figure 2.11, Tables 2.4). These results indicate that the fluoroionophore **12** is more sensitive to Li^+, especially at low concentrations. The ligand to metal stoichiometry and stability constant

Table 2.3. Effect of $LiClO_4$ on the photophysical properties of squaraine fluoroionophores 12, 13 and model compound 15 in 30% (v/v) acetonitrile-toluene mixtures

$[LiClO_4]$	**12**		**13**		**15**[a]	
	0 mM	1 mM	0 mM	1 mM	0 mM	1mM
λ_{max} (Abs)	639	640	637	637	644	644
λ_{max} (Em)	661	661	657	657	662	662
Φ_f	0.51	0.47	0.51	0.36	0.67	0.66
% quenching		8		29		1

[a] Reference compound (Chart 8)

for **12** on complexation with metal cations have been investigated using Equation 3,

$$\frac{1}{\Phi_f^0 - \Phi_f} = \frac{1}{\Phi_f^0 - \Phi_f'}\left[\frac{1}{K_S[M]} + 1\right] \quad (3)$$

Table 2.4: Effect of $NaClO_4$ on the photophysical properties of squaraine fluoroionophores 12, 13 and model compound 15 in 30% (v/v) acetonitrile-toluene mixtures

$[NaClO_4]$	12		13		15[a]	
	0 mM	1 mM	0 mM	1 mM	0 mM	1mM
λ_{max} (Abs)	639	639	637	637	644	644
λ_{max} (Em)	661	661	657	657	662	662
Φ_f	0.51	0.49	0.51	0.41	0.67	0.67
% quenching		4		20		0

[a] Reference compound (Chart 8)

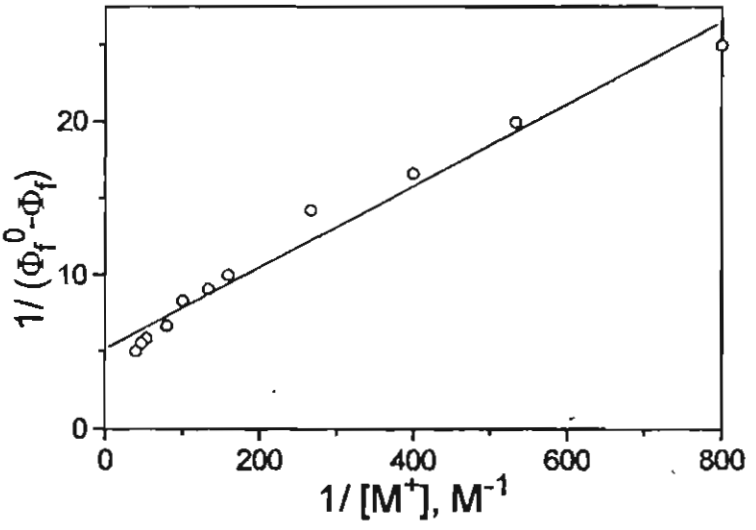

Figure 2.12. Plot of $1/(\Phi_f^0-\Phi_f)$ versus reciprocal of lithium ion concentration for the fluorescence quenching of **12** in presence of $LiClO_4$.

where, K_s is the stability constant, Φ_f^0, the quantum yield of fluorescence of free ligand, Φ_f' the quantum yield of fluorescence of complexed ligand, Φ_f the observed quantum yield of fluorescence and [M] is the concentration of metal perchlorate. Plot of $1/(\Phi_f^0 - \Phi_f)$ against the reciprocal of lithium ion concentration showed a linear dependence in the concentration range of 0-10 mM, indicating a 1:1 metal to ligand complexation for **12** (Figure 2.12). Stability constant (K_s = 2.71 x 10^2 M^{-1}] was obtained from the ratio of intercept and slope. The deviation from linearity found above 10 mM can be due to the formation of 2:1 metal to ligand complexes.

The changes in absorption spectra of **13**, on addition of lithium perchlorate (0-2.5 mM) in 30% (v/v) acetonitrile-toluene mixture are shown in Figure 2.13. A well defined isosbestic point at 625 nm indicates the existence in equilibrium of the uncomplexed and complexed fluoroionophores (Figure 2.13). Similar changes in absorption spectra were observed

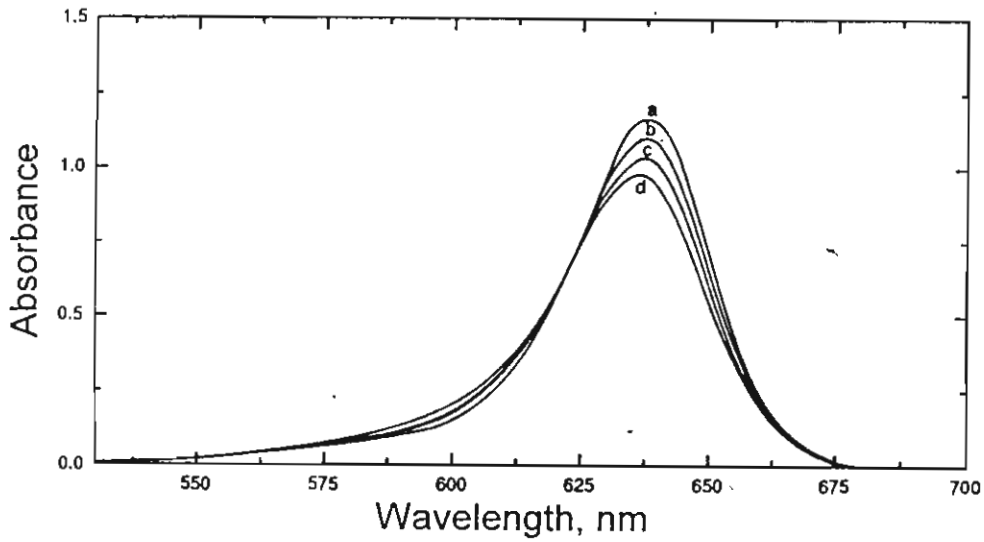

Figure 2.13. Effect of $LiClO_4$ concentrations on the absorption spectrum of **13** (7.4 μM) in 30% (v/v) acetonitrile-toluene mixture. [$LiClO_4$] (a) 0, (b) 0.25, (c) 0.5 and (d) 2.5 mM.

on addition of sodium perchlorate. The emission maximum remain unchanged on addition of $LiClO_4$ (Figure 2.14) as well as $NaClO_4$ (Figure 2.15). Upon addition of 1 mM of lithium perchlorate, 29% quenching of fluorescence was observed and for 1 mM of sodium perchlorate, 20% quenching of fluorescence was observed (Figure 2.16, Tables 2.3 and 2.4). The metal to ligand stoichiometry and the stability constants were determined from the Benesi-Hildebrand analysis of the emission data. Plot of $1/(\Phi_f^0 - \Phi_f)$ versus reciprocal of metal ion concentration showed a linear dependence for lithium perchlorate (Figure 2.17) as well as sodium perchlorate (Figure 2.18) in the concentration range of 0-2 mM, indicating a 1:1 metal to ligand complexation. Stability constants K_s were calculated as 1560 M^{-1} for lithium perchlorate and 1300 M^{-1} for sodium perchlorate.

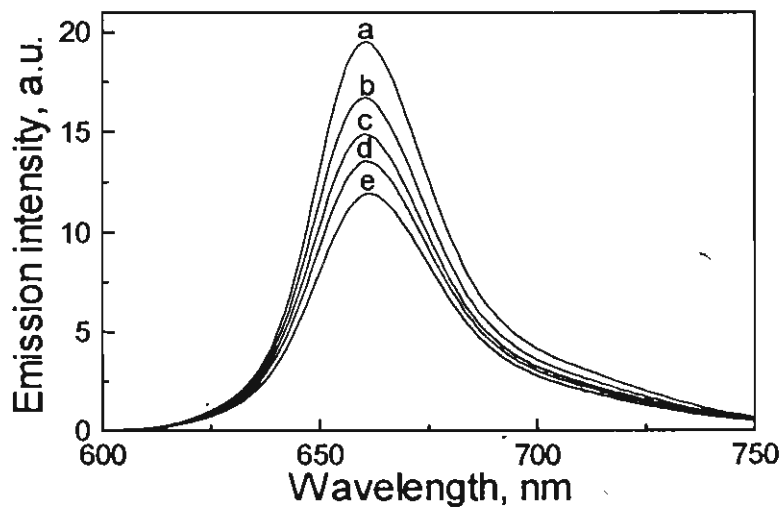

Figure 2.14. Influence of $LiClO_4$ concentrations on the emission spectrum of **13** (7.4 μM) in 30% (v/v) acetonitrile-toluene mixture. [$LiClO_4$] (a) 0, (b) 0.5, (c) 1.25, (d) 2.5 and (e) 5.0 mM.

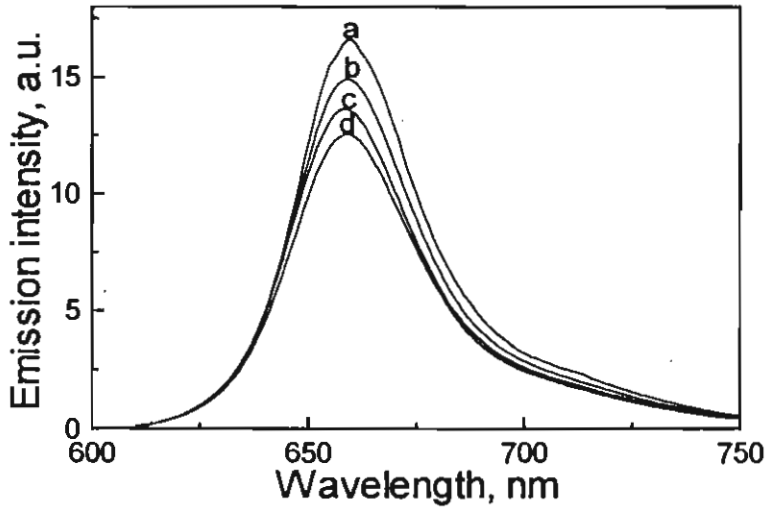

Figure 2.15. Influence of $NaClO_4$ concentrations on the emission spectrum of **13** (7.4 μM) in 30% (v/v) acetonitrile-toluene mixture. [$NaClO_4$] (a) 0, (b) 1.25, (c) 3.75, and (d) 7.5 mM.

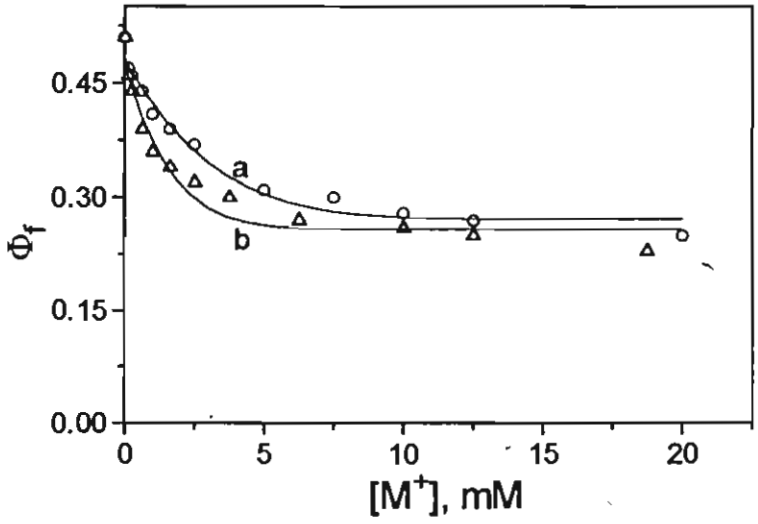

Figure 2.16. Plot of quantum yield of fluorescence (Φ_f) of **13** (7.4 μM) versus metal ion concentration in 30% (v/v) acetonitrile-toluene mixture. (a) $NaClO_4$; (b) $LiClO_4$.

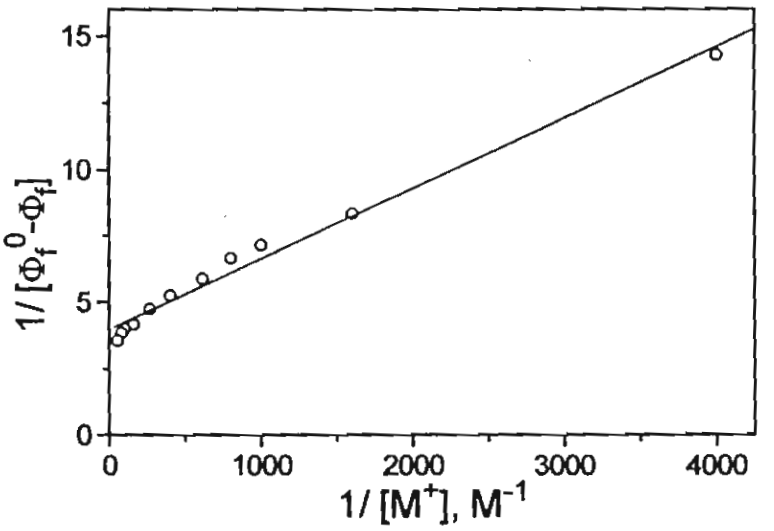

Figure 2.17. Plot of $1/(\Phi_f^0-\Phi_f)$ versus reciprocal of lithium ion concentration for the fluorescence quenching of **13** in presence of $LiClO_4$.

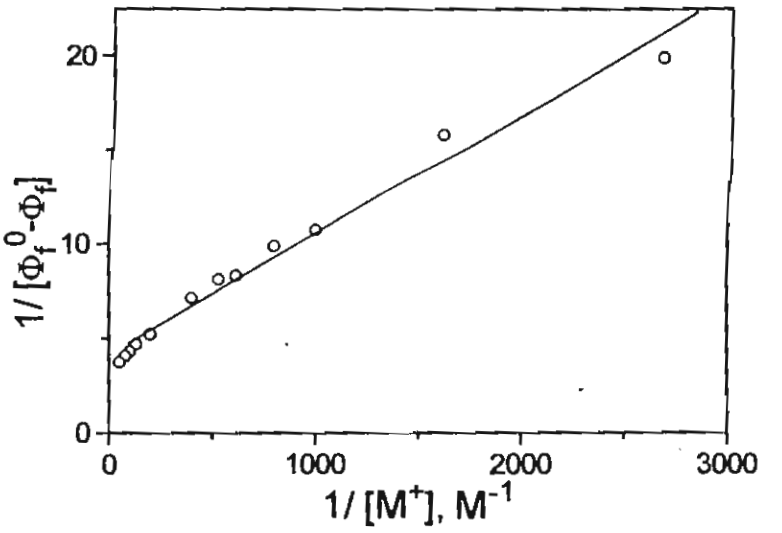

Figure 2.18. Plot of $1/(\Phi_f^0-\Phi_f)$ versus reciprocal of sodium ion concentration for the fluorescence quenching of **12** in presence of $NaClO_4$.

Blank experiments were carried out with a similar squaraine dye, bis(4-dioctadecylphenyl)squaraine,[51] **15** (Chart 8), which does not possess the crown-ether appendages. A slight reduction in quantum yield of fluorescence (1%) was observed on addition of 1 mM of $LiClO_4$ to a solution of **15** in acetonitrile-toluene mixture (30/70, v/v) whereas in the case $NaClO_4$, absorption and emission properties remain unchanged. At higher concentrations (5 mM) of $LiClO_4$, absorption as well as emission maxima shift to longer wavelength by 1 nm and 6% quenching of fluorescence was observed (Table 2.3-2.4). In the case of $NaClO_4$ (5 mM), the absorption as well as emission maxima remain unchanged and a slight quenching of fluorescence (1%) was observed. These results clearly indicate that the complexation of the metal ions is predominantly by the crown-ether moiety of the dyes.

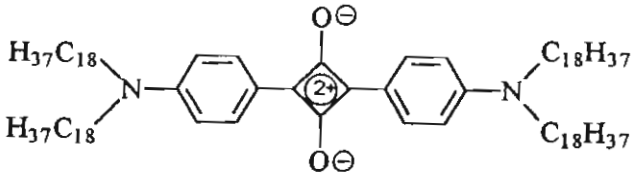

15

Chart 8

The absorption and emission spectra of squaraine dyes have been suggested to arise from charge transfer transitions. Eventhough the charge-transfer is primarily confined to the central C_4O_2 unit (from the oxygen atom to the four membered ring), there is a minor contribution from the anilino moiety also. Complexation of the cation by the crown-ether moiety induces a reduction in the electron donating ability of the nitrogen atom and thereby hindering its ability to contribute to the intramolecular charge transfer process leading to a hypsochromic shift of the absorption band. The

reason for the decrease in fluorescence quantum yield brought about by metal ion complexation is not obvious. Law,[52] had earlier reported that for unsymmetrical squaraines such as the 4-(dimethylamino)phenyl-4′-(methoxy)phenyl squaraine dye and its derivatives, introduction of asymmetry through the less electron donating anisole ring has a significant impact on the absorption and fluorescence properties. Such unsymmetrical squaraines are reported to have a blue shifted absorption and emission bands and the fluorescence quantum yields are significantly lower. These effects were ascribed to the rapid free rotation of the C-C bond between the C_4O_2 unit and the anisole ring. Due to the less electron donating nature of the anisole ring the double bond character of the bond between the C_4O_2 unit and the anisole ring will be reduced making free rotation around this bond easier. This argument may also hold for the crown-ether squaraines, complexed with metal ions, since the complexation of the metal ion by one of the crown-ether moieties induces asymmetry in the molecule and reduces the electron donating ability of one of the rings. As a result, easier free rotation of the bond between the C_4O_2 unit and the phenyl ring containing the metal ion becomes possible, leading to enhancement in the nonradiative decay process.

The selectivities observed for Li^+ than Na^+ in the case of **12** and **13** can be explained by comparing the cavity size of the crown-ether moieties with the ionic diameter and charge densities of the metal ions[14] (Table 2.5). Ionic diameter of Li^+ ion matches well with the cavity size of N-aza-12-crown-4-ether moiety and hence can complex more efficiently than Na^+. Fluoroionophore **13** is also more selective to Li^+ ion, eventhough the ionic diameter of Na^+ ion matches well with the cavity size of N-aza-15-crown-5-

ether moiety (1.7-2.2 Å). This can be explained on the basis of the charge densities of the two ions.[14] Charge density of lithium ion is higher than sodium ion and hence will be strongly solvated. The solvated Li^+ ion fits well

Table 2.5: Ionic radii of various alkali metal ions and the cavity size of different crown-ethers

Metal cation/ Ligand	Ionic diameter/ Cavity size of the crown-ether Å
Li^+	1.36
Na^+	1.94
K^+	2.66
N-Aza-12-crown-4-ether	1.2-1.5
N-Aza-15-crown-5-ether	1.7-2.2
N-Aza-18-crown-6-ether	2.6-3.2

to the crown-ether cavity of **13** and leads to a more stable complex. Such effects were previously reported by Valeur and co-workers.[12] The size of the crown-ether cavity of **14** (2.6-3.2 Å) is much larger than the size of Li^+ and Na^+ ions and hence fluorescence quenching was not observed.

2.4.5. Electrochemical Recognition of Alkali Metal Ions[32]

The dye **12** exhibits two reversible oxidation peaks at 705 and 1030 mV vs Ag/AgCl in acetonitrile with tetrabutylammonium perchlorate (TBAP) as the electrolyte and the dye could be subjected to several

oxidation/reduction cycles without undergoing any significant chemical changes. Both of these potentials are significantly greater than the corresponding oxidation potentials of bis[4-(dimethylamino)phenyl]squaraine (710-790 mV vs SCE), and its derivatives.[53] These oxidation peaks are sensitive to metal ions present in the electrolyte. With TBAP as the

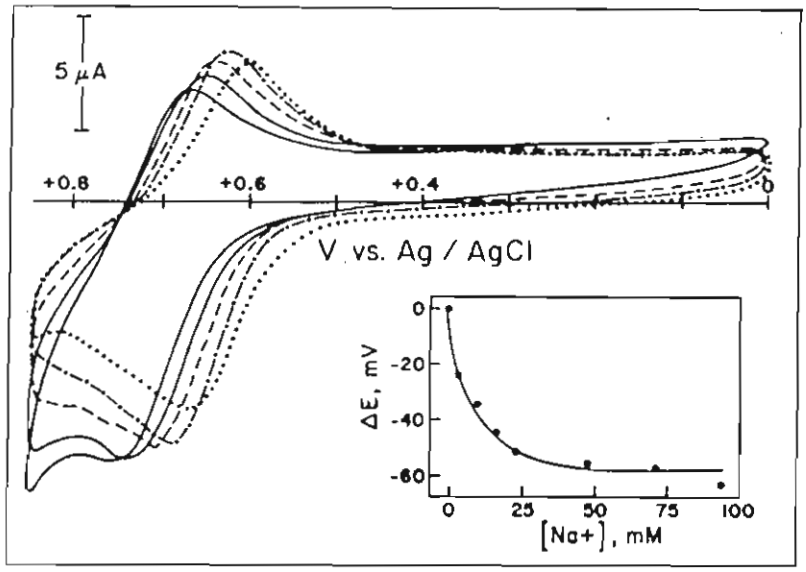

Figure 2.19. Electrochemical oxidation of **12** (5.7 mM) in CH_3CN containing 0.1 M TBAP. The concentrations of Na^+ were: A, 0; B, 3.3; C, 10; D, 16.4 and E, 93.7 mM. The inset shows the shift in the anodic peak versus the concentration of Na^+ ion (working electrode, glassy carbon; reference electrode, Ag/AgCl in 0.1 M $AgNO_3$; electrolyte, 0.1 M TBAP in CH_3CN; scan rate, 100 mV s^{-1}. The solid line represents a qualitative trend in attaining saturation.

electrolyte, the dye shows reversible oxidation with E_{pa} and E_{pc} at 670 and 740 mV, respectively. Upon addition of small amounts of $NaClO_4$, these peaks shift towards less positive potentials (Figure 2.19). The dependence

of the shift in the anodic peak on the concentration of Na^+ ions is shown in the inset of Figure 2.19. A saturation in this shift was evident at metal ion concentrations greater than 25 equivalents of the dye. This behaviour parallels the metal ion quenching of fluorescence of **12**. The shift in the oxidation potentials of **12** on addition of Li^+, Na^+ and K^+, measured in the presence of excess metal ion concentration could be attributed to the metal ion binding by the crown-ether moiety of **12**. Dyes **13** and **14** (with K^+) also exhibited similar results. The metal cation recognition capability of crown-ether squaraine dyes makes them potentially useful in biological applications. The selective complexation of metal ions as well as the redox-active nature of these molecules make them highly suited for developing chemical sensors as well as redox-active switches for metal ions.

2.4.6. Flash Photolysis Studies[32]

Direct excitation led to the photoionization of these dyes along with the formation of small amounts of triplets. The transient absorption spectra obtained by the nanosecond laser flash photolysis of **12** in deaerated acetonitrile solution show a bleaching at 630 nm and transient absorption maxima at 540 and 680 nm were observed. The absorption at 540 nm was prompt and was readily quenched by dissolved oxygen. Although the inter-system crossing efficiency of squaraines are generally low, this absorption band has been attributed to triplet excited state of the dye. However, even in air saturated solutions significant amount of transient absorption was observed at 680 nm, indicating the presence of species other than the triplet state. This could be attributed to the radical cations of the dye. Since both S_0 and S_1 states exhibit significant absorption at the excitation wavelength

(532-nm), multiphotonic excitation of the dye is possible within the duration of the laser pulse. These effects were more evident at high laser intensities as the dye molecules photoionize. Similar biphotonic photoionization has been reported earlier for bis[4-(dimethylamino)phenyl]squaraine.[31] Photoionization of **12** yields dye radical cations and solvated electrons. The reaction of these solvated electrons with the ground state dye molecules produces dye radical anions. In air-saturated solutions the anion radical formation was suppressed as dissolved oxygen scavenges away the solvated electron. Thus, excited triplet, radical anion and radical cation are the major reaction intermediates that result from direct excitation of the dye.

The triplet excited states of these dyes were generated using the triplet-triplet energy transfer method using 1-pyrenecarboxaldehyde and C_{60} as sensitizers. It was observed that the lifetime of the triplet formed was dependent upon the ground state dye concentration. This indicates the participation of the ground state in deactivating the triplet excited dye. The decay of the triplet state (540- 560 nm), follows the formation of a species with absorption maximum at 680 nm. The spectral features of the transient observed at 680 nm match with those of the transient observed in the photoionization experiments. This suggests the formation of dye radical cations and anions via the quenching of the triplet state with the ground state of the dye.

2.5. Conclusion

A series of new crown-ether-linked squaraine fluroionophores have been synthesized and characterized. The ^{13}C NMR spectra of these dyes

substantiated their highly symmetric structure. The fluoroionophores **13** and **14** form aggregates in water. Addition of β-cyclodextrin leads to the break-up of the aggregate and the formation of a fluorescent dye-β-CD-complex. These fluoroionophores complex with alkali metal ions selectively and thus can be used as ion-sensitive near-infrared probes. Direct laser excitation of these dyes resulted in the production of different transient intermediates such as excited triplet, radical anion and radical cation. The triplet excited state, radical anion, and radical cation of all the three dyes exhibit strong absorption in the visible region. Although substituent groups on the phenyl ring are generally capable of influencing the intramolecular charge transfer in the excited state, the size of the crown-ether moiety seems to have no major effect.

2.6. References

1. Lehn, J. M. *Angew. Chem. Int. Ed. Engl.*, **1990**, *29*, 1304.
2. Bissel, R. A.; de Silva, A. P.; Gunaratne, H. Q. N.; Lynch, P. L. M.; Maguire, G. E. M.; Sandanayake, K. R. A. S. *Chem. Soc. Rev.* **1992**,187.
3. de Silva, A. P.; Gunaratne, H. Q. N.; McRoy, C. P. *Nature* **1993**, *364*, 42.
4. Lakowicz, J. *Topics in Fluorescence Spectroscopy Vol. 4: Probe Design and Chemical Sensing*; Plenum press: New York, **1994**.
5. Blasius, E.; Janzen, K.-P. *Top. Curr. Chem.* **1981**, *98*, 163.
6. Barzykin, A. V.; Fox, M. A.; Ushakov, E. N.; Stanislavsky, O. B.; Gromov, S. P.; Fedorova, O. A.; Alfimov, M. V. *J. Am. Chem. Soc.* **1992**, *114*, 6381.
7. Lohr, H.-G.; Vogtle, F. *Acc. Chem. Res.* **1985**, *18*, 65
8. Valeur, B. In *Topics in Fluorescence Spectroscopy Vol. 4: Probe Design and Chemical Sensing*; Lakowicz, J., Ed.; Plenum press: New York, **1994**, p 21.
9. Fery-Forgues, S.; Le Bris, M.-T.; Guette, J.-P.; Valeur, B. *J. Chem. Soc. Chem. Commun.* **1988**, 384.
10. Fery-Forgues, S.; Le Bris, M.-T.; Guette, J.-P.; Valeur, B. *J. Phys. Chem.* **1988**, *92*, 6233.
11. Fery-Forgues, S.; Bourson, J.; Dallery, L.; Valeur, B. *New. J. Chem.* **1990**, *14*, 617.
12. Bourson, J.; Valeur, B. *J. Phys. Chem.* **1989**, *93*, 3871.

13. Martin, M. M.; Plaza, P.; Hung, N. D.; Meyer, Y. H.; Bourson, J.; Valeur, B. *Chem. Phys. Lett.* **1993**, *202*, 425.
14. Bourson, J.; Pouget, J.; Valeur, B.; *J. Phys. Chem.* **1993**, *97*, 4552.
15. Letard, J. F.; Lapouyade, R.; Rettig, W. *Pure and Appl. Chem.* **1993**, *65*, 1705.
16. Thomas, K. J.; Thomas, K. G.; Manojkumar, T. K.; Das, S.; George, M. V. *Proc. Indian Acad. Sci. (Chem. Sci.)* **1994**, *106*, 1375.
17. Beer, P. D. *Endeavour New Ser.* **1992**, *16*, 182.
18. Saji, T. *Chem. Lett.* **1986**, 275.
19. Beer, P. D. *J. Chem. Soc. Chem. Commun.* **1985**, 1115.
20. Beer, P. D.; Sikanyika, H.; Slawin, A. M. Z.; Williams, D. J. *Polyhedron*, **1989**, *8*, 879.
21. Beer, P. D.; Sikanyika, H.; Blackburn, C.; McAleer, J. F. *J. Chem. Soc. Chem. Commun.* **1989**, 1831.
22. Czarnik, A. W. In *Frontiers in Supramolecular Organic Chemistry and Photochemistry*; Schneider. H-J. and Durr, H., Eds.; VCH: New York, **1991**, p 109.
23. Parker, D. In *Crown Compounds Toward Future Applications*; Cooper, S. R., Ed.; VCH: New York, **1992**, p 51.
24. Sutherland, I. O. In *Crown Compounds Toward Future Applications*; Cooper, S. R., Ed.; VCH: New York, **1992**, p 235.
25. Ueno, A.; Osa, T.; In *Photochemistry in Organized and Constrained Media*; Ramamurthy, V., Ed.; VCH: New York, **1991**, p 739.
26. Konopelski, J. P.; Kotzba-Hibert, F.; Lehn, J.-M.; Desvergne, J.-P.; Castellan, A.; Laurent, H. B. *J. Chem. Soc. Chem. Commun.* **1985**, 433.

27. Vogtle, F., Knops, P. *Angew. Chem. Int. Ed. Engl.* **1991**, *30*, 958.

28. Jonker, S.A.; Van Dijik, S.I.; Goubitz, K.; Reiss, C.A.; Schuddeboom, W.; Verhoever, J. W. *Mol. Cryst. Liq. Cryst.* **1990**, *183*, 273.

29. Tsien, R. Y. In *Fluorescent Chemosensors For Ion And Molecule Recognition*, Czarnik, A. W. Ed: ACS Symposium Series 538, Washington DC, **1992**, p 130.

30. Czarnik, A. W. In *Fluorescent Chemosensors For Ion And Molecule Recognition*, Czarnik, A. W. Ed: ACS Symposium Series 538, Washington DC, **1992**, p 1.

31. Kamat, P. V.; Das, S.; Thomas, K. G.; George, M. V. *J. Phys. Chem.* **1992**, *96*, 195.

32. These studies were carried out by Dr. P. V. Kamat at the Notre Dame Radiation Laboratory, USA.

33. Natatsuji, Y.; Wakita, R.; Harada, Y.; Okahara, M. *J. Org. Chem.* **1989**, *54*, 12.

34. Schultz, R. A.; White, B. D.; Dishong, D. M.; Arnold, K. A.; Gokel, G. W. *J. Am. Chem. Soc.* **1985**, *107*, 6659.

35. Bigelow, R. W.; Freund, H.-J. *J. Chem. Phys.* **1986**,*107*, 159.

36. Law, K. Y. *J. Phys. Chem.* **1989**, *93*, 5925.

37. Das, S.; Thomas, K. G.; Ramanathan, R.; George, M. V.; Kamat, P. V. *J. Phys. Chem.* **1993**, *97*, 13625.

38. Kamat, P. V.; Hotchandani, S.; de Lind, M.; Thomas, K. G.; Das, S.; George, M. V. *J. Chem. Soc. Faraday Trans.* **1993**, *89*, 2397.

39. Patrick, B.; George, M. V.; Kamat, P. V. Das. S.; Thomas, K. G. *J. Chem. Soc. Faraday Trans.* **1992**, *88*, 671.

40. Buncel, E.; McKerrow, A. J.; Kazmaier, P. M. *J. Chem. Soc. Chem. Comm.* **1992**, 1242.

41. Das, S.; Thanulingam, T. L.; Thomas, K. G.; Kamat, P. V.; George, M. V. *J. Phys. Chem.* **1993**, *97*, 13620.

42. Law, K. Y.; Chen, H. *J. Phys. Chem.* **1989**, *93*, 2533.

43. Hotchandani, S.; Das, S.; Thomas, K. G.; George, M. V.; Kamat, P. V. *Res. Chem. Intermed.* **1994**, 20, 927.

44. Liang, K.; Law, K. Y.; Whitten, D. G. *J. Phys. Chem.* **1994**, 98, 13379.

45. Chen, H.; Law. K. Y.; Perlstein, J.; Whitten, D. G. *J. Am. Chem. Soc.* **1995**, *117*, 7257.

46. Chen, H.; Herkstroeter, W. G.; Perlstein, J.; Law. K. Y.; Whitten, D. G. *J. Phys. Chem.* **1994**, *98*, 5138.

47. Chen, H.; Law, K. Y.; Whitten, D. G. *J. Phys. Chem.* **1996**, *100*, 5949.

48. Chen, H.; Farahat, M. S.; Law, K. Y.; Whitten, D. G. *J. Am. Chem. Soc.* **1996**, *118*, 2584.

49. Ashwell, G. J.; Jefferies, G.; Hamilton, D. G.; Lynch, D. E.; Roberts, M. P. S.; Bahra, G. S.; Brown, C. R. *Nature* **1995**, *375*, 385.

50. Das, S.; Thomas, K. G.; George, M. V.; Kamat, P. V. *J. Chem. Soc. Faraday Trans.* **1992**, *88*, 3419.

51. Law, K. Y. *J. Phys. Chem.* **1987**, *91*, 5184.

52. Law, K. Y. *J. Phys. Chem.* **1985**, *89*, 9818.

53. Law, K. Y.; Facci, J. S.; Bailey, F. C.; Yanus, J. F. *J. Imaging Sci.* **1990**, *34*, 31.

CHAPTER 3

SYNTHESIS AND PHOTOPHYSICAL STUDIES OF A NEAR-INFRARED ABSORBING CATIONIC SQUARAINE DYE

3.1. Abstract

The photophysical properties of a near infrared (NIR) absorbing cationic squaraine dye, **10** were investigated. This dye was found to exist in an acid-base equilibrium in aqueous and other protic solvents. The pK_a of this equilibrium in water-acetonitrile (4:1) mixture was estimated as 4.9. In water and other protic solvents the dye is normally present in the nonfluorescent deprotonated form. However, the protonated form obtained by the addition of appropriate amounts of an acid is fluorescent; for example, the Φ_f value obtained in methanol in presence of acetic acid (~40 μM) was 0.21. In aprotic solvents the dye however, exists in the fluorescent protonated form and the Φ_f value measured in chloroform was 0.24. The singlet and triplet excited states of the cationic squaraine dye were characterized using laser flash photolysis studies. The absorption spectrum of the cationic squaraine dye in water-acetonitrile mixture (4:1) was found to be highly sensitive to the presence of trace amounts of transition and lanthanide metal cations. On complexation with these metal cations characteristic new absorption bands are formed, which are blue shifted with respect to the normal absorption band. Absorption maxima of the complex is characteristic of the metal ion used. The dye is capable of detecting nanomolar quantities of Cu^{2+}, La^{3+}, Eu^{3+}, Tb^{3+}, Gd^{3+} and Lu^{3+}, micromolar quantities of Hg^{2+} and Pb^{2+} and millimolar quantities of cations such as Mn^{2+} and Zn^{2+} in aqueous solutions. The cationic squaraine dye is insensitive to alkali and

alkaline earth metal cations, which makes it possible to detect submicromolar quantities of transition and lanthanide metal ions even in the presence of high concentrations (mM) of the former cations. The high fluorescence intensity of the cationic squaraine dye in acetonitrile facilitates the detection of metal ions such as copper using fluorescence spectroscopy.

3.2. Introduction

Design of organic materials as building blocks for optical data storage, NIR lasers and biosensors is currently an active area of research.[1,2] One of the desired properties of such materials is their ability to absorb and emit in the NIR region.[2] Only a small fraction of the known organic and organometallic molecules emit in the infrared region.[3-5] The important classes of IR sensitive dyes so far reported are the cyanines, oxazines, phthalocyanines and polynuclear aromatic hydrocarbons.[3,5-16]

Among the various compounds reported to be fluorescent in the IR region, cyanines (for an example see Chart 1) are the most widely used.[3] They have been used as laser dyes and as saturable absorbers in mode-locked and Q-switched laser systems.[6,7] Although the ability of most of the cyanines to undergo photooxidation makes them suited for applications in photographic films and saturable absorbers, it makes them less desirable for the design of fluorophores.[3] The tuning ranges of these dyes in dye lasers are also limited due to their small Stoke's shifts.[3] The excited state dipoles of most cyanines do not have much difference from those of the ground state, and thus exhibit very limited solvent dependent shifts in emission wavelengths.[3] Some of the recently developed cyanine laser dyes have larger Stoke's shift and improved stability and their emission may also be

more solvent sensitive.[8] The squarylium cyanines, recently reported by Terpetschnig and Lakowicz[9] showed improved photostability. Only few IR cyanine dyes have been reported so far, for biochemical and biophysical applications. The *bis*-alkylindocarbocyanine[10] family of dyes used in fluorescence recovery after photobleaching microscopy studies are photounstable. Most of these cyanines are relatively new and much more studies are necessary before they can be compared with commonly used fluorophores such as fluorescein or rhodamines for applications in microscopy, cell sorting, or fluorescence immunoassay.[3] The styryl series of dyes, which are structurally related to cyanines, are found to be more efficient laser dyes than the corresponding cyanines because they exhibit larger Stoke's shifts, but otherwise share most of the characteristics of the cyanines.[3] In general, eventhough cyanines are widely used as IR dyes, they have significant drawbacks with regard to design of fluoro- and chromoionophores.

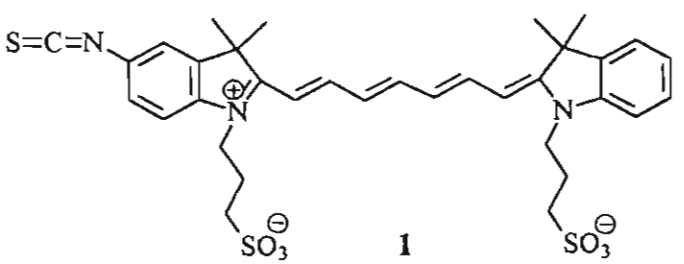

1

CY-7-isothiocyanate

Em = 777 nm

Chart 1

Soper et al. have reported detection sensitivity at the single molecule level in the NIR region using pulsed-laser excitation and time-gated detection for the NIR fluorescent dye IR-132 in methanol.[11] Recently, Soper and Mattingly have studied the fluorescence properties, lifetimes and other photophysical properties of tricarbocyanine dyes[12], IR-125 and IR-132

(Chart 2). In aqueous solvents IR-132 underwent extensive ground state aggregation whereas IR-125 showed little evidence of aggregation. The fluorescence lifetimes for both dyes demonstrated negligible dependence on solution viscosity, indicating that photoisomerization is not a major nonradiative path for these tricarbocyanine dyes. Internal conversion, resulting from the small electronic energy difference between the ground and the singlet state seems to be the major nonradiative pathway for decay of the singlet excited state.

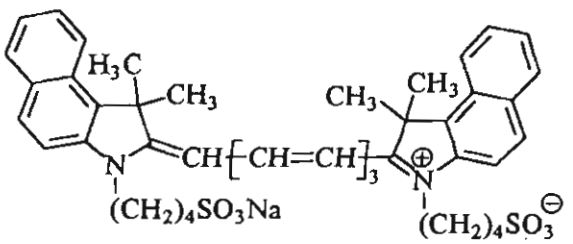

IR-125

2

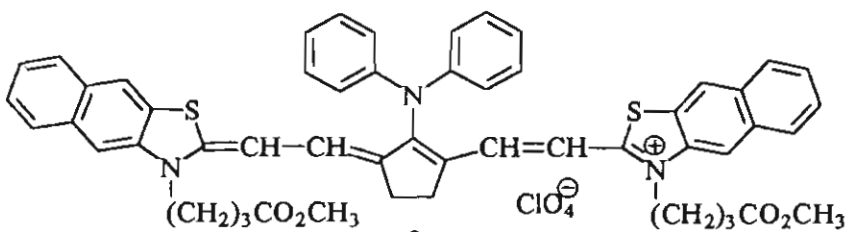

IR-132

3

Chart 2

Oxazines form another major class of IR fluorescent dyes and their photostability is much better. than that of the cyanines. Oxazines are synthesized by condensation of the appropriate *p*-nitrosoaniline derivatives with phenols.[13] Though they have better Stoke's shifts, the major limitation of these class of dyes are their absorption and emission are not very close towards the red.[3] The most commonly used phenoxazine dye, Nile Blue

(Chart 3) is often contaminated by the corresponding oxazone Nile Red, which is readily formed by the weak acid hydrolysis of the former.[14] Nile Red exhibits solvent sensitivity in its emission, but its absorption and emission are at much shorter wavelengths than Nile Blue.[10] Oxazines may be easier to solubilize since they are relatively compact compared to cyanines.[3]

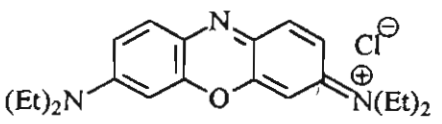

4

Oxazine 1, Em = 658 nm

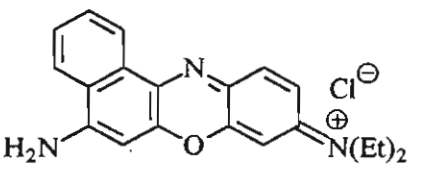

5

Nile blue, Em = 660 nm

Chart 3

Polynuclear aromatic hydrocarbons (PAH) (Chart 4) represents a diverse group of fluorophores which have not been as well exploited as compared to cyanines.[7,15] Unlike cyanines, PAH are of low commercial interest primarily because of the difficulty to synthesize a variety of derivatives.[3] PAH such as perylene, pyrene and coronene are very useful fluorophores in the UV-visible range of the spectrum, while they have little use in the IR region, primarily because the IR-emitting PAH are large molecules and are difficult to solubilize. Some of the PAH have very good fluorescence quantum yields in organic solvents. Carcinogenicity is another limiting factor for PAH such as benzo[a]pyrenes.

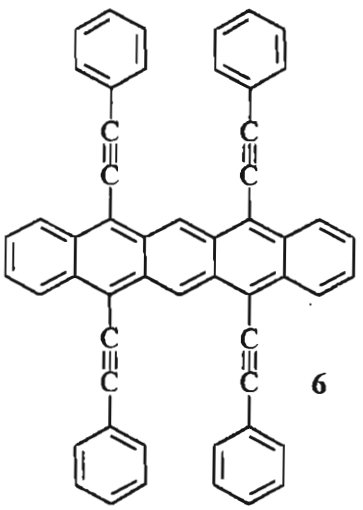

6

5,7,12,14-tetrakis(phenylethynyl) pentacene (Em = 740 nm)

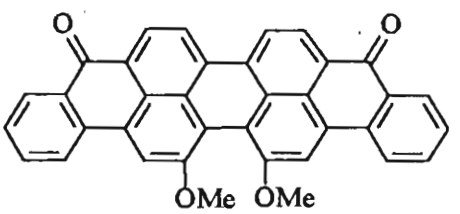

7

16,17-dimethoxy violanthrone (Em = 713 nm)

Chart 4

Phthalocyanines and naphthocyanines (Chart 5) form another class of very stable IR fluorophores.[16] Most of the phthalocyanine derivatives can be made by prolonged heating of a phthalimide or phthalic acid derivative with a metal in powder or salt form at elevated temperatures. Several of the phthalocyanines absorb in the NIR region and either fluoresce or phosphoresce.[3] The electronic transitions of phthalocyanines are complex and have been extensively studied. The unsubstituted phthalocyanines and naphthocyanines are very insoluble in solvents other than, for instance, nitrobenzene. Sulfonated phthalocyanines are water soluble and exhibit spectra comparable to the parent derivatives.

A few other dyes are also known to be fluorescent in the IR and NIR region.[4] However the number of such dyes are limited and are not well characterized. Some anthraquinone dyes have been described as fluorescent in the IR region, but their emissions have not been well characterized.[3]

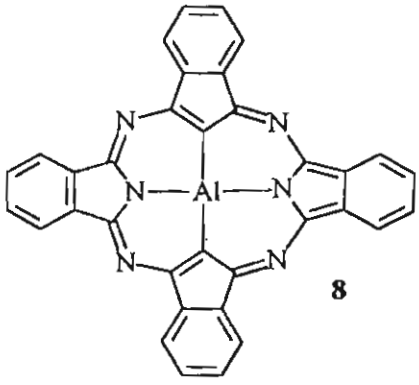

8

Al Phthalocyanine
(Em = 680 nm)

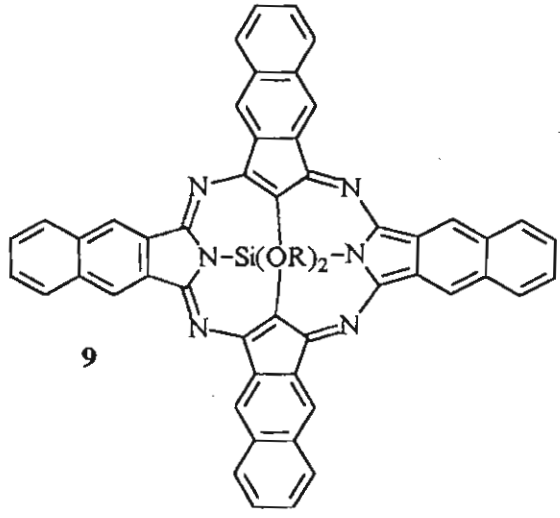

9

Bis(trialkylsiloxy)silicon naphthocyanine
(Em = 780 nm)

Chart 5

Near infrared absorbing ion and molecular probes find a lot of biological applications due to the inherently low biomolecular interference in this region.[5,11,17] Some of the desirable attributes of chromogens for application in naturally occurring systems are (i) ability to function in aqueous media,[17,18] (ii) ability to detect specific metal ions in the presence of other closely related species[17,19] and (iii) absorption and emission in the near infrared (NIR) region.[11,12,17] With a few exceptions[17,19-24] most of these studies have been concerned with non-aqueous solutions of metal ions or the chromophores used tend to possess absorption in the short wavelength region.

Since squaraines are highly fluorescent in the visible and NIR region, their potential as fluoroionophores[25,26] and fluorophores in biological applications[27] have recently been explored. However these studies have dealt with 1,3-disubstituted squaraines. The synthesis and characterization

of a new class of water soluble dyes known as cationic squaraines have been reported recently.[28] In this Chapter of the thesis, the detailed photo-physical studies of the cationic squaraine dye, **10** (Chart 6) have been reported. This dye is soluble in water with strong absorption in the NIR region and possess a suitable geometry for strong complexation with metal cations. These properties make the cationic squaraine dye ideal for the detection of trace metal ions in aqueous systems and these aspects have also been discussed in detail.

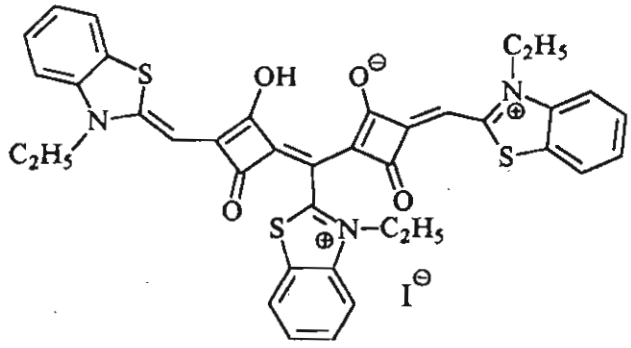

10

Chart 6

3.3. Experimental Section

3.3.1. Materials and Methods

All melting points are uncorrected and were determined on a Aldrich Meltemp apparatus. Absorption spectra were recorded on a Shimadzu 2100 or on a GBC UV-vis spectrophotometer. IR spectra were recorded on a Perkin Elmer Model 882 spectrophotometer. NMR spectra were recorded on a Varian 300 MHz FT NMR spectrometer and the mass spectra on a JEOL

JMS AX 505 HA mass spectrometer. Fluorescence spectra were recorded on a SPEX Fluorolog F-112X spectrofluorimeter. The solutions were excited at 730 nm and the emission was followed from 740 nm to 880 nm. The fluorescence quantum yield, Φ_f was determined relative to IR-125 in DMSO (Φ_f = 0.13).[12,29] Stock dye solutions (2.5 x 10^{-5} M) were made by dissolving the cationic squaraine dye in dry acetonitrile. Two mL of this dye solution was diluted to 10 mL using water and this solution was further purged with argon. All spectroscopic measurements were carried out in a quartz cuvette, closed with a septum. Appropriate concentrations of metal cations were added by injecting μL quantities of argon bubbled metal salt solutions. Complexes of all the metal ions studies except with Cu^{2+} and Mn^{2+} are stable in H_2O/CH_3CN (4:1) mixture and the solutions were kept for 15 minutes for equilibration before carrying out the measurements. In the case of Cu^{2+} and Mn^{2+}, the measurements were carried out immediately after the addition of the metal ions. The pH of the solution remained unchanged on addition of metal ions. Spectroscopic grade solvents, double distilled water and analytical grade metal salts were used for the experiments.

Picosecond laser flash photolysis[30] experiments were performed with 355-nm laser pulses from a mode-locked, Q-switched Quantal-YG-501 DP Nd:YAG laser system (output 1.5 mJ/pulse, pulse width ~18 ps). Details of the experiments are described in Section 2.3.2. Nanosecond laser flash photolysis studies were carried out using the third harmonic of a Quanta-Ray CDR-1 Nd:YAG pulsed laser (355-nm, 6 ns pulse width, 2-5 mJ/pulse). Details of the experimental setup are described in Section 2.3.2.

3.3.2. Synthesis of Cationic Squaraine Dye 10

Cationic squaraine dye, **10** was synthesized according to a reported procedure.[28] A mixture of 3-ethyl-2-methylbenzothiazolium iodide (1.32 g, 4 mmol) and squaric acid (0.23 g, 2 mmol) was refluxed for 3h in a solvent mixture containing 2 mL of benzene and 8 mL of *n*-butanol, accompanied by azeotropic distillation of water. Purification was carried out by recrystallizing twice from a mixture (3:1) of dichloromethane and ethyl acetate to give 0.4 g (44%) of **10**, mp 218 °C (decomp.); IR ν_{max} (KBr) 1750, 1633, 1410, 1243 cm^{-1}; UV-vis λ_{max} (CH_3CN) 783 nm (ε 3,00,000 $M^{-1}cm^{-1}$); ^1H NMR ($CDCl_3$)) δ 1.1-1.4 (m, 9 H, CH_3), 4.4-4.6 (m, 4 H, NCH_2), 4.8 (m, 2 H, NCH_2), 6.1 (s, 2H, vinyl), 7.2-8.0 (m, 10 H, aromatic), 8.1-8.2 (m, 2 H, aromatic); HRMS, exact mol wt calcd for $C_{18}H_{30}N_3S_3O_4$ (M^+), 688.1398, found 688.1434 (FAB high resolution mass spectrometry).

3.4. Results and Discussion

3.4.1. Acid-Base Equilibrium Properties

The cationic squaraine dye **10** absorbs strongly in the near infrared region and the spectrum was found to be dependent upon the pH of the solution. Figure 3.1 shows the absorption spectra in a mixture (4:1) of water and acetonitrile at different pH values. At pH 6.5, (curve a, Figure 3.1) two absorption maxima, centered around 790 and 640 nm are observed. On lowering the pH, by the addition of dilute HCl to the solution, a decrease in the intensities of these bands were observed along with the formation of a sharp new band centered around 690 nm. These spectral changes are marked by the presence of an isosbestic point at 715 nm.

A plot of pH versus absorbance at 790 nm (inset, Figure 3.1) indicated the presence of a single acid-base equilibrium. The pK_a of **10** has been evaluated as 4.9, based on these pH dependent spectral changes. The probable structures of the acid/ base species in equilibrium with each other are shown in Scheme 1. Since the sharp absorption bands observed for

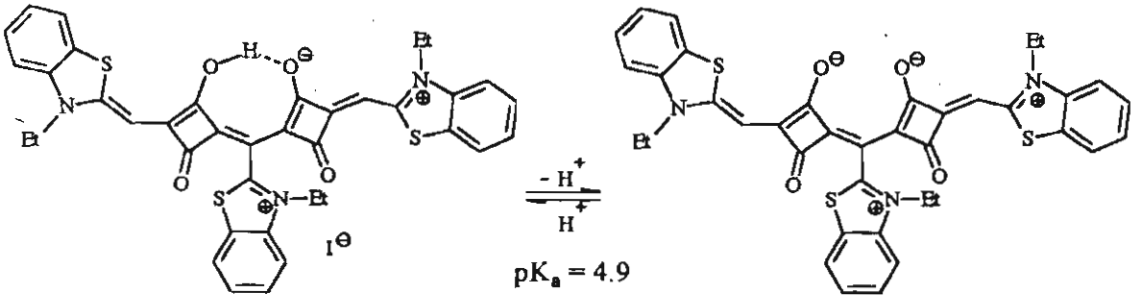

10

Scheme 1

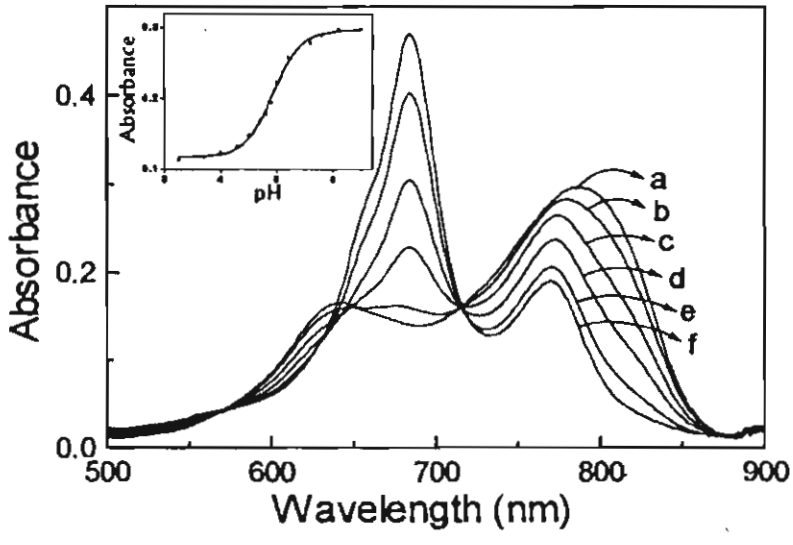

Figure 3.1. Variation in the absorption spectra of 4.7 μM of **10** in H_2O/CH_3CN (4:1): pH = (a) 6.5, (b) 5.6, (c) 5.1, (d) 4.9, (e) 4.5, (f) 4.0. Inset shows the plot of absorbance at 790 nm versus pH (pK_a = 4.9).

squaraine dyes arise mainly from an intramolecular charge transfer transition between the central cyclobutane rings and the oxygen atoms,[31-33] protonation of this oxygen atom will result in a reduction of the intramolecular charge transfer character. Accordingly, in the protonated state of **10** the absorption spectrum becomes blue shifted.

3.4.2. Absorption and Emission Properties

The cationic squaraine dye **10** exists in two distinct forms in solution, depending on the pH. The absorption and emission properties of this dye are highly sensitive to the nature of the solvent. In aprotic solvents the dye exists predominantly in the protonated form. For example, in acetonitrile the absorption spectrum of **10** is sharp with a maximum at 783 nm (Figure 3.2). Since this form corresponds to the protonated form,

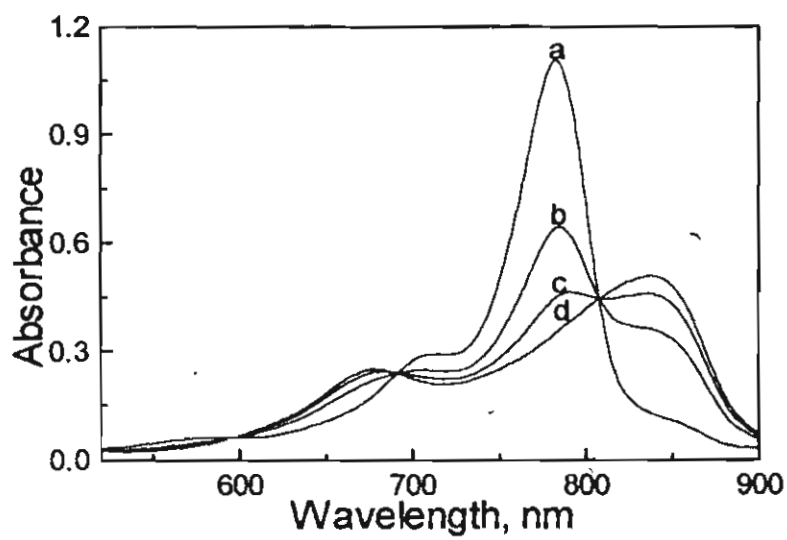

Figure 3.2. Absorption spectrum of the cationic squaraine dye, **10** (5.7 μM) in dry CH_3CN containing various amounts of triethylamine (TEA): [TEA] (a) 0; (b) 5.5; (c) 28 and (d) 580 μM.

deprotonation can be carried out by adding water or base such as triethylamine. The effect of various concentrations of triethylamine on the absorption spectrum of **10** in acetonitrile is shown in Figure 3.2. On addition of triethylamine, the spectrum shows two new absorption maxima, one around 830 nm and the other at 660 nm, while the original peak at 783 nm decreases in intensity. These changes are marked by the presence of two isosbestic points at 695 and 810 nm, which confirm the existence of an acid-base equilibrium as shown in Scheme 1. Addition of water also leads to similar changes in the absorption spectrum of **10** in acetonitrile.

Table 3.1: Absorption and emission properties of 10 in different solvents

Solvent	λ_{max} (nm)		Φ_f
	Abs	Em	
Chloroform	797	826	0.24
Dichloromethane	795	824	0.26
Acetone	787	822	0.21
Acetonitrile	783	812	0.31
Methanol[a]	780	812	0.21
Methoxyethanol[a]	788	825	0.10
Trifluoroethanol[a]	760	790	0.40
n-Butanol[a]	793	818	0.13

[a] in presence of acetic acid (~0.04 mmol)

In protic solvents such as water or methanol, the dye exists in its deprotonated form with a broad absorption band. However, protonation by the addition of acid leads to noticeable changes in the absorption spectra. For example, in methanol **10** possess a broad absorption band centered around 805 nm with a shoulder at 650 nm and the fluorescence intensity is negligible. On addition of acetic acid (40 μM), the absorption spectrum becomes sharp with a maximum centered at 780 nm. The emission maximum was observed at 825 nm and the fluorescence quantum yield was found to be 0.21. Similar behaviour was also observed on addition of acetic acid to the solutions of **10** in other protic solvents. The fluorescence quantum yield observed in trifluoroethanol containing acetic acid (40 μM) was 0.40.

The absorption and fluorescence properties of the cationic squaraine dye was studied in different solvents and the results are summarized in Table 3.1. In dry acetonitrile, **10** has an absorption maximum at 783 nm and the corresponding emission band was at 812 nm, with a fluorescence quantum yield of 0.31. The deprotonated form, obtained by the addition of appropriate amounts of a base was found to be nonfluorescent. The high fluorescence intensity of the protonated form of **10** was ascribed to hydrogen bonding between the central O^- and OH groups of the cyclobutane rings, which is expected to rigidize the configuration of the excited state and suppress energy loss due to rotor motion.

3.4.3. Excited State Properties

The excited singlet state of the protonated form of the cationic squaraine dye, **10** was characterized using picosecond laser flash photolysis. Since the dye has a small absorption in the UV region, the 355-nm laser

pulse could be used for excitation of the dye. The time-resolved transient absorption spectra of $^{1}\mathbf{10}^{+\bullet}$ in acetonitrile are shown in Figure 3.3. The singlet excited state has a characteristic absorption maximum at 650 nm. The exponential decay of the transient absorption at 650 nm (inset, Figure 3.3), indicated a singlet excited lifetime of 1.13 ns. Although at lower laser intensities, recovery of most of the dye bleaching was observed, some irreversible degradation was observed at higher laser intensities. The spectral characteristics and lifetimes of the excited states are summarized in Table 3.2.

Table 3.2: Excited state properties of 10 in acetonitrile

Transient	Abs. Max. (nm)	Lifetime
$^{1}\mathbf{10}^{+\bullet}$	640	1.13 ns
$^{3}\mathbf{10}^{+\bullet}$	620	$9 \pm 1\mu s$
$\mathbf{10}^{2+\bullet}$	630	$77\mu s$

As a result of poor intersystem crossing efficiency, the triplet excited state could not be generated by direct excitation. The triplet excited state of the dye was therefore generated via photosensitization using pyrenecarboxaldehyde as triplet sensitizer (E_T = 186 kJ mol^{-1}). Excitation of the sensitizer with 355-nm laser pulse in the presence of the dye led to the formation of dye triplets. Time resolved transient absorption spectra recorded during the formation of $^{3}\mathbf{10}^{+\bullet}$ in acetonitrile using triplet excited 1-pyrenecarboxaldehyde as a sensitizer are shown in Figure 3.4. The

spectra recorded immediately after the laser flash exhibits an absorption maximum at 440 nm corresponding to the formation of the sensitizer triplet within the laser pulse duration. The sensitizer triplet decays as the acceptor triplet ($^3\mathbf{10}^{+*}$) is formed by a diffusion controlled process. The difference absorption maximum recorded 11.2 μs after the laser pulse excitation shows

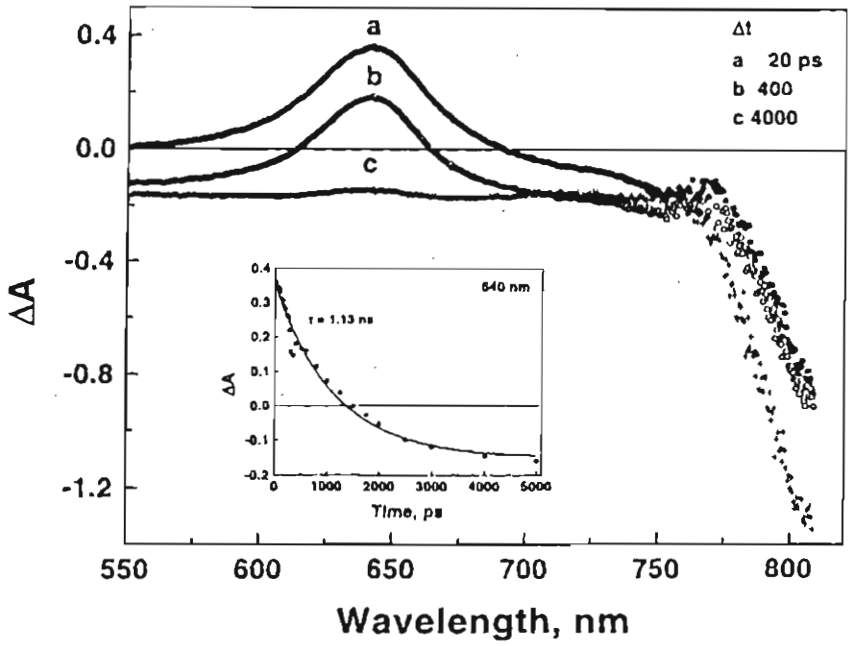

Figure 3.3. Difference absorption spectra of singlet excited $\mathbf{10}^+$ in acetonitrile. Time-resolved transient absorption spectra were recorded, following 355-nm laser pulse excitation of 10 μM $\mathbf{10}^+$ in acetonitrile. The spectra were recorded at time intervals: (a) 20, (b) 400 and (c) 4000 ps, after laser pulse excitation. Inset shows decay profile at 640 nm.

a maximum at 620 nm and bleaching at wavelengths greater than 660 nm. The bleaching around 700 nm further confirms the depletion of ground state dye molecules to form excited state squaraine dye triplets. The isosbestic

point observed in the 550 nm region indicates that only two factors (^{3}dye* absorption and dye depletion) contribute to the difference absorption spectra in Figure 3.4.

The inset of Figure 3.4 shows the decay of ^{3}Sens* at 440 nm and the growth of $^3\mathbf{10}^{+*}$ at 620 nm. The extinction coefficient of $^3\mathbf{10}^{+*}$ at the absorption maximum can be determined by recording the maximum absorbance values of ^{3}Sens* and $^3\mathbf{10}^{+*}$ as reported earlier.[32] In the present experiments we estimate the difference extinction coefficient of $^3\mathbf{10}^{+*}$ to be 7.0 x 10^3 M^{-1} cm^{-1} at 620 nm. The triplet excited state is sufficiently long lived with a lifetime of 9 ± 1 μs.

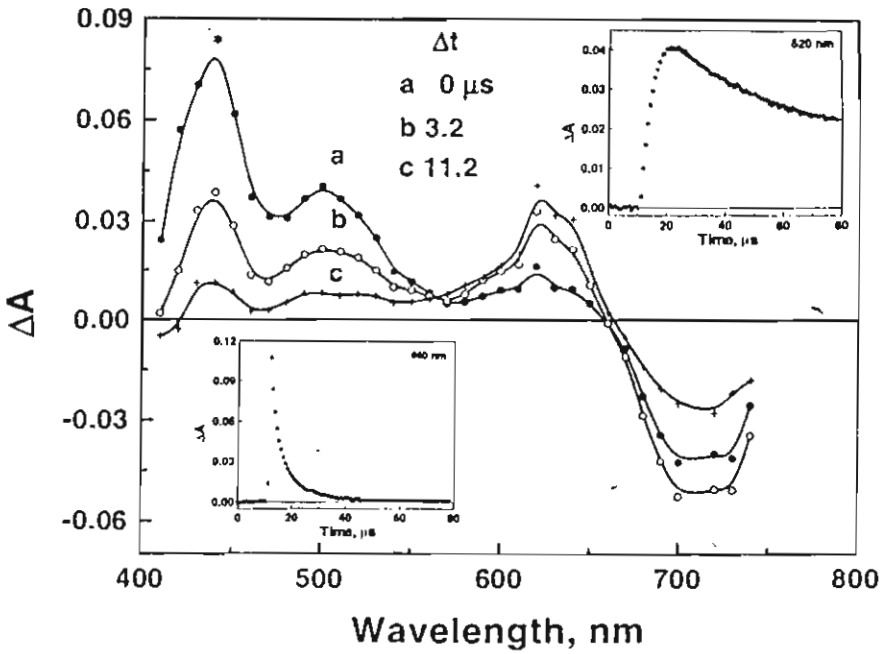

Figure 3.4. Triplet-triplet sensitization of $\mathbf{10}^+$. The transient absorption spectra were recorded following 355-nm laser (6 ns) excitation of 0.1 mM pyrenecarboxaldehyde in acetonitrile containing 20 μM $\mathbf{10}^+$. The spectra were recorded at (a) 0, (b)3.2 and (c) 11.2 μs after laser pulse excitation. Insets show the decay profile of the sensitizer triplet at 440 nm and the growth profile of $\mathbf{10}^+$ triplet at 620 nm.

Since the dye underwent degradation under high laser intensities, we probed this process further with nanosecond laser flash photolysis setup. Laser pulses of 355-nm with high intensity (> 10 mJ/pulse) was used for these experiments. The transient absorption spectrum obtained in deaerated acetonitrile solution is shown in Figure 3.5. An intense difference maximum at 630 nm and bleaching at wavelengths greater than 660 nm were

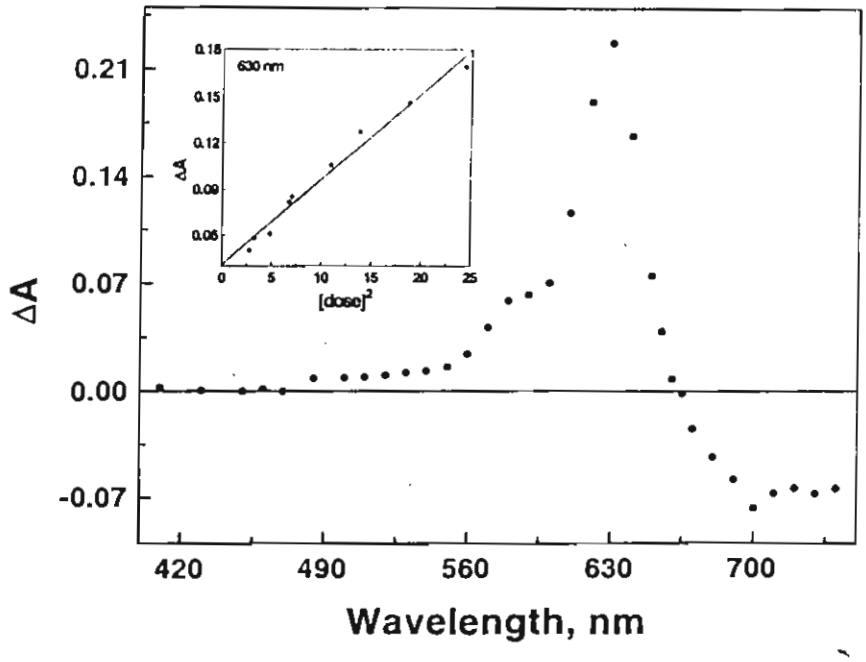

Figure 3.5. Photoionization of $\mathbf{10}^{+}$. The transient absorption spectrum was recorded, following 355-nm laser pulse (6 ns) excitation of 10 μM $\mathbf{10}^{+}$.

observed. The transient absorption at 630 nm is prompt and is not quenched readily by dissolved oxygen. The linear dependence of the transient absorption at 630 nm to the square of the laser intensity (inset, Figure 3.5)

confirms the biphotonic photoionization process. This transient has been attributed to the oxidized form of $\mathbf{10}^{+}$. Photoionization of $\mathbf{10}^{+}$ yields dye radical cations and solvated electrons.

Usually, the reaction of these solvated electrons with the ground state dye molecules produce dye radical anions. This property is similar to the photoionization behaviour observed for the crown derivatives of squaraine dyes. Since we did not see any significant effect of dissolved oxygen on the transient absorption spectrum in Figure 3.5, we consider the absorption of the reduced form of the dye to be relatively small in the spectral region chosen in the study. The transient and the bleaching did not recover during the time period of ~100 μs. This is indicative of the fact that the cation radical of the dye eventually undergoes permanent degradation.

3.4.4. Detection of Transition Metal Ions Present in Aqueous Medium

An interesting property of **10** is its capability to detect trace amounts of transition metal ions present in aqueous medium. Since the dye and the dye-metal ion complexes undergo slow precipitation in purely aqueous media, the experiments were carried out in water-acetonitrile mixture (4:1). Addition of low concentrations of copper ions to a solution of **10** in a mixture (4:1) of water and acetonitrile at pH 6.7 led to a decrease in the intensities of the absorption maxima at 790 and 640 nm, which was accompanied by the formation of a sharp new band around 670 nm (Figure 3.6). It has been observed that addition of even 50 nM (4 ppb) of Cu^{2+} leads to a notable change in the absorption spectrum. The stability constants for the complex formation of **10** with Cu^{2+} was estimated using the Benesi-Hildebrand equation (Equation 1) for 1:1 metal to ligand stoichiometry.

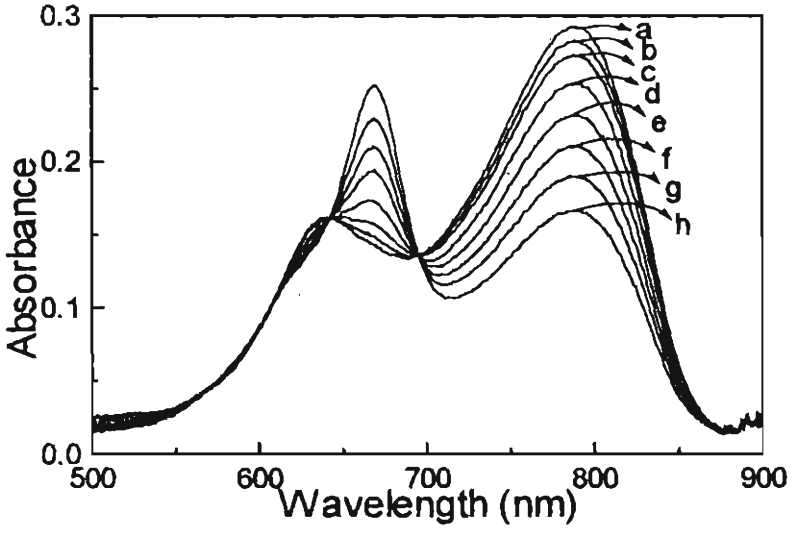

Figure 3.6. Effect of Cu^{2+} concentrations on the absorption spectrum of **10** (4.7 μM) in H_2O/CH_3CN (4:1) : [Cu^{2+}] (a) 0, (b) 0.15, (c) 0.3, (d) 0.6, (e) 1.2, (f) 1.8, (g) 2.4, (h) 3.0 μM.

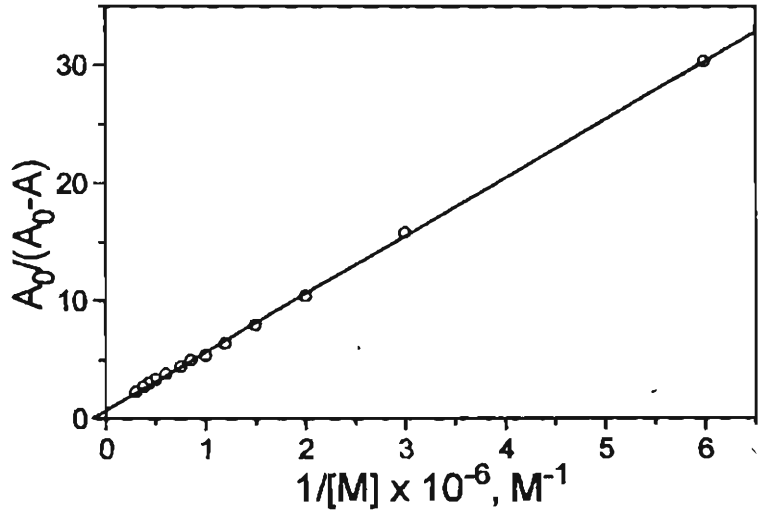

Figure 3.7. Plot of $A_0 / (A_0-A)$ versus reciprocal of Cu^{2+} concentration for the complexation of **10** with Cu^{2+} in water-acetonitrile mixture (4:1).

$$\frac{1}{A - A_0} = \frac{\varepsilon_L}{\varepsilon_L - \varepsilon_{ML}} \left[\frac{1}{K_S [M]} + 1 \right] \qquad (1)$$

where, A is the absorbance of the solution containing different concentrations of metal ions, A_0 is the absorbance of the free ligand, K_s is the stability constant and [M] is the concentration of the metal ion. ε_L and ε_{ML} are the molar extinction coefficients of the free ligand and the complex, respectively. The complex formation, studied by following the changes in absorbance at 670 nm on addition of copper ions, (Figure 3.7) indicated a 1:1 ligand to metal stoichiometry with a stability constant of $1.5 \times 10^5\ M^{-1}$.

Complexation of **10** with various transition metal cations such as Hg^{2+}, Mn^{2+} and Zn^{2+} and other metal ions like Pb^{2+} have also been studied. Effect of addition of Hg^{2+} and Pb^{2+} on the absorption spectrum of **10** is shown in Figures 3.8 and 3.9, respectively. The complexation of the cationic squaraine dye with different metal ions led to the formation of new absorption maxima. The absorption maximum and equilibrium constants measured for different metal ions are shown in Table 3.3. With the exception of the complexes of Hg^{2+} and Cu^{2+} which have a maximum at 670 nm, the other complexes have their own characteristic absorption maxima. The marked difference in absorption maxima of the complexes of the dye makes it possible to detect various metal ions in a mixture using procedures such as higher order derivative spectrophotometry[35] or known statistical methods.[36] With the exception of Cu^{2+} and Hg^{2+}, the hypsochromic shift observed for the dye-metal ion complex increases with increasing charge density of the cation (Table 3.3). The minimum concentration detectable for Cu^{2+} is 40 nM, Hg^{2+} is 2 μM, Pb^{2+} is 20 μM, Mn^{2+} is 40 μM and Zn^{2+} is 0.4 mM.

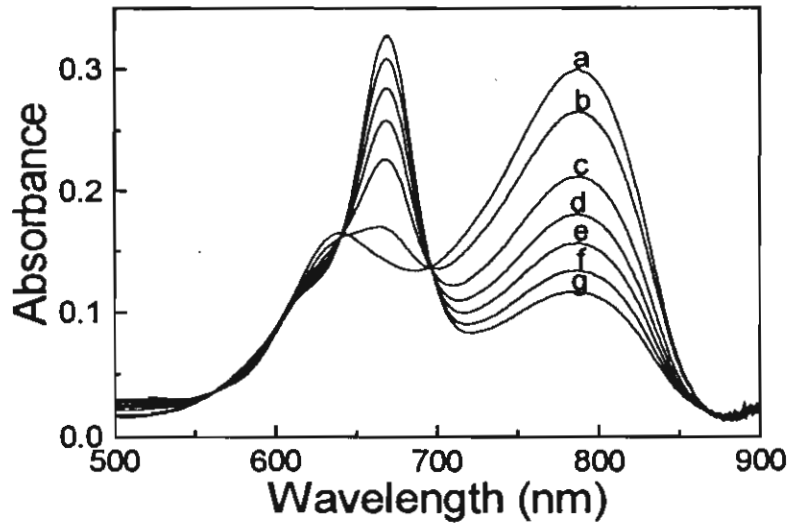

Figure 3.8. Effect of Hg^{2+} concentrations on the absorption spectrum of **10** (4.7 μM) in H_2O/CH_3CN (4:1) : [Hg^{2+}] (a) 0, (b) 3.33, (c) 5.55, (d) 6.65, (e) 7.76, (f) 8.87, (g) 9.98 μM.

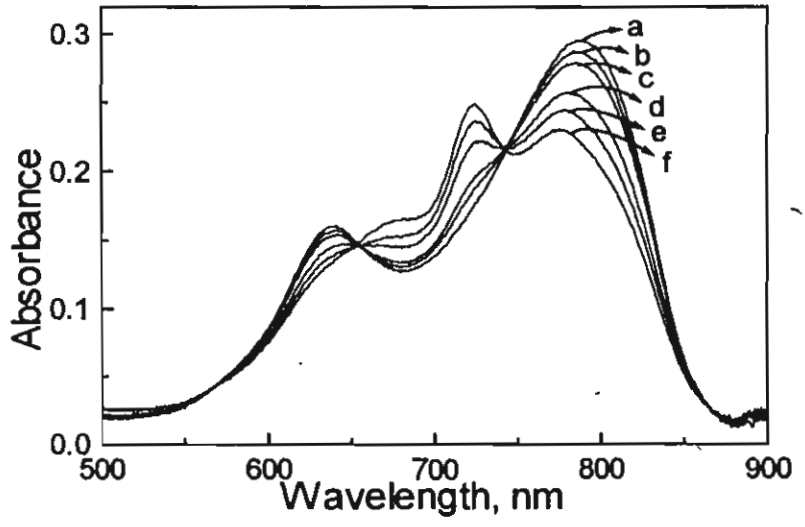

Figure 3.9. Effect of Pb^{2+} concentrations on the absorption spectrum of **10** (4.7 μM) in H_2O/CH_3CN (4:1) : [Pb^{2+}] (a) 0, (b) 22, (c) 44, (d) 133, (e) 222, and (f) 267 μM.

Table 3.3: Complexation properties of 10 with various transition metal cations

Solvent	Metal cation	λ_{max} (nm)	log K_s	Charge density	Detection limit
CH_3CN	-	783	-	-	-
CH_3CN	Cu^{2+}	705	4.97	-	nM
H_2O/CH_3CN (4:1)	-	790,640	-	-	-
H_2O/CH_3CN (4:1)	Cu^{2+}	670	5.19	2.778	nM
H_2O/CH_3CN (4:1)	Pb^{2+}	732	3.52	1.667	μM
H_2O/CH_3CN (4:1)	Mn^{2+}	720	2.87	2.500	μM
H_2O/CH_3CN (4:1)	Hg^{2+}	670	3.90	1.818	μM
H_2O/CH_3CN (4:1)	Zn^{2+}	718	-	2.703	mM

Although Hg^{2+} and Cu^{2+} complexes absorb at the same wavelengths, the differences in equilibrium constants for complex formation permit the analysis of nanomolar quantities of the latter even in the presence of micromolar quantities of the former. Determination of Cu^{2+} in the presence of Hg^{2+} using **10** in water-acetonitrile mixture (4:1) is shown in Figure 3.10. The absorption spectrum of **10** remained unaffected on addition of

up to 1.1 μM of Hg^{2+} (trace a, Figure 3.10). Whereas addition of even nanomolar quantities of Cu^{2+} (~50 nM) to the above solution containing 1.1 μM of Hg^{2+} (curve b) causes the decrease in the intensities of absorption band of the dye which is accompanied by the formation of the 670 nm band characteristic of Cu^{2+}-dye complex.

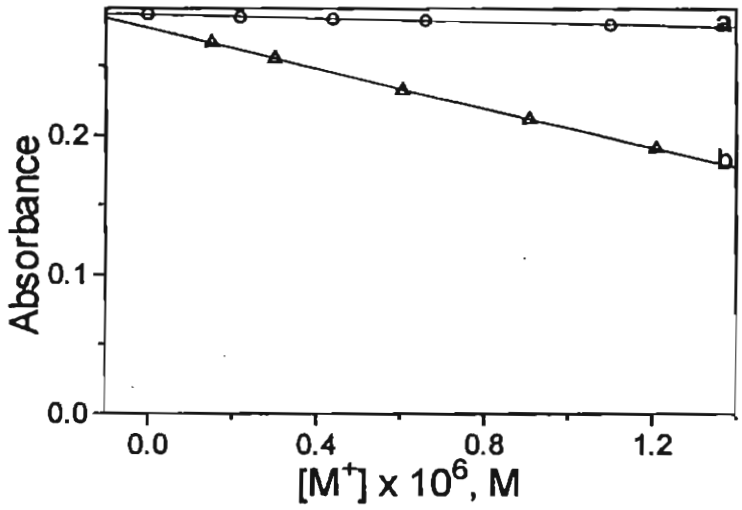

Figure 3.10. Determination of Cu^{2+} in the presence of Hg^{2+} using **10** (4.7 μM) in H_2O/CH_3CN (4:1) following the absorbance at 790 nm: (a) effect of addition of Hg^{2+} (upto 1.1 μM), (b) effect of addition of Cu^{2+} in presence of 1.1 μM of Hg^{2+}.

The complexation of the metal ion is assumed to take place at the O^- atoms of the central cyclobutane rings. In the anionic form of the dye **10**, the oxygen atoms of the two cyclobutane rings are ideally located to yield the suitable geometry for strong complexation with metal ions. The long wavelength absorption bands of the 1,3-disubstituted squaraine dyes are essentially due to an intramolecular charge transfer transition which is

primarily confined to the C_4O_2 unit.[31-33] The long wavelength absorption of the cationic dye is similar to those of the 1,3-disubstituted analogues, except that it is significantly red shifted. These transitions could arise out of similar intramolecular charge transfer transition, as reported for the earlier dyes. The large bathochromic shift observed in the case of **10** could be attributed to the extended conjugation present in its structure with respect to the disubstituted squaraine derivatives. On complexation with metal ions, a decrease in the intensity of the long wavelength band is accompanied by the formation of a blue shifted new band, in each case. Complexation of metal ions reduces significantly the electron donating property of the two oxygen atoms. The hypsochromic shift in the absorption spectra, upon complexation, can be attributed to a reduction in the electron donating ability of the O^- atoms on complexation by the metal ions.

3.4.5. Determination of Lanthanide Metal Cations

The cationic squaraine dye, **10** is capable of complexing with lanthanide metal cations present in aqueous media. To a solution of **10**, in water-acetonitrile mixture (4:1) the addition of nanomolar quantities of trivalent lanthanide metal cations resulted in significant changes in its absorption spectrum. The new band which is characteristic of the metal ion used appeared at shorter wavelengths. We have studied the complexation properties of representative lanthanide ions such as La^{3+}, Eu^{3+}, Gd^{3+}, Tb^{3+} and Lu^{3+}. The changes in the absorption spectra of **10** on addition of Eu^{3+} and Tb^{3+} are given in Figures 3.11 and 3.12, respectively. In general, on increasing the atomic number of lanthanide ion, the absorption maxima of the complex shifts towards the blue region and the stability constant slowly

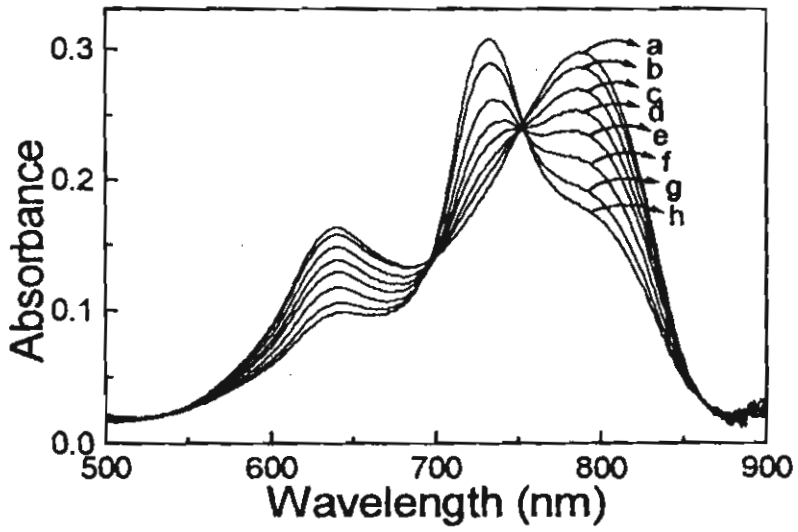

Figure 3.11. Effect of Eu^{3+} concentrations on the absorption spectrum of **10** (4.7 μM) in H_2O/CH_3CN (4:1) : [Eu^{3+}] (a) 0, (b) 0.11, (c) 0.34, (d) 0.57, (e) 0.91, (f) 1.36, (g) 1.82, (h) 2.28 μM.

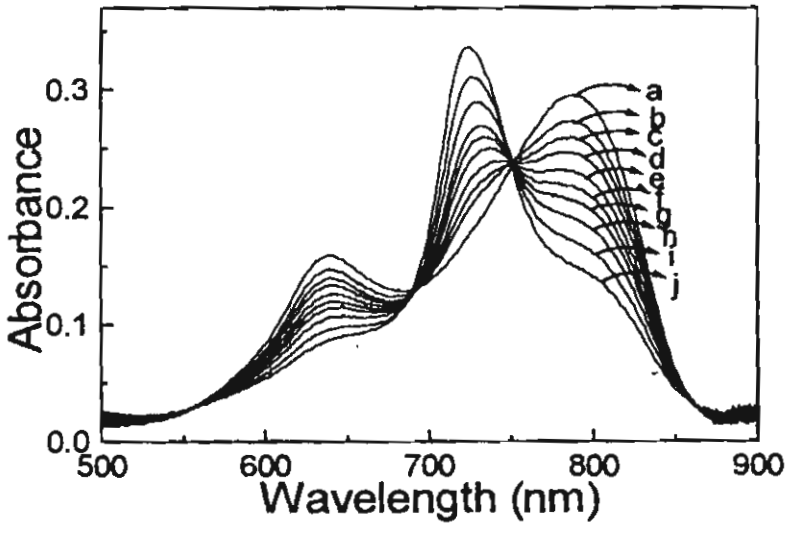

Figure 3.12. Effect of Tb^{3+} concentrations on the absorption spectrum of **10** (4.7 μM) in H_2O/CH_3CN (4:1) : [Tb^{3+}] (a) 0, (b) 0.44, (c) 0.88, (d) 1.32, (e) 1.76, (f) 2.20, (g) 2.64, (h) 3.52, (i) 5.29, (j) 8.80 μM.

decreases. For example, the λ_{max} of the La^{3+} complex is at 735 nm, Eu^{3+} is 733 nm, Gd^{3+} is 727 nm, and Tb^{3+} is 724 nm. But this observation is not true towards the end of the lanthanide series. For example the λ_{max} of the Lu^{3+} complex at 732 nm, which is higher than that observed for Tb^{3+} (724 nm). Among the lanthanide metal ions studied, the absorption maxima of the complexes are at different wavelengths (Table 3.4), which is characteristics of the metal ion used. Thus, it is possible to discriminate the various lanthanide ions by monitoring the λ_{max} of the complex.

These metal ion complexes are found to be substantially stable under the experimental conditions. It was observed that the pH of the solution remains unchanged after the addition of the final concentration of the

Table 3.4: Complexation properties of 10 with lanthanide metal cations

Solvent	Metal cation	λ_{max} (nm)	log K_a	Charge density	Detection limit
H_2O/CH_3CN (4:1)	-	790,640	-	-	-
H_2O/CH_3CN (4:1)	La^{3+}	735	5.90	2.953	nM
H_2O/CH_3CN (4:1)	Eu^{3+}	733	5.75	3.158	nM
H_2O/CH_3CN (4:1)	Gd^{3+}	727	5.44	3.198	nM
H_2O/CH_3CN (4:1)	Tb^{3+}	724	5.23	3.250	nM
H_2O/CH_3CN (4:1)	Lu^{3+}	732	5.24	3.529	nM

metal ions. Addition of strong acids such as trifluoroacetic acid resulted in the break-up of the dye-metal ion complexes and formation of the protonated form of the dye, indicating that the complexation process is reversible. Furthermore, it is evident that the deprotonated form of the cationic squaraine dye is the species which is involved in the metal ion complexation process.

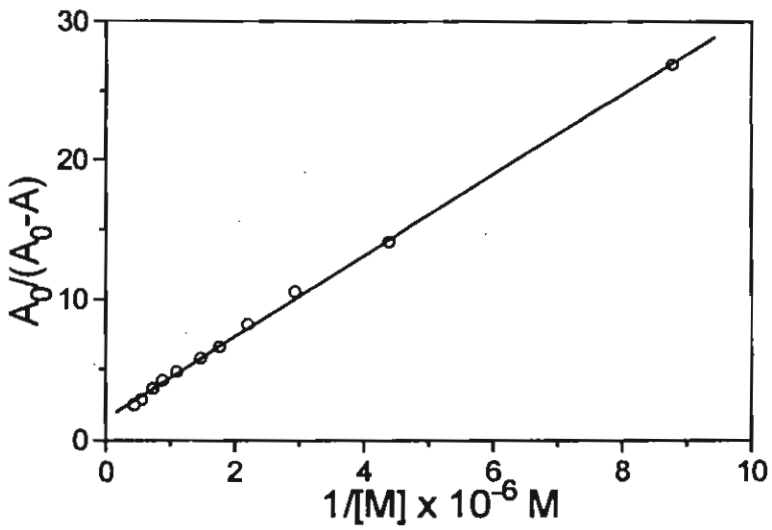

Figure 3.13. Plot of $A_0 / (A_0-A)$ versus reciprocal of Eu^{3+} concentration for the complexation of **10** with Eu^{3+} in water-acetonitrile mixture (4:1).

Benesi-Hildebrand analysis (Equation 1) of the absorption spectrum showed the formation of a 1:1 metal to ligand complexation in the case of lanthanides also. However, at higher concentrations of the metal ions (>1 μM), deviation of the curve from linearity was observed (Figures 3.13 and 3.14) which could probably be due to the formation of higher order

complexes. The equilibrium constants for the formation of complexes with various lanthanides are given in Table 3.4.

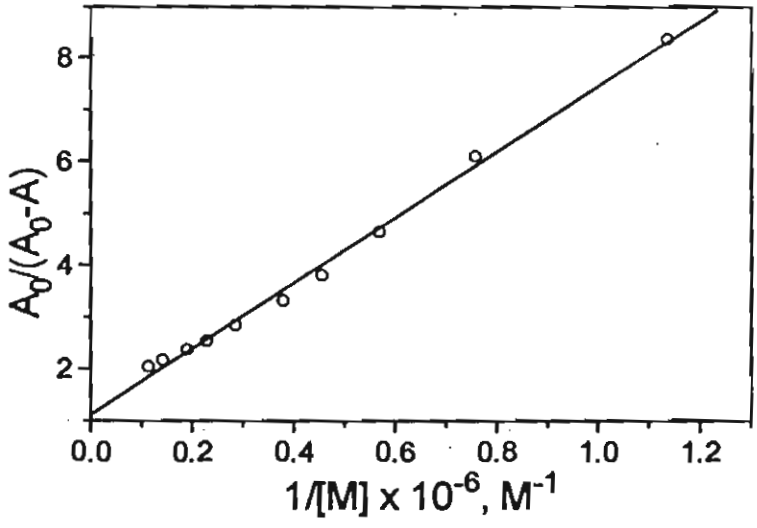

Figure 3.14. Plot of $A_0 / (A_0-A)$ versus reciprocal of Tb^{3+} concentration for the complexation of **10** with Tb^{3+} in water-acetonitrile mixture (4:1).

As discussed in Section 3.4.4, the complexation of the metal ion could be attributed to take place at the oxygen atoms of the central cyclobutane ring. Comparison of the shift in absorption maxima with charge density of the metal ions within the lanthanide series indicates that the hypsochromic shift does indeed increase with increasing charge density of the metal ion (Table 3.4). The ability of **10** to detect submicromolar quantities of rare earth metal cations in aqueous medium and its ability to discriminate among the various ions make it potentially useful in the qualitative and quantitative analysis of rare earth metal ions.

3.4.6. Detection of Transition Metal Ions Selectively in the Presence of Alkali and Alkaline Earth Metal Ions

An interesting property of the cationic squaraine dye is its ability to selectively complex various metal ions. Even high concentrations (millimolar) of alkali and alkaline earth metal cations do not affect the absorption spectrum of **10** in acetonitrile-water mixture (4:1) making it possible to detect transition and rare earth metal cations even in the presence of large amounts of alkali and alkaline earth metal cations. We have studied the complexation properties of **10** with copper and mercury ions in the presence of millimolar quantities of metal ions such as Li^+, Na^+, K^+ and Ca^{2+}. The presence of the latter did not affect the complexation properties of the cationic squaraine dye with the former. Plot a in Figure 3.15 shows the effect

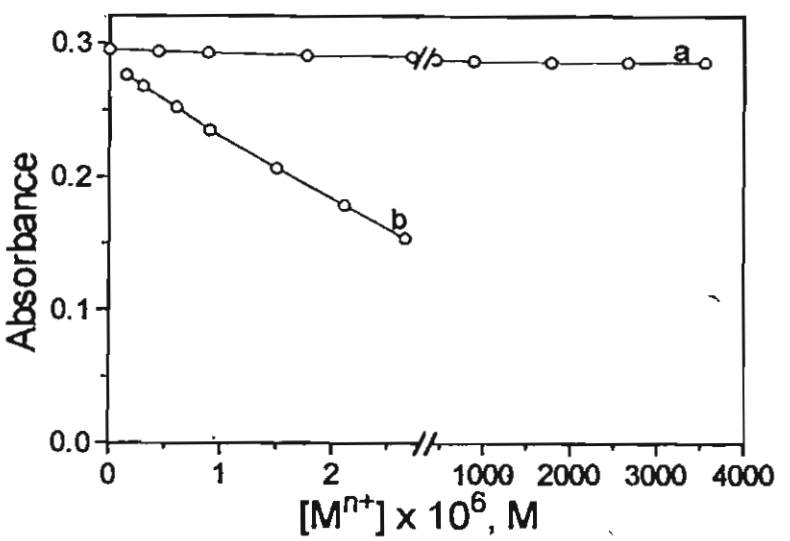

Figure 3.15. Determination of Cu^{2+} in the presence of Na^+ using **10** (4.7 μM) in H_2O/CH_3CN (4:1) following the absorbance at 790 nm: (a) effect of addition of Na^+ (upto 3.55 mM), (b) effect of addition of Cu^{2+} containing 3.55 mM of Na^+.

of addition of various concentrations of sodium chloride to a solution of **10** in water-acetonitrile (4:1) mixture. The absorption spectrum remains unchanged even by the addition of millimolar quantities of alkali metal ions. On addition of nanomolar quantities of Cu^{2+} to the solution containing 3.55 mM of Na^{+} (curve b, Figure 3.15) resulted in the formation of the blue shifted peak (670 nm), which is characteristic of the dye-copper complex. The detection limit remained unaffected by the presence of Na^{+}. Similarly, the detection of other transition metals and lanthanides is also possible in the presence of alkali and alkaline earth metal ions.

3.4.7. Detection of Copper ions (Cu^{2+}) in Acetonitrile Using 10

Since the dye exists in the protonated form in aprotic solvents with high fluorescence quantum yield, fluorescence spectroscopy can also be used for the detection of metal ions in nonaqueous media. In acetonitrile the absorption spectrum of **10** is sharp and intense with a maximum at 783 nm (Figure 3.16, curve a) and the emission band is centered at 812 nm with a fluorescence quantum yield of 0.31. Upon addition of trace amounts of copper perchlorate a substantial change in the absorption and fluorescence properties was observed. Addition of nanomolar quantities of Cu^{2+} ions to the solution leads to the formation of a characteristic new band at 705 nm (Figure 3.16). This can be attributed to the formation of a complex between Cu^{2+} and the ligand. Complexation of **10** with metal ions also leads to a reduction in the fluorescence yield of the dye (Figure 3.17). The changes in the absorption spectra are marked by a clear isosbestic point at 730 nm (Figure 3.16). The features of the Cu^{2+}-dye complex were analyzed using the Benesi-Hildebrand equation (Equation 1), assuming a 1:1 metal to

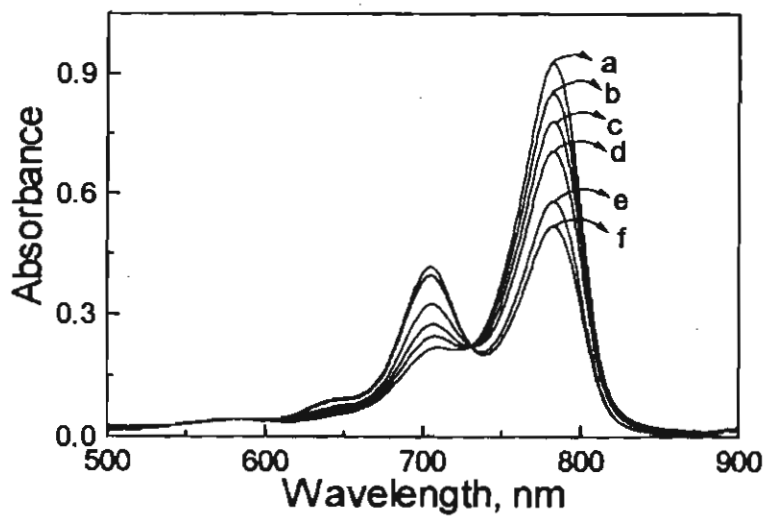

Figure 3.16. Effect of Cu^{2+} concentrations on the absorption spectrum of **10** (4.7 μM) in CH_3CN : [Cu^{2+}] (a) 0, (b) 0.32, (c) 0.64, (d) 1.9, (e) 2.5 and (f) 3.2 μM.

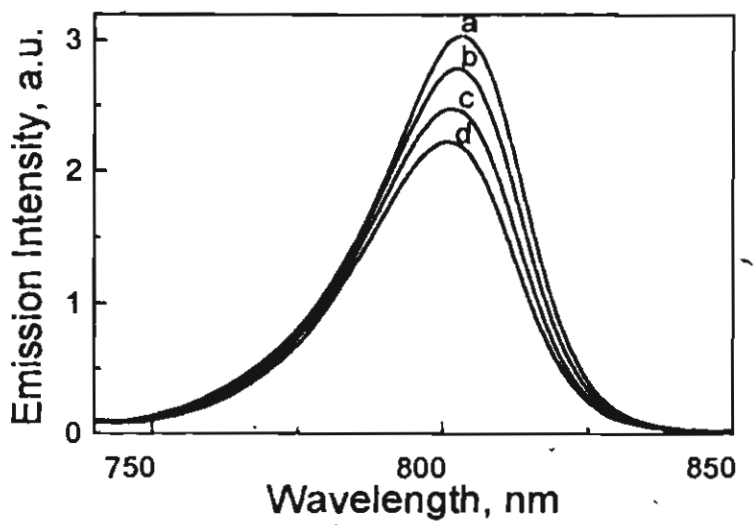

Figure 3.17. Effect of addition of Cu^{2+} ions on the fluorescence spectrum of **10**: [Cu^{2+}] (a) 0, (b) 0.64, (c) 1.9, (d) 3.2 μM.

ligand stoichiometry. A plot of $A_0/(A-A_0)$ versus the reciprocal concentration of copper ions gave a straight line (Figure 3.18). The equilibrium constant was calculated from the ratio of the intercept/slope as $9.3 \times 10^4\ M^{-1}$.

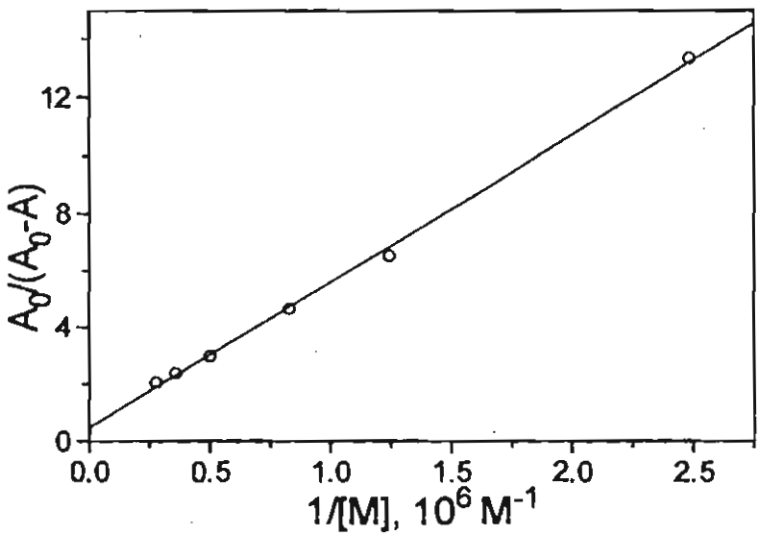

Figure 3.18. Plot of A_0 / (A_0-A) versus the reciprocal of Cu^{2+} concentration for the complexation of **10** with Cu^{2+} in CH_3CN.

The stability constant was determined using the Benesi-Hildebrand analysis of the emission data also, using the equation,

$$\frac{1}{\Phi_f^0 - \Phi_f} = \frac{1}{\Phi_f^0 - \Phi_f'}\left[\frac{1}{K_s\,[M]} + 1\right] \qquad (2)$$

where, Φ_f^0 is the fluorescence quantum yield of the free ligand, Φ_f is the observed fluorescence quantum yield, Φ_f' is that of the complex, M is the concentration of the metal ion used and K_s is the stability constant. The

value of K_s (9.3×10^4 M^{-1}) is the same as that obtained from the studies on the changes in the absorption of the dye on metal ion addition.

3.5. Conclusion

A detailed study of the photophysical and metal ion recognition properties of the cationic squaraine dye has been carried out. The cationic squaraine dye was found to exist in the protonated or deprotonated form, depending upon the pH of the solution. The pK_a of the dye was estimated as 4.9 in water-acetonitrile (4:1) mixture. The dye exists predominantly in the protonated form in organic aprotic solvents, whereas the deprotonated form predominates in water and other protic solvents. The protonated form of the dye was found to have a high fluorescence quantum yield. In dry acetonitrile, the quantum yield was found to be 0.31 which is reasonably high compared to other reported IR fluorescent dyes. The high fluorescence quantum yield of this dye has significant implications in the design of IR fluorescence probes for a number of biological and other applications. The singlet excited state of the dye showed a characteristic absorption band at 640 nm with a lifetime of 1.13 ns. Laser flash photolysis studies indicated the poor intersystem crossing efficiency of the dye. However, the triplet excited state produced by energy transfer using 1-pyrenecarboxaldehyde as sensitizer, showed a lifetime of 9 μs. Nanosecond laser flash photolysis studies indicated the photoionization of **10** via a biphotonic process.

The cationic squaraine dye binds several transition and lanthanide metal cations in aqueous solutions. The equilibrium constant and the maximum of the absorption band of the dye-metal ion complex is characteristic of the metal ion used. On complexation with metal cations blue shifted

bands are formed in the absorption spectrum. The detection limit for metal ions such as Cu^{2+} and lanthanides are found to be in the nanomolar range. The cationic squaraine dye does not complex with alkali and alkaline earth metal cations, facilitating the detection of transition and lanthanide metal cations even in the presence of large amounts of the former. Detection of the metal ions such as Cu^{2+} in acetonitrile is also possible using fluorescence measurements, since the dye is fluorescent in nature. These properties make the cationic squaraine dye highly suited for the quantitative analysis of trace metals present in various systems.

3.6. References

1. Emmelius, M.; Pawlowski, G.; Vollmann, H. W. *Angew. Chem. Int. Ed. Engl.* **1989**, *28*, 1445.
2. Fabian, J.; Zahradnik, R. *Angew. Chem. Int. Ed. Engl.* **1989**, *28*, 677.
3. Thompson, R. B. in *Fluorescence Spectroscopy, Vol. 4: Probe Design and Chemical Sensing*, Lakowicz, J. (Ed): Plenum Press, New York, **1994**, p 151.
4. Demas, J. N.; De Graff, B. A. in *Topics in Fluorescence Spectroscopy, Vol. 4: Probe Design and Chemical Sensing*, Lakowicz, J. R. (Ed.): Plenum Press, New York, **1994**, p 71.
5. Casay, G. A.; Shealy, D. B.; Patonay, G. in *Topics in Fluorescence Spectroscopy, Vol. 4: Probe Design and Chemical Sensing*, Lakowicz, J. R. (Ed.): Plenum Press, New York, **1994**, p 183.
6. Schafer, F. P. in *Dye Lasers*, Springer-Verlag, New York , **1982**.
7. Maeda, M. In *Laser Dyes: Properties of Organic Compounds for Dye Lasers*, Academic Press, New York, **1984**.
8. Drexhage, K. H. in *Dye Lasers*, 3rd Ed., Schafer, F. P. (Ed.): Springer-Verkag, New York, **1990**, p 155.
9. Terpetschnig, E.; Lakowicz, J. R. *Dyes and Pigments*, **1993**, *21*, 227.
10. Hougland, R.P. In *Handbook of Fluorescence Probes and Research Chemicals*, 5th Ed., Molecular Probes, Eugene, Oregon, **1992**.
11. Soper, S. A.; Mattingly, Q. L.; Vegunta, P. *Anal. Chem.* **1993**, *65*, 740.
12. Soper, S. A.; Mattingly, Q. L. *J. Am. Chem. Soc.* **1994**, *116*, 3744.
13. Waring, D. R.; Hallas, G. *The Chemistry and Application of Dyes*, Plenum Press, New York, **1990**.

Greenspan, P.; Fowler, S. D. *Kodak Lab. Chem. Bull.* **1985**, *56*, 1.

Rauhut, M. M.; Roberts, B. G.; Maulding, D. R.; Bergmark, W.; Coleman, R. *J. Org. Chem.* **1975**, *40*, 330.

Fabian, J. G.; Nakazumi, H.; Matsuoka, M. *Chem. Rev.* **1992**, *92*, 1197.

Fluorescent Chemosensors for Ion and Molecule Recognition; Czarnik, A. W., Ed.; ACS Symposium Series 538: Washington DC, 1993;

Bisell, R. A.; de Silva, A. P.; Gunaratne, H. Q. N.; Lynch, P. L. M.; Maguire, G. E. M.; Sandanayake, K. R. A. S. *Chem. Soc. Rev.* **1992**, 187.

Fabbrizzi, L.; Poggi, A.; *Chem. Soc. Rev.* **1995**, 197.

Czarnik, A. W. *Acc. Chem. Res.* **1994**, *27*, 302.

Walkup, G. K.; Imperiali, B. *J. Am. Chem. Soc.* **1996**, *118*, 3053.

Czarnik, A. W. *Chem. Bio.* **1995**, *2*, 423.

Sasaki, D. Y.; Shnek, D. R.; Pack, D. W.; Arnold, F. H.; *Angew. Chem. Int. Ed. Engl.* **1995**, *34*, 905.

Fabbrizzi, L.; Licchelli, M.; Pallavicini, P.; Perotti, A.; Sacchi, D.; *Angew. Chem. Int. Ed. Engl.* **1994**, *33*, 1975.

Das, S.; Thomas, K. G.; Thomas, K. J.; Kamat, P. V.; George, M. V. *J. Phys. Chem.* **1994**, *98*, 9291.

Das, S.; Thomas, K. G.; Thomas, K. J.; George, M. V.; Bedja, I.; Kamat, P. V. *Anal. Proc.* **1995**, *32*, 213.

Terpetschnig, E.; Szmacinski, H.; Ozinskas, A.; Lakowicz, J.R. *Anal. Biochem.* **1994**, *217*, 197.

Nakazumi, H.; Natsukawa, K.; Nakai, K.; Isagawa, K.; *Angew. Chem. Int. Ed. Engl.* **1994**, *33*, 1001.

Benson, R. C.; Kues, H. *J. Chem. Eng. Data* **1977**, *22*, 379.

30. These studies were carried out by Dr. P. V. Kamat at the Notre Dame Radiation Laboratory, USA.

31. Bigelow, R. W.; Freund, H.-J. *Chem. Phys.* **1986**, *107*, 159.

32. Law, K. Y. *J. Phys. Chem.* **1987**, *91*, 5184.

33. Kamat, P. V.; Das, S.; Thomas, K. G.; George, M. V. *J. Phys. Chem.* **1992**, *96*, 195.

34. Sauve, G.; Kamat, P. V.; Thomas, K. G.; Thomas, K. J.; Das, S.; George, M. V. *J. Phys. Chem.* **1996**, *100*, 2117.

35. Rao, T. P.; Sukumar, R. *Anal. Lett.* **1986**, *19*, 1731.

36. Scarminio, I.; Kubista, M. *Anal. Chem.* **1993**, *65*, 409.

CHAPTER 4

SYNTHESIS AND PHOTOPHYSICAL STUDIES OF WATER SOLUBLE SQUARAINES CONTAINING CARBOXYLIC GROUPS

4.1. Abstract

Two new water soluble squaraine dyes, bis[3(*p*-carboxybenzyl)benzothiazol-2-ylidene]squaraine (**7**) and bis[3(carboxymethyl)benzothiazol-2-ylidene]squaraine (**8**) have been synthesized and characterized. The photophysical properties of these dyes have been studied in detail. Both **7** and **8** form dimer aggregates in water which have absorption bands, blue shifted to those of the monomeric forms. These dyes have a stronger tendency to form aggregates in D_2O than in H_2O. In the presence of low concentrations ($< 3 \times 10^{-4}$ M) of polyvinylpyrrolidone (PVP), enhancement in aggregate formation of **7** was observed, whereas **8** remains unaffected under these conditions. Addition of higher concentrations ($> 3 \times 10^{-4}$ M) of PVP leads to the disruption of the aggregate and formation of a new species with absorption bands, red shifted to those of the corresponding monomers. An enhancement in fluorescence quantum yield was also observed along with this process. The nature of these interactions have been investigated. Addition of β-cyclodextrin or cetyltrimethylammonium bromide (CTAB) above its critical micellar concentration also leads to an enhancement in fluorescence quantum yield of these dyes. It is proposed that hydrophobic interaction between the chromophoric units is the main driving force for the

formation of the blue-shifted sandwich type aggregates in water. The red-shifted species were attributed to the monomeric forms, microencapsulated in a hydrophobic environment provided by PVP. Picosecond laser flash photolysis studies of the aggregates show clear evidence for the break-up of the aggregate from the excited state to yield an excited state-ground state monomer pair which rapidly recombine to form the ground state dimer.

4.2. Introduction

Aggregation is a phenomenon observed for many organic compounds including dyes[1-4] such as xanthene, methylene blue, certain cyanines, and crystal violet. It is frequently encountered in crystals and in organized media such as Langmuir-Blodgett (LB) films where the close packing of chromophores with certain favoured orientations leads to strong coupling of the interacting dipoles and distinct changes in spectral and photophysical properties.[5-7] Eventhough the molecules are situated away from each other, aggregation is observed for certain dyes in the solution state also.[8,9] Based on the orientation of the dipoles and the spectral features, aggregates can be classified into two types, H-type and the J-type aggregates. The H-aggregate is characterized by a head-to-head (sandwich type) orientation of the transition dipole and a blue shift in the electronic transition, compared to the monomer.[10] A head-to-tail transition dipole arrangement and a red shift in the absorption band are the characteristic features of J-aggregates.[11-13] Since aggregation modifies the absorption spectrum and photophysical properties of a dye, which affects its ability to emit at a certain wavelength or to act as a photosensitizer,[9] it has fundamental

consequences in applications in areas as diverse as in photographic technology, tunable lasers, fluorescence depolarization diagnostic devices, and photomedicine.[14]

Absorption and emission spectroscopy are the techniques most widely used to study aggregation of complex organic molecules in aqueous solution since spectral shifts, nonconformity with Beer-Lambert's law, and fluorescence quenching at high concentrations are all indicative of second-order spectroscopic interference between dye chormophores. The strength of the aggregation between two or more dye molecules depends on the structure of the dye, the solvent, the temperature, and the presence of electrolytes. Various mechanisms have been proposed to explain the driving force of aggregation. These forces include van der Waals interactions, intermolecular hydrogen bonding, hydrogen bonding with the solvent, and coordination with metal ions.[9] The spectral features of dye aggregates have been correlated with its structure in the exciton theory by Kasha and Hochstrasser,[15,16] and by Kuhn and co-workers.[17,18] The theory put forward by the latter generally gives better agreement with the experimental observations. According to exciton theory[19], the splitting of the excited state is a consequence of the two possible arrangements (in-phase and out-of-phase oscillation) of the transition dipoles of the chromophores in the dimer. The interaction energy between the chromophores is a function of the transition moment of the monomer, the angle and distance between the transition dipoles. Transition from the ground state to any one of the split excited states is determined by the geometry of the dimer.

There have been several reports on the photophysics and photochemistry of various dye aggregates in solution. The aggregation behaviour of rhodamine 6G (Chart 1) has been studied by many research groups because of its applications in tunable lasers.[9,20,21] Formation of aggregates decreases its emission intensity due to nonradiative decay. Aggregation of rhodamine

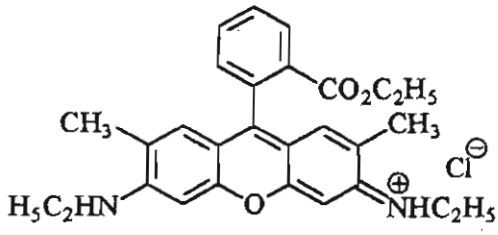

1

Rhodamine 6G

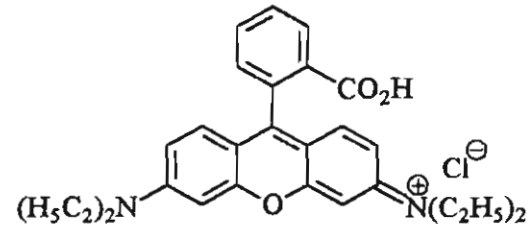

2

Rhodamine B

Chart 1

6G is a function of its concentration and it occurs in both aqueous and organic solvents. In water the aggregation process was reported to be exothermic (ΔH ~-6.9 kcal mol^{-1}) and H-aggregates were formed.[20] However, in ethanol the dimer spectrum was red shifted with respect to the monomer indicating the formation of J-type aggregates.[21] Furthermore, according to Ruiz-Ojeda et al.[21] dimerization in ethanol was endothermic with an enthalpy of 9.3 kcal mol^{-1}. Aggregation in ethanol involves breaking of two hydrogen bonds between ethanol and the monoethylamino groups of rhodamine 6G and formation of one hydrogen bond between the monoethylamino groups. This interpretation is consistent with the different geometries observed for the dimer in water and ethanol.

Several research groups have extensively studied the aggregation properties of rhodamine B in aqueous as well as in organic solutions.[9] It has been generally observed that H-aggregates were formed in water. Hydrophobic interactions and hydrogen bonding were proposed to be the driving forces of the aggregation in aqueous solutions. Levschin et al.[22] have reported that aggregates were not detectable in ethanol and other organic solvents up to rhodamine B concentration of 5×10^{-3} M. However, Selwyn and Steinfeld find aggregation in ethanol and ether-pentane-alcohol (EPA) to be stronger than in water.[23] The absorption band of the dimer in these solvents was red shifted as compared to the monomer band, indicating that the geometry of the dimer in the organic solvents is different from that obtained in aqueous solution. From these studies they concluded that dimerization of rhodamine B in EPA is driven exclusively by dispersion forces whereas hydrogen bonding with solvent molecules plays an important role in the association in ethanol.

Fluorescein and its derivatives are another class of dyes that undergo aggregation in solution. The existence of trimers and higher aggregates in aqueous solution have also been reported for fluorescein, eosin and erythrosin[9] (Chart 2). Detailed studies by Rohatgi and co-workers[24,25] on the aggregation properties of a series of halofluorescein dyes have showed that the tendency to aggregate increases with increasing halogen substitution and also with the presence of more polarizable halogens. It is worth noting that the dimerization constants for these dyes in ethanol and glycerol were similar to those obtained in water indicating that similar forces are involved in all these solvents.[9] The good correlation with the

polarizability of the halogens suggests that hydrophobic forces play an important role in the association process. Based on these studies they concluded that association of fluorescein in aqueous solution is mediated by hydrogen bonding with the water molecules.

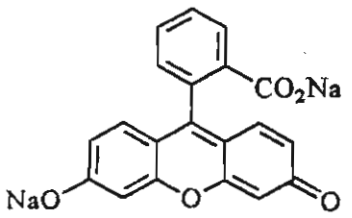

3
Fluorescein

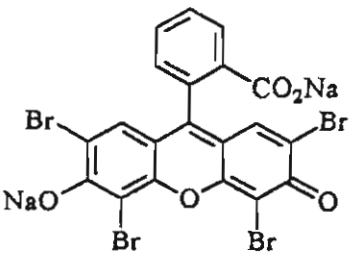

4
Eosin

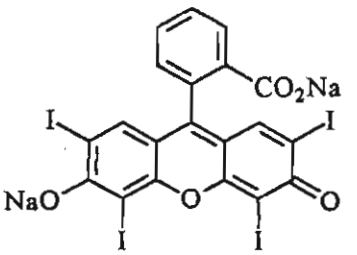

5
Erythrosin

Chart 2

Neckers and co-workers have studied the aggregation processes of Rose Bengal dyes (Chart 3) extensively.[9] They observed that in aqueous solutions, Rose Bengal ethyl ester exists as a monomer[8,9] up to a concentration of 3×10^{-5} M. Addition of salts such as potassium nitrate significantly changes the shape of the absorption spectrum. This process was attributed to the aggregate formation induced by the cations. Based on the analysis of the spectral changes with ionic strength and dye concentration, they have suggested a mechanism for aggregation, which involves coordination between the metal cation and the xanthene chromophore. It has also been observed that the equilibrium constant increases moderately with the polarizability of the cation. However, this effect was not pronounced and they have concluded that the dimerization step is driven mainly by the hydrophobicity of the dye. Later, the same authors have studied the

intramolecular aggregation properties of Rose Bengal by connecting two dye units through a methylene chain.[9] They have observed that the stability of the aggregate formed does not increase or decrease monotonically with the length of the methylene chain.

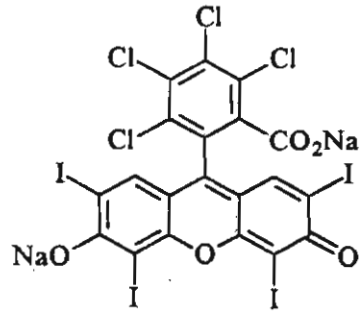

6

Rose Bengal

Chart 3

Squaraines are capable of forming different types of aggregates depending on the structure and the surrounding medium (see Section 1.6). Although there are a few reports on the aggregation behaviour of certain squaraine dyes, [26-34] the diverse consequences of the aggregation process demand more fundamental knowledge. We have synthesized two new water soluble squaraine dyes with carboxylic functional groups. This Chapter of the thesis describes the synthesis and characterization, photophysical and aggregation properties of **7** and **8** (Chart 4) in purely aqueous media. The effect of adding polyvinylpyrrolidone, β-cyclodextrin and micelles on the photophysical and aggregation properties of **7** and **8** are also reported.

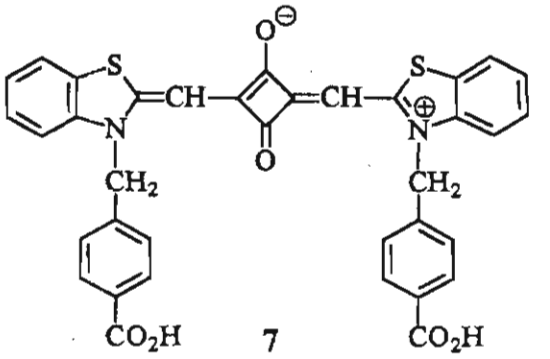

7

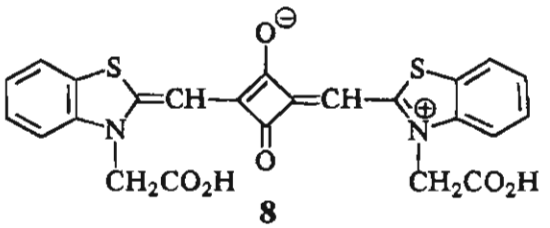

8

Chart 4

4.3. Experimental Section

4.3.1. Materials and Methods

Polyvinylpyrrolidone (Mol. Wt. ~44,000) obtained from SD Fine Chemicals (Bombay) was further purified by dissolving it in chloroform and reprecipitating with hexane, followed by repeated washings with hexane.

All melting points are uncorrected and were determined on a Aldrich MEL-TEMP apparatus. IR spectra were recorded on a Perkin-Elmer Model 882 IR spectrometer and the UV-visible spectra on a Shimadzu 2100 spectrometer or on a GBC UV-VIS 918 spectrophotometer. ^{1}H and ^{13}C NMR spectra were recorded on either a Varian 300 MHz or a JEOL EX-90 FT-NMR spectrometer. Mass spectra were recorded on a JEOL AX 505 HA

mass spectrometer. Emission spectra were recorded on a SPEX Fluorolog F112X spectrofluorimeter. Quantum yields of fluorescence were measured by the relative method using optically dilute solutions with bis[4-(dimethylamino)-2-hydroxyphenyl]squaraine ($\Phi_f = 0.84$)[35] as reference. The changes in absorptivity on addition of PVP, β-CD and CTAB have been taken into account for all quantum yield measurements and the solutions were excited at 590 nm where these changes are minimum. Polymer concentrations are expressed in terms of monomer units. All the experiments in aqueous solutions were carried out at pH 8.0, which was obtained by adding the appropriate amount of KOH.

Picosecond laser flash photolysis experiments[36] were performed with 355-nm or 532-nm laser pulses from a mode-locked, Q-switched Quantel YG-501 DP Nd:YAG laser system (see Section 2.3.2 for details). All the lifetimes and rate constants reported in this study have an experimental error of ± 5%. Because of the instability of the dye to laser excitation, the dye solution was continuously flowed through the sample cell.

4.3.2. Synthesis of 3-(*p*-Carboxybenzyl)-2-methylbenzothiazolium Bromide

3-(*p*-Carboxybenzyl)-2-methylbenzothiazolium bromide was synthesized[37] by heating a mixture of 2-methylbenzothiazole (1.32 g, 8.8 mmol) and *p*-bromomethylbenzoic acid (1.90 g, 8.8 mmol) for 15 h. The product was recrystallized from methanol to give 1.28 g (40 %), of a pure sample, mp 265 °C; IR ν_{max} (KBr) 3600-3200 (CO_2H), 1704, 1434, 1384, 1236, 765 cm^{-1}; ^1H NMR (CD_3OD) δ 3.3 (3 H, s, CH_3), 6.2 (2 H, s, CH_2), 7.2-7.5 (2 H, d, aromatic), 7.75-8.5 (6 H, m, aromatic); ^{13}C NMR (DMSO-d_6)

δ 178.83, 167.25, 141.18, 137.66, 131.21, 130.41, 130.11, 129.48, 128.77, 127.48, 125.04, 117.25; Anal. Calcd for $C_{16}H_{14}NO_2SBr$: C, 52.76; H, 3.87; N, 3.85; found: C, 52.57; H, 3.85; N, 4.33; HRMS, exact mol wt calcd for $(C_{16}H_{14}NO_2S)^+$, 284.0745; found, 284.0735 (FAB high resolution mass spectrometry).

4.3.3. Synthesis of 3-(Carboxymethyl)-2-methylbenzothiazolium Bromide

3-(Carboxymethyl)-2-methylbenzothiazolium bromide was synthesized[37] by heating a mixture of 2-methylbenzothiazole (1.49 g, 10 mmol) and bromoacetic acid (1.39 g, 10 mmol) for 5 h. The product was recrystallized from methanol to give 2.0 g (70%), of a pure product, mp 218 °C; IR ν_{max} (KBr) 3600-3200 (CO_2H), 1740, 1444, 1248, 767 cm^{-1}; ^1H NMR (CD_3OD) δ 3.3 (3 H, s, CH_3), 5.75 (2 H, s, CH_2), 7.8-8.5 (4 H, m, aromatic); ^{13}C NMR (CD_3OD) δ 180.86, 168.18, 143.57, 132.02, 130.92, 130.65, 126.28, 118.24, 52.66; Anal. Calcd for $C_{10}H_{10}NO_2SBr$: C, 41.68; H, 3.50; N, 4.86; found: C, 41.29; H, 3.90; N, 5.35; HRMS, exact mol wt calcd for $(C_{10}H_{10}NO_2S)^+$, 208.0432, found: 208.0453 (FAB high resolution mass spectrometry).

4.3.4. Synthesis and Characterization of 7 and 8

Squaraine dyes **7** and **8** were synthesized by refluxing the appropriate 2-methylbenzothiazolium bromide (2 mmol) and squaric acid (1 mmol) in a solvent mixture containing 5 mL of benzene and 7 mL of *n*-butanol, in presence of quinoline (2 g, 23 mmol) accompanied by azeotropic distillation of water. Purification was carried out by repeated washing with boiling methanol to give a 10 % yield of

bis[3(*p*-carboxybenzyl)benzothiazol-2-ylidene]squaraine, **7**, mp 315 °C (decomp). The dye **8** was purified by repeated washings with chloroform, followed by methanol to give a 20% yield of a pure sample, mp 235 °C.

Analytical results and spectral data are given below.

7: mp 315 °C (decomp); IR ν_{max} (KBr) 3600-3200 (CO_2H), 1707 (CO), 1550, 1460, 1428, 1242 cm^{-1}; UV λ_{max} (H_2O, pH = 8) 645 nm (ε 190,000 M^{-1} cm^{-1}); ^1H NMR (DMSO-d_6) δ 5.66 (4 H, s, CH_2), 5.76 (2 H, s, CH), 7.23-7.96 (16 H, m, aromatic); Anal. Calcd for $C_{36}H_{24}N_2S_2O_6$: C, 67.07; H, 3.75; N, 4.34; S, 9.94. found: C, 66.95; H, 3.93; N, 4.33; S, 9.69; HRMS, exact mol wt calcd for $C_{36}H_{25}N_2S_2O_6$ $(M+H)^+$ 645.1154; found 645.1131 (FAB high resolution mass spectrometry).

8: mp 235 °C (decomp); IR ν_{max} (KBr) 3600-3200 (CO_2H), 1734, 1658, 1565, 1459, 1430, 1351, 1262 cm^{-1}; UV λ_{max} (H_2O, pH = 8) 641 nm (ε 1,70,000 M^{-1} cm^{-1}); ^1H NMR (DMSO-d_6) δ 5.12 (4 H, s, CH_2), 5.67 (2 H, s, CH), 7.23-7.87 (8 H, m, aromatic); Anal. Calcd for $C_{24}H_{16}N_2S_2O_6$: C, 58.53; H, 3.27; N, 5.69; S, 13.02. found: C, 58.10; H, 3.66; N, 5.60; S, 12.77; HRMS, exact mol wt calcd for $C_{24}H_{16}N_2S_2O_6(M+H)^+$ 493.0528; found 493.0522 (FAB high resolution mass spectrometry).

4.4. Results and Discussion

4.4.1. Acid-Base Equilibria of 7 and 8

It has been observed that the photophysical properties of **7** and **8** are highly sensitive to the pH of the medium. The protonation-deprotonation process leads to changes in the absorption spectra of **7** and **8**. In acidic

medium (pH < 6.0), the squaraine dye 7 shows an absorption band in the range of 500-750 nm region with a maximum around 565 nm. On increasing the pH by the addition of base (KOH) to this solution formation of a sharp band centered at 645 nm was observed. These spectral changes were marked by the presence of an isosbestic point at 595 nm (Figure 4.1).

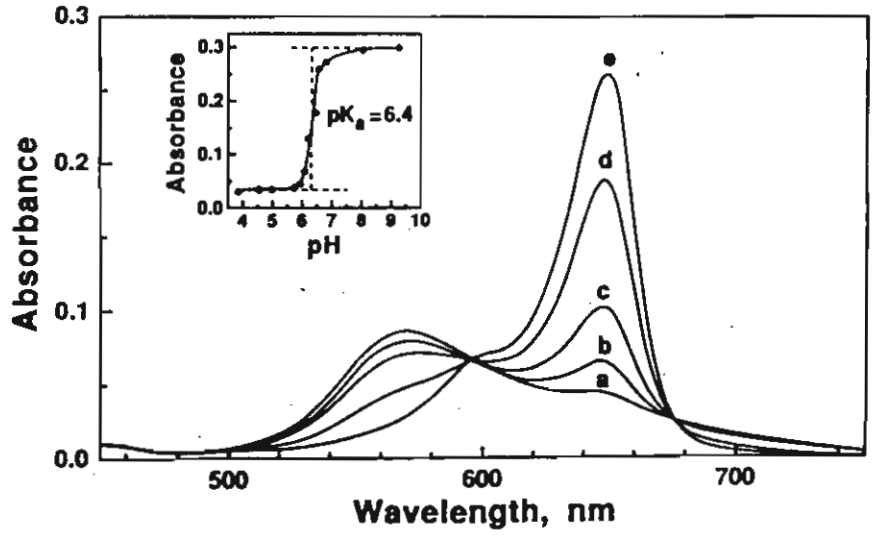

Figure 4.1.Effect of pH on the absorption spectrum of 7 (1.4 μM) in aqueous medium at 300 K. pH (a) 5.93, (b) 6.11, (c) 6.18, (d) 6.37 and (e) 6.72. Inset shows the plot of absorbance at 645 nm versus pH.

A plot of the absorbance at 645 nm versus pH indicated a single protonation-deprotonation equilibrium for 7, with a pK_a of 6.4 (inset, Figure 4.1). The pK_a of 6.4 of 7 probably corresponds to the deprotonation at the ring nitrogen since pK_a for deprotonation of the carboxylic group would not be expected to be much different from 4.2, reported for benzoic acid.

The squaraine dye **8** also exhibits similar acid-base equilibrium properties. In acidic medium (pH < 4.4), the absorption band of **8** is very broad in the range of 550-750 nm (Figure 4.2). On increasing the pH of the solution, a sharp intense band develops at 641 nm. The extinction coefficient of this band has been estimated as 170,000 M^{-1} cm^{-1}. A plot of absorbance at 640 nm against the pH of the solution showed the presence of two distinct protonation-deprotonation equilibria (inset, Figure 4.2). From

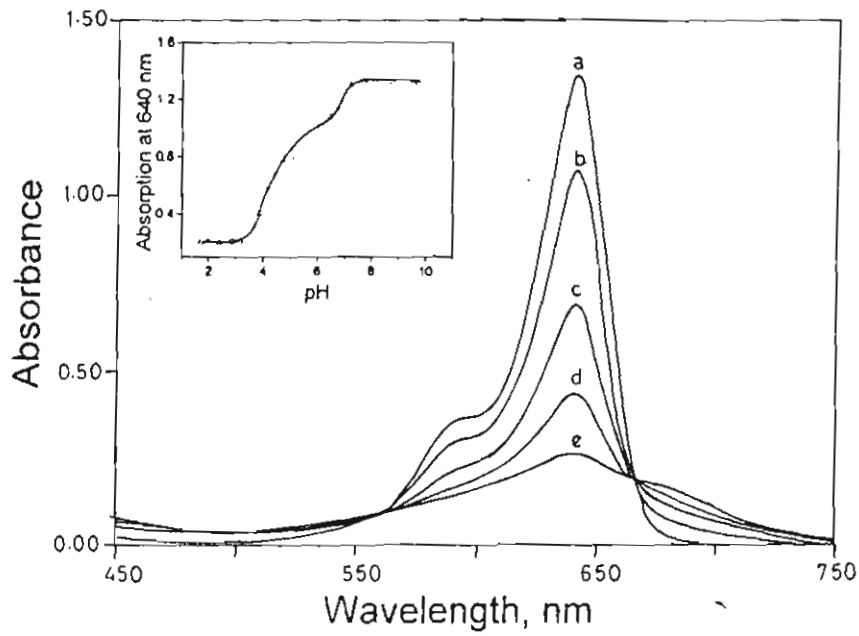

Figure 4.2. Effect of pH on the absorption spectrum of **8** (8 μM) in aqueous medium at 300 K. pH (a) 9.7, (b) 6.49, (c) 4.50, (d) 3.89 and (e) 3.43. Inset shows the plot of absorbance at 640 nm versus pH.

this plot, the pK_a values were estimated as 6.7 and 4.4. The pK_a observed at 6.7 can be assigned to the deprotonation of the benzothiazole ring nitrogen and the one at 4.4 to the deprotonation of the carboxylic groups.

In the case of the squaraine dye **8**, the carboxylic group is in close proximity to the chromophore and hence protonation/deprotonation at this site can influence the absorption spectrum of the dye.

4.4.2. Absorption and Emission Properties of 7 and 8

The squaraine dyes 7 and 8 were found to be soluble only in protic solvents (in presence of base) and in highly polar solvents such as DMF and DMSO. The absorption and emission properties of 7 and 8 have been studied in these solvents and are summarized in Table 4.1. In protic solvents,

Table 4.1: Absorption and emission properties of 7 and 8 in different solvents

Solvent	7		Φ_f	8		Φ_f
	λmax (nm)			λmax (nm)		
	Abs	Em		Abs	Em	
Water*	645	659	0.027	641	658	0.03
Methanol*	656	673	0.17	650	667	0.12
Trifluoroethanol*	642	657	0.19	640	657	0.10
Methoxyethanol*	663	679	0.38	659	675	0.20
DMSO	679	702	0.32	667	687	0.14
DMF	678	693	0.28	676	691	0.16

* In presence of KOH (~10^{-4} M)

hypsochromic shifts in the absorption and emission maxima and a decrease in Φ_f with increasing hydrogen bonding ability of the solvent were observed which are similar to those reported for some bis(benzothiazolylidene)-squaraines.[38] These effects have been attributed to hydrogen bonding of the oxygen atoms of the central cyclobutane ring with solvent molecules. The strength of such interactions are expected to depend upon the relative acidity of the alcohols. The electron density at the oxygen site will be strongly reduced on changing from the ground to the excited singlet state. Such a change will weaken the hydrogen bond between the alcohol and the excited state of the dye. However, in aprotic polar solvents such as DMF and DMSO the spectra were considerably red-shifted and the fluorescence quantum yield was relatively higher (Table 4.1).

4.4.3. Aggregation Properties of 7 and 8 in Water

It has been observed that the absorption bands of these dyes in water are highly dependent on the concentration and temperature of the solution. At very low concentrations ($< 10^{-6}$ M) the absorption spectrum of 7 showed a sharp band at 645 nm with an extinction coefficient of 190,000 M^{-1} cm^{-1}. With increasing concentration of 7 ($>10^{-6}$ M), a new band develops at 595 nm and the relative intensity of this band increases with decrease in temperature (Figure 4.3). Figure 4.4 shows the absorption spectra measured for different concentrations of 7 in water, at 280 K. At higher concentrations, the intensity of the 595 band went up significantly and became more intense than the 645 nm band, suggesting that this band is due to the formation of aggregates.

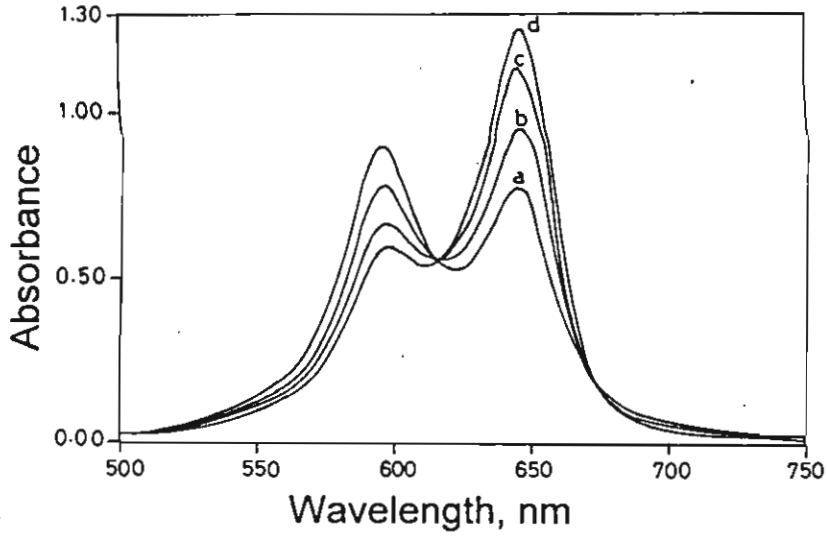

Figure 4.3. Absorption spectrum of 7 (12 μM) in water at temperatures: (a) 280, (b) 291, (c) 301 and (d) 308 K.

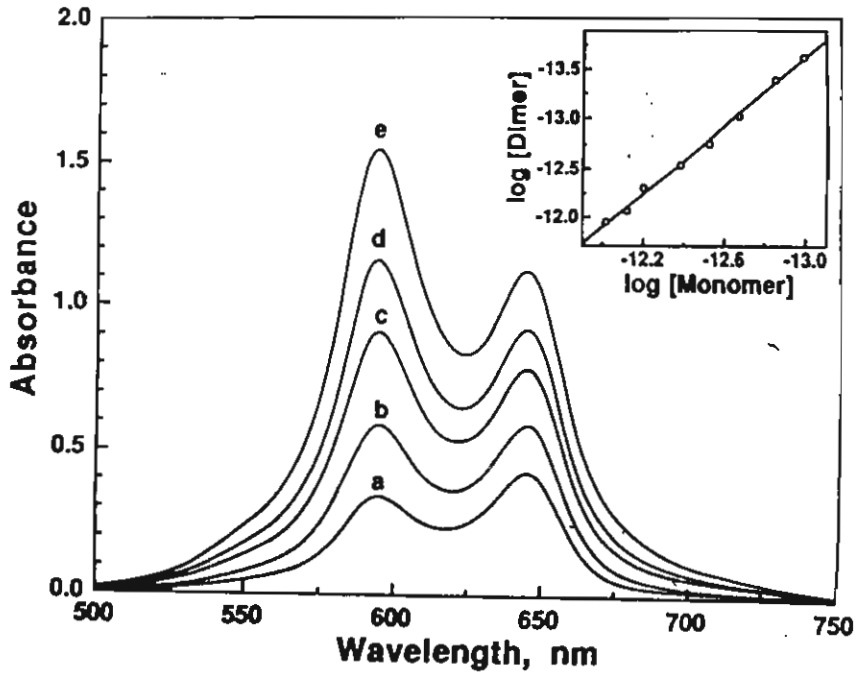

Figure 4.4. Absorption spectra of 7 in water at 280 K: [7] (a) 4.73,(b) 7.57, (c) 11.35, (d) 14.19 and (e) 18.92 μM. Inset shows the plot of log [dimer] versus log [monomer] for solutions of 7 in water at 280 K.

The squaraine dye **8** also shows similar behaviour in aqueous media. At low concentrations (< 10^{-6} M), **8** exhibits a sharp intense band at 641 nm with an extinction coefficient of 170,000 M^{-1} cm^{-1}. With increasing concentration (Figure 4.5), a new band was formed at 590 nm. As in the case of **7**, the newly formed band was found to be temperature and concentration dependent with an extinction coefficient of 340,000 M^{-1} cm^{-1}, suggesting that the band is due to the formation of aggregates.

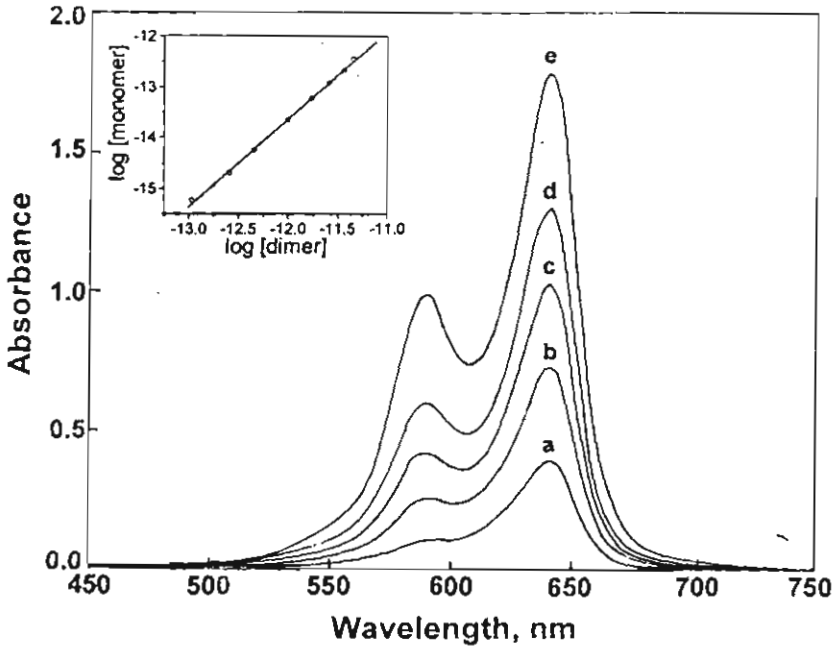

Figure 4.5. Absorption Spectra of **8** in water at 280 K: [**8**] (a) 2.82, (b) 5.65, (c) 8.47, (d) 11.3 and (e) 16.93 μM. Inšet shows the plot of log [dimer] versus log [monomer] for solutions of **8** in water at 280 K.

According to exciton theory[19,39] the excited state energy level of the monomeric dye splits into two upon aggregation, one level being lower and the other higher in energy than the monomer excited state. For head-to-tail

aggregates (J-type), transition to the higher energy state is forbidden, whereas for head-to-head aggregates (H-type) the lower excited state is forbidden. The blue shifted bands observed in the present study indicate that H-type aggregates are formed for 7 and **8** . The concentrations of the monomer and aggregate forms as well as the extinction coefficient of the aggregate were estimated, assuming negligible spectral overlap between the monomer and aggregate at the peak positions and that the aggregates formed are dimers. These values are summarized in Table 4.2. A plot of log [aggregate] versus log [monomer] (insets, Figures 4.4 and 4.5) was linear with a slope of **8**, confirming that dimer aggregates are formed for both dyes.

Table 4.2: Parameters for the aggregation of 7 and 8 in water

	7		8
	H_2O	D_2O	H_2O
K_{308K}, 10^5 M^{-1}	0.54	1.19	0.14
$-\Delta G$ (k cal mol^{-1})	6.73	7.01	5.78
$-\Delta H$ (k cal mol^{-1})	8.15	9.47	4.66
$-\Delta S$ (eu)	4.82	7.89	-3.81
ε (monomer), $M^{-1}cm^{-1}$	1,90,000 (645 nm)	1,55,000 (645 nm)	1,70,000 (641 nm)
ε (dimer), $M^{-1}cm^{-1}$	2,40,000 (595 nm)	2,30,000 (600 nm)	3,40,000 (590 nm)

The equilibrium constants and the thermodynamic parameters for the aggregation process have been evaluated by studying the aggregation process at different temperatures. These results are summarized in Table 4.2. The Arrhenius plot of log K versus 1/T for **7** and **8** are shown in Figure 4.6. Enthalpies of formation ΔH_0, have been calculated using the van't Hoff equation. The standard free energy and entropy changes have been calculated by means of equations $\Delta G^0 = -RT\ln K$ and $\Delta S^0 = (\Delta H - \Delta G^0)/T$.

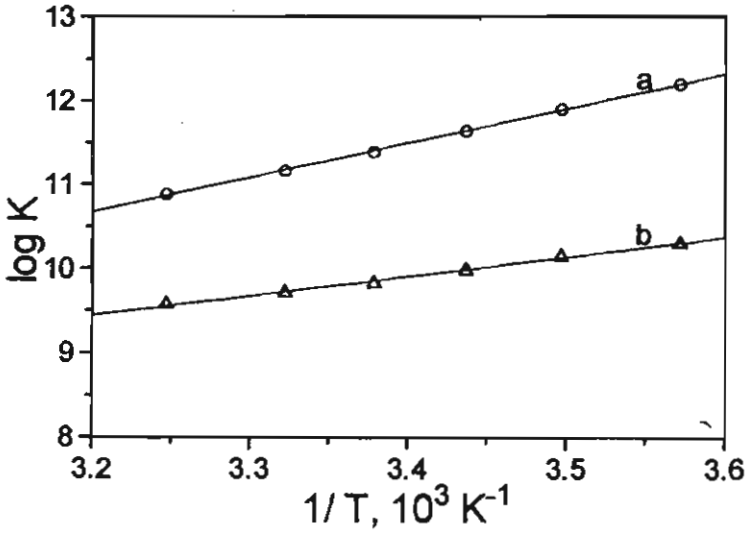

Figure 4.6. Arrhenius plot of log K versus 1/T in water for the aggregation of : (a) **7** and (b) **8**.

The equilibrium constant for dimerization of **8** was nearly an order of magnitude less than that of **7**. The standard free energy and enthalpy changes associated with the aggregation of **7** was also higher in comparison to that of **8**. These effects can be explained on the basis of the hydrophobicity of the two dyes. Both of these dyes have a hydrophobic core (the

chromophoric part) and a hydrophilic part (carboxylic groups). In a highly hydrophilic solvent such as water, the hydrophobic forces tend to form aggregates whereas the carboxylic groups favour dissolution. The presence of two additional phenyl groups enhances the hydrophobic character of 7 as compared to 8 giving it a stronger tendency to aggregate in water.

4.4.4. Aggregation of 7 in D_2O

The aggregation of 7 has been studied in D_2O. Figure 4.7 shows the absorption spectrum of 7 in D_2O, recorded at different temperatures. The absorption maximum of the monomeric form was unchanged, whereas that of the dimer was red-shifted (λ_{max} = 600 nm), compared to that in H_2O. The equilibrium constant, as well as thermodynamic functions were estimated and are given in Table 4.2. These values indicate that 7 has a stronger

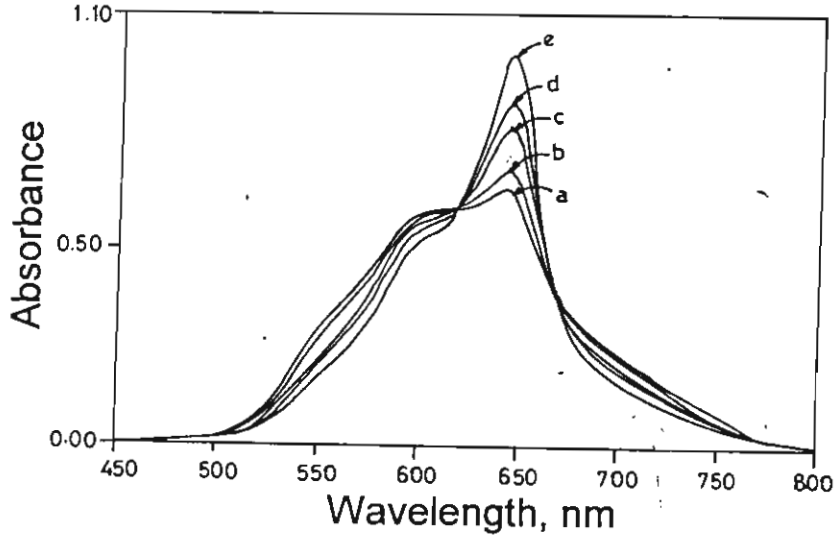

Figure 4.7. Absorption spectrum of 7 (6.5 μM) in D_2O at temperatures: (a) 303, (b) 308, (c) 313, (d) 318 and (e) 323.

tendency to aggregate in D_2O than in water. The difference in the ability of 7 to form dimers in H_2O and D_2O may be related to the differences in hydrogen bonding ability of the two solvents. Since deuterium bonds are reported to be stronger than hydrogen bonds in neutral water complexes[40] it will be more difficult for the dyes to disrupt these bonds. Hence aggregate formation will be relatively more favoured in D_2O.

4.4.5. Effect of Addition of Polyvinylpyrrolidone (PVP) on the Aggregation Process

It has been found that addition of low concentrations of polyvinylpyrrolidone (PVP) has a significant effect on the aggregation behaviour of 7, whereas that of **8** was unaffected. Figure 4.8 shows the effect of addition of low concentrations of PVP (< 0.30 mM) on the absorption spectrum of 7 in water. A decrease in the intensity of the monomer band and an increase in the intensity of the aggregate band which were also accompanied by a shift in its absorption maximum to 612 nm were observed. A substantial decrease in the fluorescence quantum yield was also observed. The ratio of the absorbance at the two maxima (A_{612}/A_{645}) increases with increasing concentrations of 7 at fixed PVP concentrations, confirming that the 612 nm band results from dye aggregation. It is proposed that the formation of a complex between 7 and PVP, (7....PVP)' can bring about non-homogeneous distribution of 7 in solution. Increased concentration of 7 around the polymer chains can enhance aggregate formation (Equations 1 and 2), the driving force being the hydrophobic interaction between 7 and PVP.

$$7 + PVP \rightleftharpoons (7....PVP)' \qquad (1)$$

$$2(7....PVP)' \rightleftharpoons (7....PVP)'_2 \qquad (2)$$

Considering the reaction scheme shown in equations 1 and 2, the following relationship (Equation 3) can be obtained,[8]

$$\frac{[7]^2}{[(7.....PVP)]'} = \frac{1}{K_1^2 K_2 [PVP]^2} \qquad (3)$$

where, K_1 and K_2 are the equilibrium constants for the reactions 1 and 2, respectively. Since the extinction coefficient of 7 is known, the concentration of 7 and $(7....PVP)'_2$ could be determined. A plot of $[7]^2/[(7...PVP)'_2]$

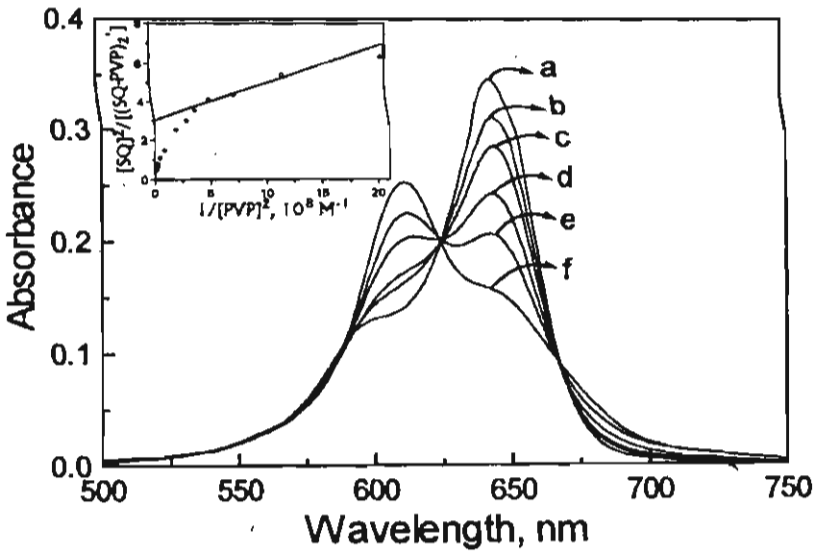

Figure 4.8. Effect of low concentrations of PVP (< 2 x 10^{-4} M) on the absorption spectrum of 7 (3.0 μM) in water at 300 K: [PVP] (a) 0, (b) 22, (c) 36 (d) 73, (e) 110 and (f) 220 μM. Inset shows the plot of $[7]^2/[(7..PVP)_2']$ versus $1/[PVP]^2$.

Table 4.3: Absorption and emission characteristics of 7 and 8 in solution containing PVP, β-CD and CTAB in water

	λ_{max} (nm)		Φ_f	K, $10^2 M^{-1}$	τ_s ps
	Abs	Em			
7	645	659	0.027	-	250
7 + 17 mM PVP	667	679	0.072	1.90	500
7 + 2.7 mM β-CD	652	667	0.15	8.68	650
7 + 4.0 mM of CTAB	664	680	0.33	-	-
8	641	658	0.03	-	180
8 + 17 mM PVP	645	675	0.126	2.20	175
8 + 2.7 mM β-CD	642	659	0.042	7.23	175
8 + 4.0 mM CTAB	663	682	0.29	-	-

versus $1/[PVP]^2$, where PVP concentration was expressed in monomer units gave a straight line (inset, Figure 4.8), which supports the above mechanism. Interestingly, at these low concentrations of PVP, no significant effect on the aggregation behaviour of **8** was observed. Since the equilibrium constant for aggregate formation was about ten fold lesser than for 7, the hydrophobic interaction of **8** with PVP is also expected to be lesser.

Addition of higher amounts of PVP (> 0.30 mM) to 7 leads to a decrease in the intensity of the aggregate band centered around 612 nm.

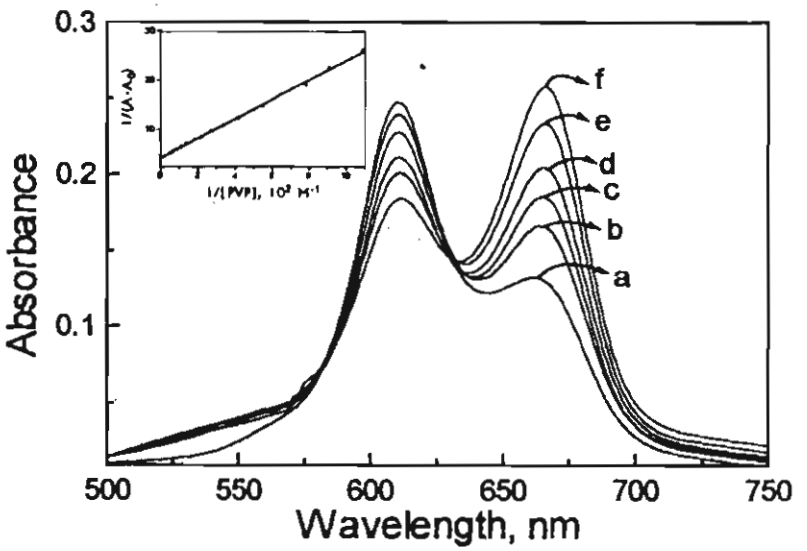

Figure 4.9. Absorption spectra of 7 (3.0 μM) in presence of higher concentrations of PVP (>3 x 10^{-4} M) measured at 300 K: [PVP] (a) 1.1, (b) 2.38, (c) 3.66, (d) 5.49, (e) 9.15 and (f) 16 mM. Inset shows the plot of $1/(A-A_0)$ versus 1/[PVP].

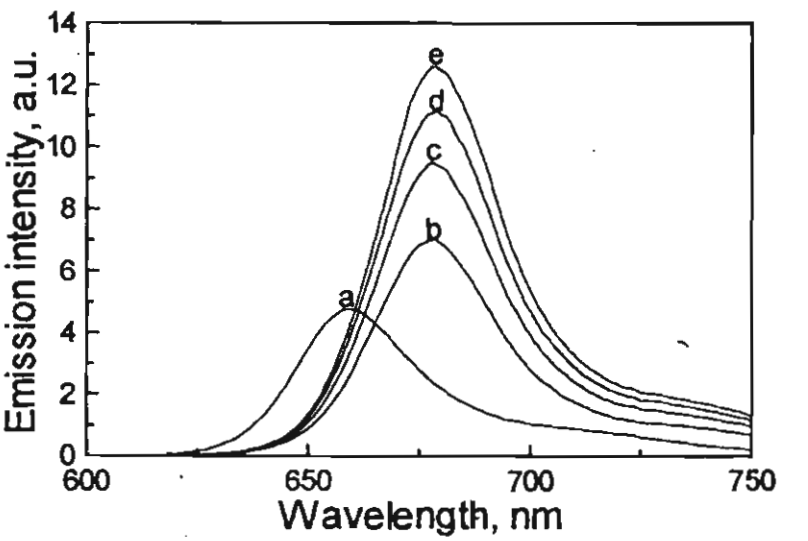

Figure 4.10. Emission spectra of 7 (3.0 μM) in presence of higher concentrations of PVP (>3 x 10^{-4} M) measured at 300 K: [PVP] (a) 0, (b) 2.4, (c) 5.5, (d) 9.2 and (e) 16.5 mM.

This change was accompanied by the formation of a new band centered around 667 nm (Figure 4.9), which was considerably red shifted from the original monomer band (λ_{max} = 645 nm). These changes were also accompanied by an increase in the fluorescence quantum yield. The fluorescence enhancement on addition of higher amounts of PVP is shown in Figure 4.10. In presence of 17 mM of PVP, Φ_f measured at 590 nm was 0.072, which was substantially higher than that in the absence of PVP (Φ_f = 0.027) (Table 4.3).

Squaraines are known to form J-type aggregates which have absorption maxima, red-shifted to those of the corresponding monomers.[26] The species formed in aqueous solution of 7 at higher concentrations of PVP, with absorption maximum at 667 nm however, does not appear to be the J-aggregate since it is highly fluorescent and also the analysis of the absorption and emission data indicates a 1:1 squaraine/PVP complex. The absorption and emission characteristics of 7 in the presence of high concentrations of PVP tends towards those observed in aprotic solvents such as DMSO and DMF (Table 4.1). The species observed in the polymer containing solution can therefore be assigned to the monomeric form of the dye, encapsulated in a hydrophopbic domain provided by the polymer. At higher concentrations of PVP, more sites will be available for 7 to complex, which can cause the aggregate to break due to a better distribution of 7 within PVP matrix. The equilibrium constant for the formation as well as the extinction coefficient of the (7....PVP) and (8...PVP) complex were determined from the relationship (Equation 4),

$$\frac{1}{A - A_0} = \frac{\varepsilon}{\varepsilon - \varepsilon'} \left[\frac{1}{K_1 [PVP]} + 1 \right] \quad (4)$$

where, A and A_0 are the absorptivity of the complexed and uncomplexed dye, respectively at 667 nm, K_1 is the equilibrium constant for complex formation according to equation 1 and ε and ε' are the molar extinction coefficients of the free dye and encapsulated dye, respectively at 667 nm. A plot of $1/(A - A_0)$ versus 1/[PVP] gives a straight line (inset, Figure 4.9), indicating a 1:1 complex formation. The values of K_1 and ε' were determined from the slope and intercept of this linear plot were 1.9×10^2 M^{-1} and 141,000 M^{-1} cm^{-1}, respectively.

Addition of PVP did not significantly affect the shapes of the absorption and emission spectra of **8**. At low concentrations of PVP (< 0.30 mM), the aggregation behaviour remains unaffected unlike in the case of 7. At

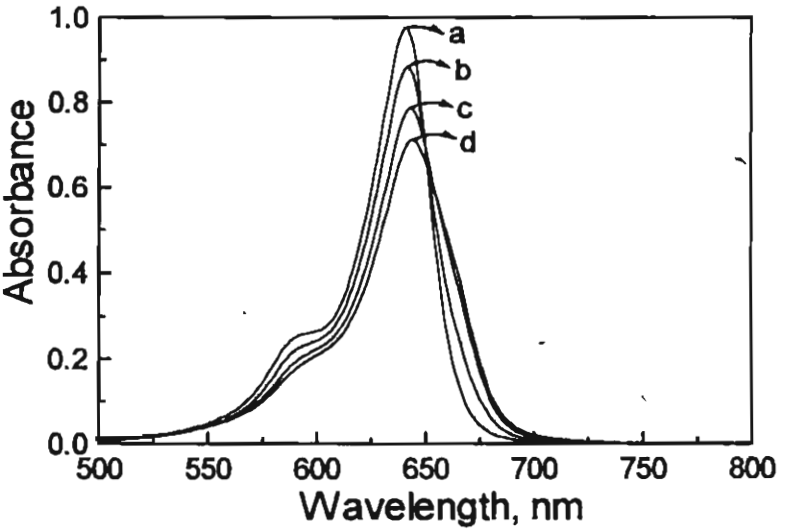

Figure 4.11. Absorption spectra of **8** (6 μM) in presence of PVP (> 10^{-3} M) measured at 300 K: [PVP] (a) 0, (b) 5.5, (c) 13, (d) 17 mM.

higher concentrations of PVP (~17 mM), a slight red shift in the absorption maxima along with the formation of an absorption shoulder around 670 nm were observed (Figure 4.11). Eventhough low concentrations of PVP has no significant effect on the aggregation behaviour of **8**, higher concentrations of PVP (> 3 x 10^{-4} M) lead to a substantial enhancement in the fluorescence quantum yield (Figure 4.12). At a concentration of 17 mM of PVP, the Φ_f value of **8** shows a four fold enhancement (Table 4.3). An emission band with a maximum around 675 nm was also observed (Table 4.3). The equilibrium constant for the **8**...PVP complex was estimated using equation 4 and this value is given in Table 4.3. These results confirm that the hydrophobic interactions of **8** are much weaker than those for **7**. The presence of two additional phenyl groups in **7** imparts greater hydrophobic character to this molecule.

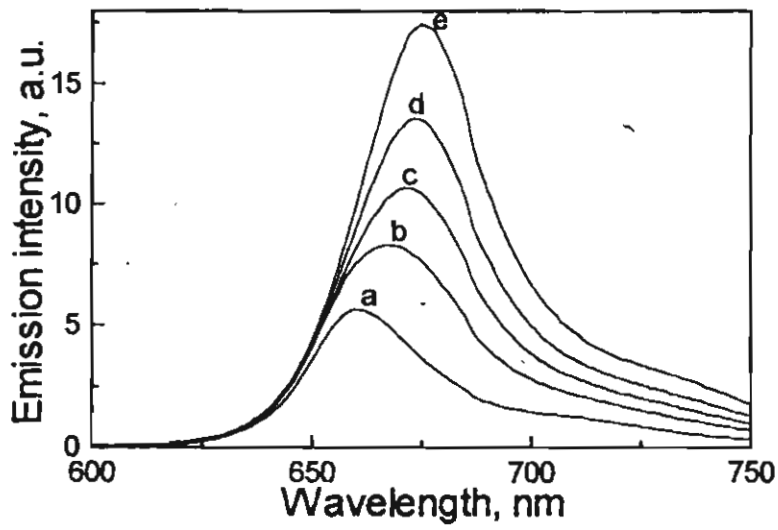

Figure 4.12. Effect of PVP on the emission spectrum of **8** (6 μM) in water at 300 K: [PVP] (a) 0, (b) 2.5, (c) 5.5, (d) 9.2 and (e) 17 mM.

4.4.6. Effect of Addition of β-Cyclodextrin (β-CD)

Addition of β-cyclodextrin to aqueous solutions of **7** and **8** brings about a bathochromic shift in their absorption and fluorescence spectra, accompanied by an enhancement in their quantum yields of fluorescence (Figures 4.13 and 4.14). These effects were less pronounced for **8** than **7**. (Table 4.3). The hydrophobic nature of the dye has been proposed to be the driving force for such interactions. Similar β-CD encapsulation was earlier reported for bis(2,4,6-trihydroxyphenyl)squaraine.[41] The equilibrium constants for the formation of the complexes between the dyes and β-CD, as well as the fluorescence yields of the complexed dye were estimated using the Benesi-Hildebrand expression for 1:1 complexation (Equation 5),

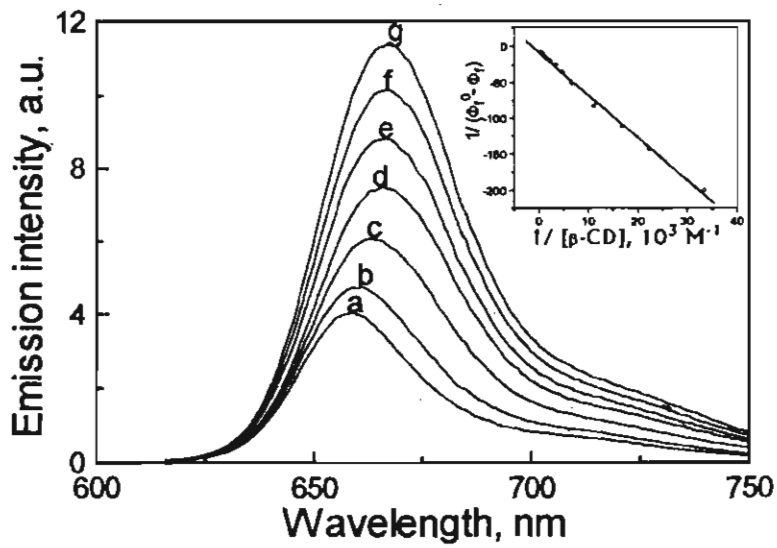

Figure 4.13. Effect of β-cyclodextrin on the emission spectrum of **7** (3.0 μM) in water at 300 K: [β-CD] (a) 0, (b) 0.06, (c) 0.45, (d) 0.6, (e) 0.9, (f) 1.5 and (g) 2.7 mM. Inset shows the plot of $1/(\Phi_f^0 - \Phi_f)$ versus 1/[β-CD].

$$\frac{1}{\Phi_f^0 - \Phi_f} = \frac{1}{\Phi_f^0 - \Phi_f'} + \frac{1}{K_3(\Phi_f^0 - \Phi_f')\,[\beta\text{-CD}]} \quad (5)$$

where, Φ_f^0 is the initial fluorescence quantum yield, Φ_f' the fluorescence of the Dye···β-CD complex and K_3 the equilibrium constant for the formation of such a complex. A plot of $1/(\Phi_f^0 - \Phi_f')$ versus $1/[\beta\text{-CD}]$ gives a straight line, indicating a 1:1 complex formation (insets, Figures 4.13 and 4.14). The values estimated for K_3 and Φ_f' for **7** and **8** are included in Table 4.3.

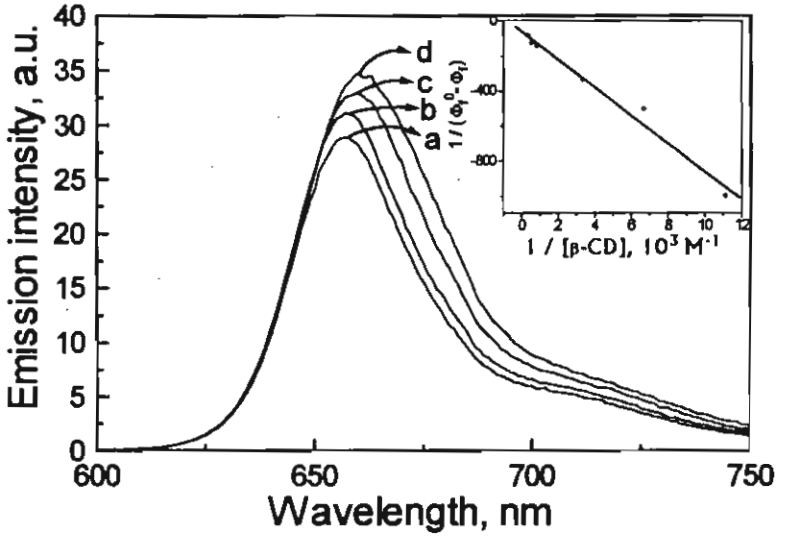

Figure 4.14. Effect of β-cyclodextrin on the emission spectrum of **8** (4 μM) in water at 300 K: [β-CD] (a) 0, (b) 0.15, (c) 1.2 and (d) 2.7 mM. Inset shows the plot of $1/(\Phi_f^0 - \Phi_f)$ versus $1/[\beta\text{-CD}]$.

The enhancement in fluorescence quantum yield for **8** on complexation with β-CD was very small (0.04 in presence of 2.7 mM of β-CD as compared to 0.03 without β-CD). β-cyclodextrin is known to provide a hydrophobic

environment, enabling it to complex with a variety of organic dyes including squaraines, in water. The enhanced hydrophilic character of **8** favours the equilibrium in favour of the uncomplexed state. These results are in agreement with the observation that the dye **8** is less hydrophobic than **7**.

4.4.7. Effect of Cetyltrimethylammonium Bromide Micelles (CTAB)

The photophysical properties of **7** and **8** were found to be affected significantly, on incorporation into CTAB micelles. The photophysical properties of **7** and **8** in cetyltrimethylammonium bromide (CTAB) have been studied using absorption and emission spectroscopy. In presence of CTAB, above its critical micellar concentration (CMC), both **7** and **8** show a bathochromic shift in the absorption (Figure 4.15) and emission spectra (Figure 4.16). This process was accompanied by a drastic enhancement in

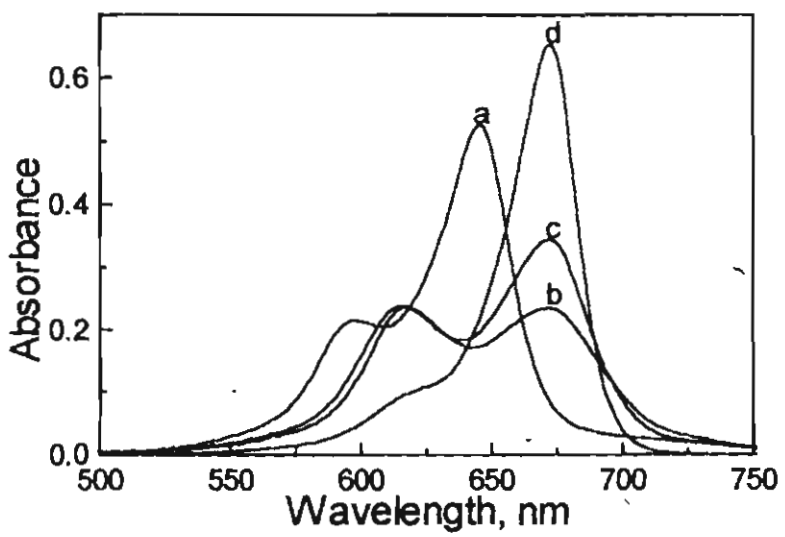

Figure 4.15. Effect of CTAB on the absorption spectrum of **7** (2.6 μM) in water: [CTAB] (a) 0, (b) 2.0, (c) 3.0 and (d) 7.41 mM.

their fluorescence intensities (Figure 4.16). The micellar media are known to provide, hydrophobic microdomains in water for guest molecules.[42] Since the dye molecules are distributed among the micelles, aggregation will not be favoured. These results are similar to those observed in the case of PVP at higher concentrations.

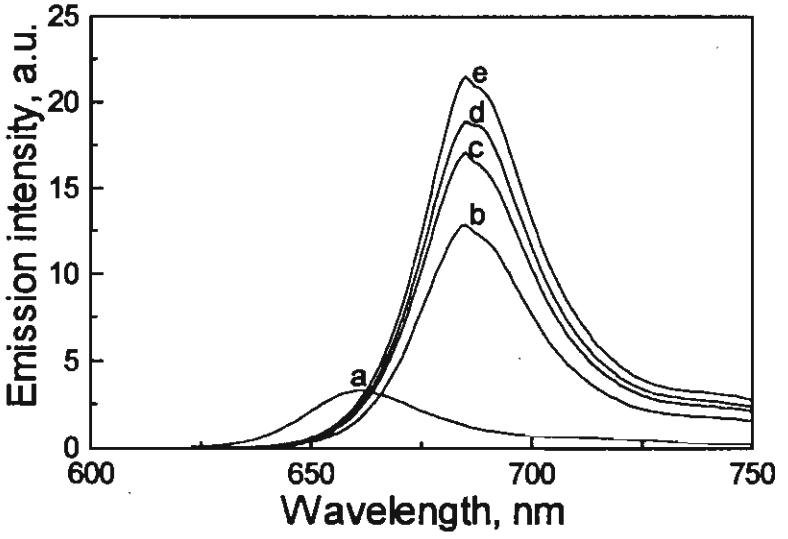

Figure 4.16. Effect of CTAB on the emission spectrum of 7 (2.6 μM) water: [CTAB] (a) 0, (b) 3.5, (c) 3.7, (d) 4.0 and (e) 6.2 mM.

4.4.8. Transient Absorption Studies[42]

The behaviour of the excited singlet state of **7** and **8** in aqueous solution with and without PVP was investigated using the picosecond laser flash photolysis technique. Figure 4.17 shows the time-resolved transient absorption spectra of an 8.2 μM solution of 7 in water. Immediately after the laser flash, the dye is excited into its singlet state to give the transient absorption spectrum (spectrum a, Figure 4.17), with a maximum at 530 nm

and a bleaching at 645 nm. Some bleaching around 600 nm, where the aggregate absorbs, was also observed. From the exponential decay of the transient absorption at 520 nm and the recovery of the bleach at 645 nm (inset, Figure 4.17), a singlet excited lifetime of 250 ± 20 ps was obtained.

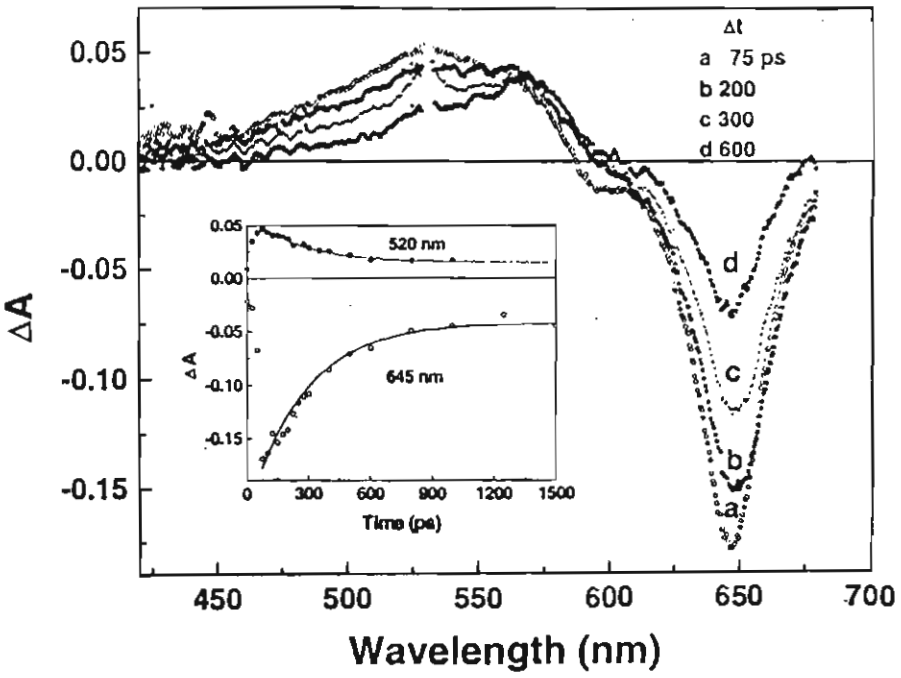

Figure 4.17. Time-resolved transient absorption spectra recorded following 532-nm laser pulse excitation of 7 (8.2 μM) in water. Inset shows the transient decay at 520 nm and bleaching recovery at 645 nm.

The recovery of absorption at 645 nm was only partial and the formation of a long-lived transient with an absorption maximum at 570 nm was evident from the spectrum recorded at 600 ps after the laser pulse excitation (spectrum d, Figure 4.17).

Figure 4.18 shows the transient absorption spectrum of an 8.2 μM solution of 7 in water containing 22 μM of PVP. At these concentrations, addition of PVP shifts the monomer/aggregate equilibrium in favour of the aggregate. The spectrum, recorded immediately after the laser pulse, shows bleaching of both the monomer and the aggregate bands at 645 nm and 600 nm, respectively. The transient spectrum measured at 100 ps shows a partial recovery of the 600 nm band, whereas a further bleach was observed at 645 nm. These results can be interpreted in terms of the reaction mechanism shown in equations 6 and 7.

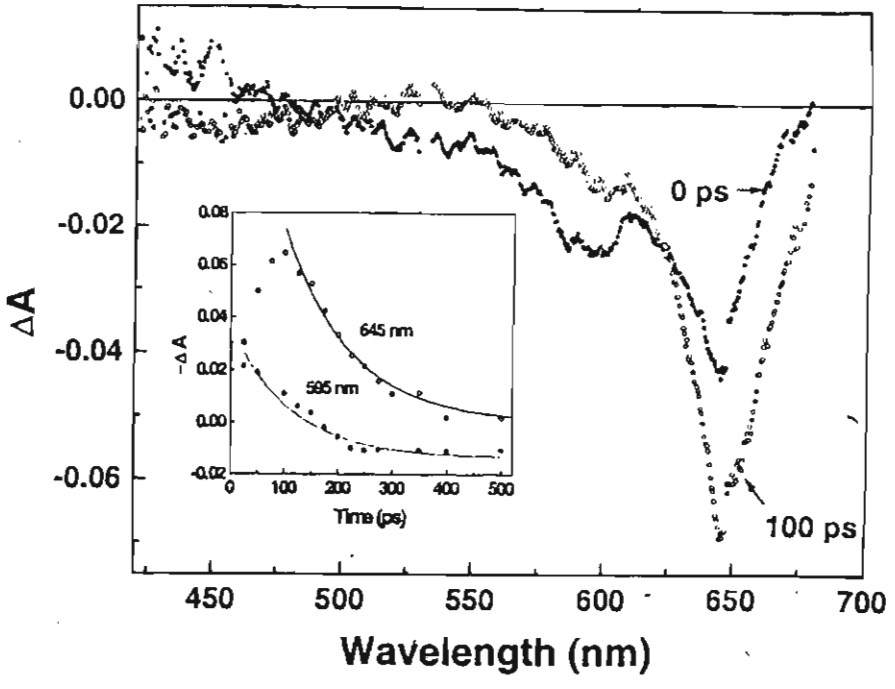

Figure 4.18. Transient absorption spectra recorded immediately (Δt = 0 ps) and 100 ps after 532-nm laser pulse excitation of 7 (8.2 μM) in aqueous PVP (22 μM) solution. Inset shows the bleaching recovery at 595 and 645 nm corresponding to the aggregate and monomer band, respectively.

$$Sq \underset{\Delta}{\overset{h\nu}{\rightleftharpoons}} {}^{1}Sq^{*} \qquad (6)$$

$$(Sq.....PVP)_2 \underset{\Delta}{\overset{h\nu}{\rightleftharpoons}} ({}^{1}Sq^{*}...PVP,\ Sq....PVP) \qquad (7)$$

The 532-nm laser pulse used for excitation, can excite both the monomer and the aggregate. According to the mechanism shown above, excitation of the monomer will lead to a depletion of the ground state and formation of the excited state. Excitation of the aggregate on the other hand will lead to a depletion of the ground state aggregate and formation of the excited state monomer as well as an equal amount of the ground state

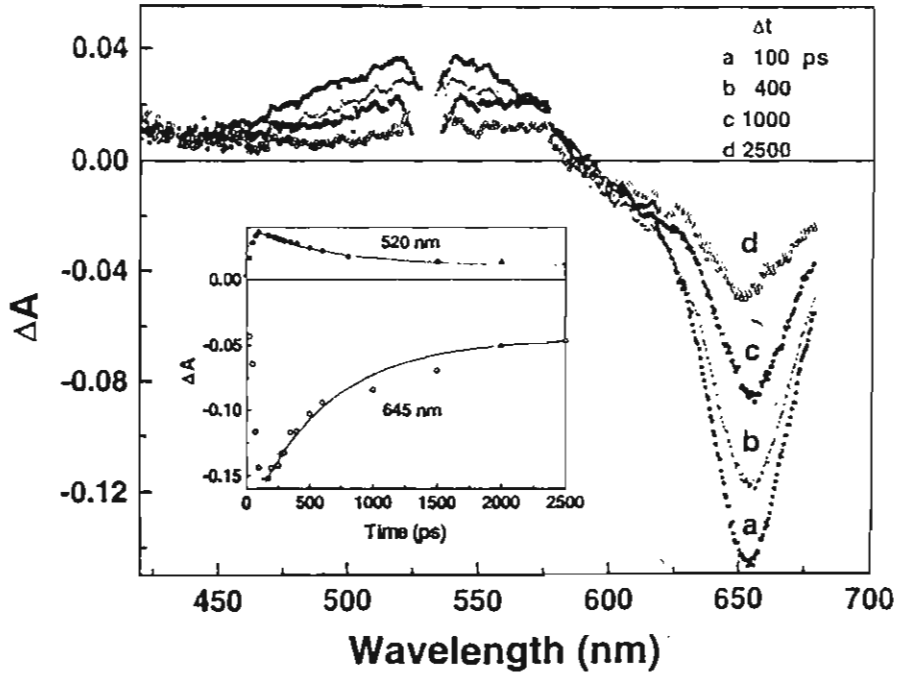

Figure 4.19. Time-resolved transient absorption spectra recorded following 532-nm laser pulse excitation of 7 (8.2 μM) in aqueous β-CD (2.7 mM) solution. Inset shows the transient decay at 520 nm and bleaching recovery at 645 nm.

monomer. If the reverse reaction 7 occurs within 100 ps, this will lead to a recovery of the ground state aggregate and a further depletion of the monomer band, which is indeed observed at 645 nm. Thus, the laser flash photolysis study clearly indicates the break-up of the excited state of the dimer to give an excited state/ground state monomer pair, which rapidly recombines within 100 ps. The subsequent decay of the excited state of the monomer occurs with a lifetime of about 125 ps.

The transient behaviour at higher PVP concentrations was similar to that observed for the monomeric dye in the absence of PVP, except that the lifetime of the excited singlet state was significantly enhanced. (τ = 500 ps).

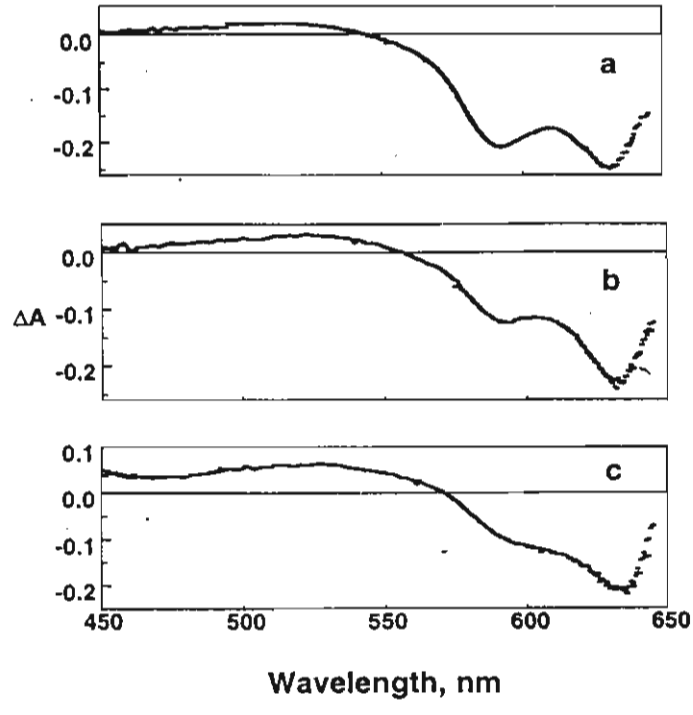

Figure 4.20. Excited singlet spectra of **8** in water (18 μM) containing (a) 0; (b) 20 μM and (c) 17 mM of PVP. The difference spectra were recorded immediately (Δt = 0 ps) following 355-nm laser pulse excitation.

This increase in lifetime parallels the enhancement observed in the fluorescence yield of 7 at high ($>10^{-4}$ M) PVP concentrations. Similar effects were observed for aqueous solutions of 7 containing β-CD (Figure 4.19). The spectral features were similar to those observed in the absence of β-CD or PVP. The excited state lifetime was longer (650 ± 20 ps), similar to that observed in aqueous solution of 7, containing high concentrations of PVP.

The singlet excited state of **8** shows a characteristic absorption maximum around 530 nm with bleaching at 590 and 640 nm. The difference absorption spectra recorded, following the 532-nm laser pulse excitation of **8** are shown in Figure 4.20. From the decay of the transient absorption at 530 nm the lifetime of **8** has been estimated as 180 ps. The singlet excited state properties are summarized in Table 4.3. Transient absorption spectra obtained in presence of PVP (Figure 4.20) and β-CD have also been recorded . It has been found that addition of PVP has little effect on the transient absorption spectra. The bleaching at 590 nm was less, whereas the one at 640 nm was retained its intensity. This is probably due to the presence of less amount of aggregates in presence of PVP. The lifetime of the singlet excited state showed a little increase in the presence of PVP and β-CD (Table 4.3).

4.5. Conclusion

Two new water soluble bis(benzothiazolylidene)squaraines were synthesized and characterized. The photophysical properties of these squaraine dyes have been investigated. The absorption spectra of these dyes are highly dependent on the pH of the solution. In acid medium, the

absorption spectra are broad and blue shifted for both these dyes. However, the spectra become sharp and intense in basic medium. The squaraine dye 7 shows one acid-base equilibrium with a pK_a value of 6.4, whereas **8** has two distinct pK_a values as 6.7 and 4.4. These dyes form H-type aggregates in water. Addition of low concentrations of PVP (< 3 x 10^{-4} M) brought about an enhancement in the aggregation of 7 whereas that of **8** remained unaffected. At high concentrations of PVP (>3 x 10^{-4} M), formation of highly fluorescent species was observed for **7** and **8** and these species have been assigned as a polymer microencapsulated monomeric forms of these dyes. Picosecond laser flash photolysis studies of the aggregates indicated the break-up of the aggregate in the excited state to yield excited state-ground state monomer pairs which undergo rapid recombination to yield the ground state aggregate. The fluorescence intensity of the dye 7 can be substantially enhanced by encapsulating it in β-CD, whereas that of **8** undergoes only a minor enhancement. In presence of cationic micelles such as CTAB, the absorption and emission spectra become red-shifted and was accompanied by an increase in the fluorescence intensity.

4.6. References

1. Yuzhakov, V. I. *Russ. Chem. Rev. (Engl. Transl.)* **1979**, *48*, 1076.
2. Rabinowitch, E. *J. Am. Chem. Soc.* **1941**, *63*, 69.
3. Mataga, N. *Bull. Chem. Soc. Jpn.* **1957**, *30*, 375.
4. West, W.; Pearce, S. *J. Phys. Chem.* **1965**, *69*, 1894 (and references cited therein).
5. Kuhn, H. In *Light-Induced Charge Separation in Biology and Chemistry*; Geischer, H., Katz, J. J., Eds.; Dahlem Konfersnzen: West Berlin, **1979**; p 151.
6. Gilman, P. B. In *Photographic Sensitivity*; Cox, R. J., Ed.; Academic Press: London, **1973**, p 187.
7. Sturmer, D. M. In *Special Topic in Heterocyclic Chemistry*; Weissberger, A., Taylor, E. C., Eds., Wiley: New York, **1977**, p 540.
8. Valdes-Aguilera, O.; Neckers, D. C. *J. Phys. Chem.* **1988**, *92*, 4286.
9. Valdes-Aguilera, O.; Neckers, D. C. *Acc. Chem. Res.* **1989**, *22*, 171.
10. Whitten, D. G.; *Acc. Chem. Res.* **1993**, *26*, 502.
11. Vaidyanathan, S.; Patterson, L. K.; Mobius, D.; Gruniger, H. R. *J. Phys. Chem.* **1985**, *89*, 491.
12. Nakahara, H.; Fukuda, K.; Mobius, D.; Kuhn, H. *J. Phys. Chem.* **1986**, *90*, 6144.
13. Duschl, C.; Kemper, D.; Frey, W.; Meller, P.; Ringsdorf, H.; Knoll, W. *J. Phys. Chem.* **1989**, *93*, 4587.
14. Blum, A.; Grossweiner, L. I. *Photochem. Photobiol.* **1971**, *14*, 551.

15. Kasha, M.; El-Bayoumi, M. A.; Rhodes, W. *J. Chem. Phys.* **1961**, *58*, 916.

16. Hochstrasser, R. M.; Kasha, M. *Photochem. Photobiol.* **1964**, *3*, 317.

17. Czikkely, V.; Forsterling, H. D.; Kuhn, H. *Chem. Phys. Lett.* **1970**, *6*, 207.

18. Czikkely, V.; Forsterling, H. D.; Kuhn, H. *Chem. Phys. Lett.* **1970**, *6*, 11.

19. McRae, F. G.; Kasha, M. In *Physical Processes in Radiation Biology*, Augenstein, I.; Rosenberg, B., Mason, S. F. Eds.; Academic: New York, **1963**; p 23.

20. Arbeloa, F.; L.; Gonzales, I. L.; Ruiz-Ojeda, P.; Arbeloa, I. L. *J. Chem. Soc. Faraday Trans. 2*, **1982**, *78*, 989.

21. Ruiz-Ojeda, P.; Katima-Amashta, I. A.; Ochoa, J. R.; Arbeloa, I. L. *J. Chem. Soc. Faraday Trans. 2*, **1988**, *84*, 1.

22. Levschin, V. L.; Lonskaya, I. S. *Opt. Spectroscopy (Engl. Transl.)* **1961**, *11*, 148.

23. Selwyn, J. E.; Steinfeld, J. I.; *J. Phys. Chem.* **1972**, *76*, 762.

24. Rohatgi, K. K.; Singhal, G. S. *J. Phys. Chem.* **1966**, *70*, 1695.

25. Rohatgi, K. K.; Mukhopadhyay, A. K. *J. Phys. Chem.* **1972**, *76*, 3970.

26. Das, S.; Thanulingam, T. L.; Thomas, K. G.; Kamat, P. V.; George, M. V. *J. Phys. Chem.* **1993**, 97,13620.

27. Hotchandani, S.; Das, S.; Thomas, K. G.; George, M. V.; Kamat, P. V. *Res. Chem. Intermed.* **1994**, 20, 927.

28. Liang, K.; Law, K-Y.; Whitten, D. G. *J. Phys. Chem.* **1994**, 98, 13379.

29. Chen, H.; Law. K. Y.; Perlstein, J.; Whitten, D. G. *J. Am. Chem. Soc.* **1995**, *117*, 7257.

30. Chen, H.; Herkstroeter, W. G.; Perlstein, J.; Law. K. Y.; Whitten, D. G. *J. Phys. Chem.* **1994**, *98*, 5138.

31. Buncel, E.; McKerrow, A.; Kazmaier, P. M. *J. Chem. Soc. Chem. Commun.* **1992**, 1242.

32. Chen, H.; Law, K. Y.; Whitten, D. G. *J. Phys. Chem.* **1996**, *100*, 5949.

33. Chen, H.; Farahat, M. S.; Law, K. Y.; Whitten, D. G. *J. Am. Chem. Soc.* **1996**, *118*, 2584.

34. Ashwell, G. J.; Jefferies, G.; Hamilton, D. G.; Lynch, D. E.; Roberts, M. P. S.; Bahra, G. S.; Brown, C. R. *Nature* **1995**, *375*, 385.

35. Kamat, P. V.; Das, S.; Thomas, K. G.; George, M. V. *J. Phys. Chem.* **1992**, *96*, 195.

36. These studies were carried out by Dr. P. V. Kamat at the Notre Dame Radiation Laboratory, USA.

37. Mills, W. H. *J. Chem. Soc.* **1922**, *121*, 455.

38. Das, S.; Thomas, K. G.; Ramanathan R.; Kamat, P. V.; George, M. V. *J. Phys. Chem.* **1993**, *97*, 13625.

39. Kasha, M.; Rawls, H. R.; El Bayoumi, A. *Pure Appl. Chem.* **1965**, *11*, 371.

40. Scheiner, S.; Cuma, M. *J. Am. Chem. Soc.* **1996**, *118*, 1511.

41. Das, S.; Thomas, K. G.; George, M. V.; Kamat, P. V. *J. Chem. Soc. Faraday Trans.* **1992**, **88**, 3419.

42. Kalyanasundaram, K. *Photochemistry in Microheterogeneous Systems*, Academic Press, Inc. Orlando, Florida **1987**.